UNIVERSITÉ LAVAL

Structure et dynamique des maximums de chlorophylle subsuperficiels en Arctique canadien

Thèse

Johannie Martin

Doctorat interuniversitaire en Océanographie
Philosophiæ doctor (Ph.D.)

Québec, Canada

Résumé

Dans l'océan Arctique, les conditions de croissance des micro-algues sont particulièrement variables et souvent contraignantes. De par sa position et sa taille modeste, cet océan est fortement influencé par les fleuves affluents et les eaux de l'Atlantique et du Pacifique. La lente propagation de ces eaux fait en sorte que, durant le premier été, le phytoplancton épuise les nutriments dans la couche de surface; le renouvellement des nutriments est ensuite limité par la très forte stratification verticale causée par l'accumulation d'eau douce. Ces conditions mènent le phytoplancton à trouver un compromis entre la limitation en lumière (en profondeur) et en nutriment (en surface), ce qui conduit à la formation d'un maximum de chlorophylle subsuperficiel (SCM). L'objectif premier de cette thèse était d'examiner, pour la première fois, la structure verticale, l'écologie et la productivité des SCM en fonction des conditions du milieu dans différents secteurs côtiers de l'Arctique canadien. Il appert que les SCM sont des structures omniprésentes et persistantes dans les eaux libres de glace. La plupart des SCM étaient associés à la nitracline, suggérant que la disponibilité en nitrate exerce une influence dominante sur leur positionnement vertical. Une étude expérimentale des relations entre la lumière, la disponibilité en azote et la productivité primaire a montré que les algues du SCM présentent de fortes compétences photosynthétiques et assimilent activement le carbone, le nitrate et d'autres sources d'azote. Bien que leur productivité à court terme soit contrainte par la faible luminosité et les basses températures, les algues du SCM contribuent largement à la production primaire journalière nouvelle, représentant une source majeure de matière organique pour l'écosystème. Comme il est difficile de mesurer la production annuelle du SCM, les résultats expérimentaux ont été jumelés à un modèle écosystémique numérique initialisé et forcé avec les conditions physico-chimiques du golfe d'Amundsen. Les simulations indiquent que la couche verticale englobant le SCM effectuerait l'essentiel de la synthèse de matière organique dans cet environnement. Vu l'impact présumé du SCM sur le réseau alimentaire, les flux verticaux de carbone et la justesse des estimations satellitaires de productivité, la meilleure compréhension de la dynamique des SCM résultant de cette thèse permet de jeter un regard nouveau sur l'écologie de l'océan Arctique dans un contexte de changements climatiques rapides.

Abstract

In the Arctic Ocean, the growth conditions of micro-algae are highly variable and often restrictive. By virtue of its location and small size, this ocean is strongly influenced by water inputs from large rivers and the adjacent Atlantic and Pacific oceans. The slow propagation of these waters ensures that the phytoplankton exhausts nutrients in surface waters during the first summer. Afterwards, upward nutrient renewal is curtailed by the strong vertical stratification imparted by the accumulation of freshwater. These conditions force the phytoplankton to find a compromise between light limitation at depth and nutrient limitation at the surface, resulting in the formation of subsurface chlorophyll maximums (SCM). The central objective of this thesis was to provide the first comprehensive analysis of the vertical structure, ecology and productivity of SCM with respect to environmental conditions across different sectors of the coastal Canadian Arctic. Results revealed the widespread occurrence of long-lived SCM in ice-free waters. Most of these SCM were closely associated with the nitracline, implying that their vertical positioning was primarily influenced by nitrate availability in the lower euphotic zone. Experimental assessments of nitrogen nutrition and photosynthetic rates showed that SCM phytoplankton possessed high photosynthetic competency and were actively assimilating carbon, nitrate and other nitrogen sources. Although low irradiance and temperature constrained short-term productivity in the lower euphotic zone, SCM contributed strongly to daily new production and thus represented a major source of organic matter in the ecosystem. Since the overall contribution of SCM to annual productivity is very difficult to measure directly, experimental results were combined with a numerical ecosystem model initialized with and forced by the physico-chemical conditions of Amundsen Gulf. The simulations indicate that SCM layers potentially contribute most of the annual new and total primary production in the southeast Beaufort Sea. Since these layers presumably exert a strong impact on the food web, vertical carbon flux and the accuracy of remote-sensing estimates of productivity, the new knowledge of SCM dynamics generated in this thesis provides crucial insights into the ecology of the Arctic Ocean in a context of rapid environmental changes.

Table des matières

Liste des tableaux

Liste des figures

« Il faut tout un village pour élever un enfant »

À tous ceux rencontrés le long de la route qui ont fait de moi la femme que je suis, plus particulièrement mon noyau : mes parents, mon frère J-F, Mélissa, Zach et Abby.

Remerciements

Cette thèse n'aurait évidemment pas pu se réaliser sans le soutien d'un nombre incalculable de gens. Loin de moi la prétention de pouvoir ici faire la liste exhaustive de chacun d'entre eux.

Tout d'abord, je tiens à remercier mon directeur de thèse, Jean-Éric Tremblay, pour l'incroyable opportunité de recherche qu'il m'a offerte. Merci d'avoir eu confiance en moi, parfois plus que moi-même. I would also like to thank my co-supervisor, Prof. Neil M. Price, for his judicious and always relevant comments throughout the years. Thank you for your patience in my struggle with the language barrier. Je voudrais aussi remercier les membres de mon comité d'encadrement, Yves Gratton et Connie Lovejoy, d'avoir fait de moi une meilleure scientifique en apportant un regard nouveau et multidisciplinaire à mes travaux. Merci à Dany Dumont, fidèle collaborateur, pour ta générosité et ton infinie patience à faire de moi une modélisatrice (plan ambitieux), mais par-dessus tout, merci pour ton amitié.

Je ne peux passer sous le silence tout le personnel du NGCC *Amundsen* pour leur aide inestimable et pour m'avoir accepté parmi eux tel l'une des leurs. Vous avez été, à bien des égards, une 2^{e} famille pour moi. Merci à mes collègues du laboratoire Tremblay : Marjolaine Blais, Mariane Berrouard, Simon Pineault, Myriam Bergeron, Geneviève Cauchon-Ouellet. Merci de m'avoir laissé m'impliquer dans vos projets respectifs; cela a toujours été un grand plaisir pour moi de pouvoir vous aider. Merci à Jonathan Gagnon, professionnel de recherche et colocataire de bureau, parce que même aujourd'hui j'entends toujours tes conseils quand vient le temps de prendre une décision. Merci à mes laboratoires d'adoption : Luc Michaud, Louis Létourneau, Catherine Lalande, Marie-Ève Garneau, Pascale Lafrance, Caroline Bouchard, Josée Michaud, Ramon Terrado, Marianne Potvin, Stéphane Thanassekos, Gérald Darnis, Keith Lévesque, Delphine Benoit, Hélen Cloutier, Alexandre Forest, Dominique Robert, Marie-Emmanuelle Rail, Caroline Sévigny, Véronique Lago. Ni le temps passé en mer, ni le temps passé à l'Université Laval n'aurait été le même sans vos sourires et votre bonne humeur. Merci à Pascal Massot, Sylvain Blondeau et Steeve Gagné, mon équipe favorite lorsque venait le temps de régler des

problèmes insolvables, vous m'avez sauvé de plusieurs nuits d'insomnie. Merci au personnel de Québec-Océan et du département de biologie, particulièrement Lynn Bélanger, Guylaine Potvin, Martine Boucher et Mélissa Laroche, d'avoir rendu la partie administrative de mes études graduées tellement plus facile.

Évidemment, je veux tout spécialement remercier ma famille et mes amis qui m'ont supportée (et endurée) durant toutes ces années, je vous suis particulièrement redevables. Merci d'avoir accepté mon mode de vie un peu bordélique, mes absences prolongées. Merci à mes parents, Pierre et Georgette, mon frère Jean-François et ma belle-sœur Mélissa; j'ai toujours senti votre amour, même à des milliers de kilomètres de vous. Merci à mon neveu et ma nièce, Zachary et Abbygaël, pour qui il vaut la peine de bâtir un monde meilleur. Merci à mon ami Mickael qui est parti beaucoup trop tôt, mais en me montrant à me battre jusqu'au bout. Merci à mes cousins, cousines, Éric, Marie-Josée, Nancy, pour les soupers hebdomadaires; vous avez été mon équilibre. Merci à Annie pour toutes ces heures passées à relire mes manuscrits; tu es probablement la 2^{e} spécialiste mondiale du SCM arctique, et à Olivier d'avoir été le conseillé « esthétique » tout au long de ce doctorat. Merci à Émilie, mon amie de toujours, de m'avoir donné une journée toutes les semaines pour me faire bouger de mon bureau et aérer l'esprit et à Jérôme pour me l'avoir laissé en garde partagée. Grâce à toi on mange aussi toutes les deux beaucoup mieux.

Avant-Propos

La présente thèse a pour but d'exposer les résultats des travaux de mon doctorat portant sur la répartition, la structure et la dynamique des maximums de chlorophylle subsuperficiels (SCM) en Arctique canadien. Cette thèse est composée de 5 chapitres; les chapitres 1 et 5 sont rédigés en français et représentent respectivement l'introduction et la conclusion générale, alors que les autres sont rédigés en anglais sous forme d'articles scientifiques, publiés (chapitres 2 et 3) ou soumis (chapitre 4):

Chapitre 2 : **Martin, J.**, Tremblay, J.-É., Gagnon, J., Tremblay, G., Lapoussière, A., Jose, C., Poulin, M., Gosselin, M., Gratton, Y. (2010). *Prevalence, structure and properties of subsurface chlorophyll maxima in Canadian Arctic waters*, publié dans Marine Ecology Progress Series. 412: 69-84.

Chapitre 3 : **Martin, J.,** Tremblay, J.-É., Price, N.M. (2012). *Nutritive and photosynthetic ecology of subsurface chlorophyll maximum in Canadian Arctic waters*, publié dans Biogeosciences, 9: 5353-5371.

Chapitre 4 : **Martin, J.**, Dumont, D., Tremblay, J.-É. (2013). *Contribution of subsurface maxima to primary production in the Beaufort Sea (Canadian Arctic): A model assessment,* publié dans Journal of Geophysical Research 118: doi: 10.1002/2013JC008843.

Les résultats obtenus lors de ce doctorat ont été recueillis lors de trois missions en mer de douze semaines et d'une de six semaines à bord du NGCC Amundsen que j'ai réalisé entre 2005 et 2008. J'ai personnellement effectué les analyses en laboratoires, les analyses statistiques, participé à l'élaboration et effectué les simulations du modèle présenté au chapitre 4, interprété les résultats, rédigé entièrement ce document ainsi que participé en tant que co-auteure aux manuscrits suivants :

Tremblay, J.-É., Simpson, K., **Martin, J.**, Miller, L., Gratton, Y., Barber, D., Price, N.M. (2008) *Vertical stability and the annual dynamics of nutrients and chlorophyll fluorescence in the coastal, southeast Beaufort Sea*. Journal of Geophysical Research. 113: C07S90, doi:10.1029/2007JC004547.

Mundy, C. J., Gosselin, M., Ehn, J., Gratton, Y., Rossnagel, A., Barber, D.G., **Martin, J**., J.-É. Tremblay, J-É., Palmer, M., Arrigo, K.R., Darnis, G., Fortier, L., Else, B., Papakyriakou, T. (2009) *Contribution of under-ice primary production to an ice-edge upwelling phytoplankton bloom in the Canadian Beaufort Sea*. Geophysical Research Letters. 36: L17601, doi:10.1029/2009GL038837.

Palmer, M.A., Arrigo, K.R., Mundy, C.J., Gosselin, M., Brunelle, C.B., Ehn, J., Rossnagel, A., Alou-Font, E., **Martin, J.**, Tremblay, J.-É., Gratton, Y. (2011) *Spatial and temporal variation of photosynthetic parameters in natural phytoplankton assemblages in the Beaufort Sea, Canadian Arctic*. Polar Biology. 34: doi: 10.1007/s00300-011-1050-x

Tremblay, J.-É., Bélanger, S., Barber, D.G., Asplin, M., **Martin, J.**, et al. (2011) *Climate forcing multiplies biological productivity in the coastal Arctic Ocean*, Geophysical Research Letters. 38: L18604, doi:10.1029/2011GL048825.

Forest, A., Tremblay, J.É., Gratton, Y., **Martin, J**., et al. (2011) *Biogenic carbon flows through the planktonic food web of the Amundsen Gulf (Arctic Ocean): A synthesis of field measurements and inverse modeling analyses.* Progress in Oceanography. 91: doi:10.1016/j.pocean.2011.05.002.

Blais, M., Tremblay, J.-É., Jungblut, A.D., Gagnon, J., **Martin, J.**, Thaler, M., Lovejoy, C. (2012) *Nitrogen fixation in coastal Arctic waters.* Global Biogeochemical Cycles. 26: doi:10.1029/2011GB004096.

Lapoussière, A., Michel, C., Gosselin, M., Poulin, M., **Martin, J.**, Tremblay, J.É. (2013) *Primary production and sinking export during fall in the Hudson Bay, Canada.* Continental Shelf Research. 52: 62-72.

Cette étude est une contribution scientifique au Réseau de centres d'excellence du Canada (RCE) ArcticNet, au Groupe interinstitutionnel de recherche océanographique du Québec (Québec-Océan), au projet Circumpolar Flaw Lead System Study (CFL) de l'Année Polaire Internationale (API) et à la Chaire de recherche du Canada sur la Réponse des écosystèmes marins arctiques au réchauffement climatique. Elle a été rendue possible grâce au soutien financier d'ArcticNet, du Conseil de recherches en sciences naturelles et en génie du Canada (CRSNG), du Fonds de collaboration internationale de la Fondation canadienne pour l'innovation et du Fonds québécois de la recherche sur la nature et les technologies (FQRNT). Un soutien financier complémentaire a été apporté par le programme de formation scientifique dans le Nord (PFSN) du Ministère des Affaires Indiennes et du Nord du Canada, de Québec-Océan, de l'Université Laval et de la Fondation Gérard D. Levesque.

.

Chapitre 1 Introduction

1.1 La production primaire en milieu pélagique

En milieu pélagique, le phytoplancton, producteur primaire fondamental, transforme le carbone inorganique dissous en composés organiques suivant le processus de photosynthèse:

$$6CO_2 + 6H_2O \xrightarrow{\text{lumière}} C_6H_{12}O_6 + 6O_2$$

Les hydrates de carbone ainsi produits permettent la synthèse des lipides, des acides nucléiques et des protéines suivant l'incorporation de nutriments tels l'azote, le phosphore et le soufre. Dans le cas particulier des diatomées, l'assimilation de silicium est nécessaire à la synthèse de la frustule sur la paroi extérieure de la cellule. Ces processus font du phytoplancton la base du réseau alimentaire marin, devenant une source de carbone et d'éléments nutritifs pour les brouteurs. Ces derniers seront à leur tour consommés par les carnivores (ex. poissons et oiseaux) et ainsi de suite, jusqu'aux plus grands prédateurs. Puisqu'une perte d'au moins 75% du carbone organique se produit à chaque niveau franchi, la quantité de phytoplancton nécessaire pour soutenir la chaîne alimentaire est importante. Globalement, le phytoplancton marin représente approximativement la moitié de la production primaire planétaire (Field et al. 1998). Par ailleurs, le phytoplancton agit comme une pompe naturelle à CO_2, transformant ce gaz à effet de serre en oxygène et en matière organique particulaire. L'exportation verticale de cette matière, soit par la chute directe du phytoplancton, soit par la chute des débris associés aux brouteurs, permet de retirer le carbone des eaux de surface et favorise un flux net de CO_2 de l'atmosphère vers l'océan (Lalli et Parsons 1997). Ce mécanisme permet, lorsque la lumière et les nutriments sont en quantités suffisantes, de séquestrer une partie du CO_2 anthropogène (Lalli et Parsons 1997; Lee et Whitledge 2005). Pour les raisons susmentionnées et dans un contexte où les écosystèmes marins sont soumis à de multiples stress (ex. l'acidification, le réchauffement

de la colonne d'eau, le changement du régime de glace arctique, l'augmentation de la stratification, l'eutrophisation côtière, les changements dans la circulation océanique) il est primordial d'étudier la production primaire et ses réponses aux changements environnementaux.

1.2 Distribution de la lumière et des nutriments en milieu océanique

Malgré des émissions solaires à peu près constantes, la lumière disponible à la surface de l'océan varie grandement en fonction de l'angle du soleil (dépendant du moment de l'année et du jour ainsi que de la latitude), de la longueur du jour et des conditions météorologiques (Lalli et Parson 1997; Fig. 1.1) faisant varier l'irradiance nécessaire aux micro-organismes photosynthétiques selon la latitude et la saison. En plus de la variation spatio-temporelle, la disponibilité en lumière fluctue grandement verticalement puisqu'une décroissance exponentielle est observée avec la profondeur, décroissance dont l'intensité varie en fonction de la turbidité de la colonne d'eau (Jerlov 1976; Fig. 1.2). De ce fait, la zone où la lumière est suffisante pour permettre la photosynthèse (c.-à-d. la zone euphotique; normalement définie comme la zone où le % de la lumière de la surface disponible est supérieur à 1%), est restreinte (généralement moins d'environ 200 m) et hautement variable (Fig. 1.2).

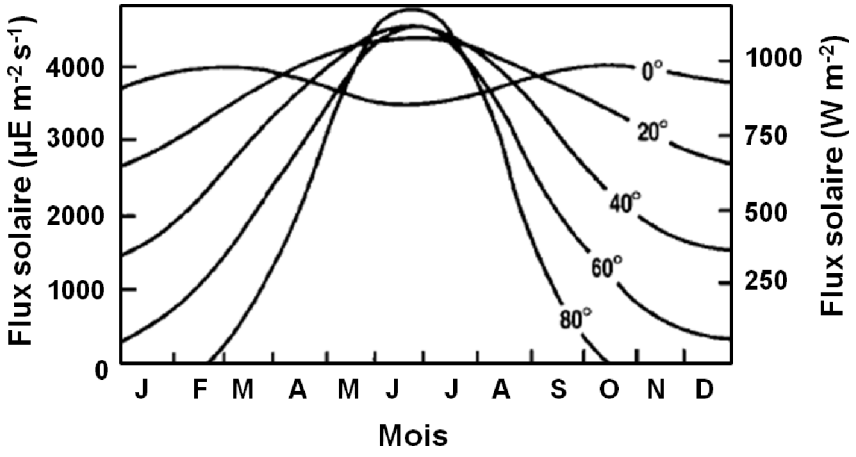

Figure 1.1 Variations du rayonnement solaire (à gauche en µE m^{-2} s^{-1} et à droite en W m^{-2}) reçu à la surface de l'océan en fonction de la latitude (ligne de contour) et du moment de l'année dans l'hémisphère nord. Adapté de Lalli et Parson 1997.

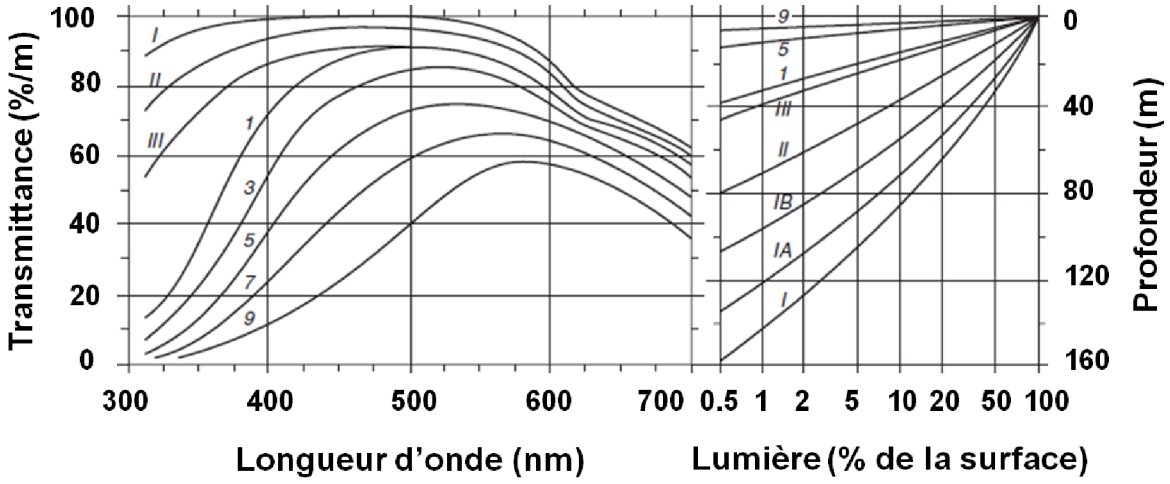

Figure 1.2 Pourcentage de la lumière transmise (transmittance en % / m) en fonction de la longueur d'onde (à gauche) et du % de la lumière (465 nm) disponible en surface (à droite) en fonction de la profondeur de la colonne d'eau pour les eaux océaniques (I à III; eaux claires à plutôt turbides) et côtières (1 à 9; turbidité croissante). Les % de la lumière disponible en surface sont présentés sur un axe logarithmique. Adapté de Jerlov 1976.

La distribution des différents nutriments nécessaires à la production primaire dans l'océan global dépend, quant à elle, d'une combinaison complexe de facteurs chimiques, biologiques et physiques. Les processus chimiques et biologiques régulent la transformation de nutriments inorganiques en nutriments organiques, mais aussi le retour des composés organiques à la forme élémentaire (reminéralisation). Les processus physiques quant à eux, redistribuent ces mêmes nutriments à travers la colonne d'eau et entre les bassins océaniques par les phénomènes de transport et de mélange (Williams et Follows 2003). À ces processus, il faut ajouter les apports extérieurs de l'atmosphère, des fleuves ainsi que la fixation de l'azote moléculaire (effectuée par les organismes diazotrophes; Gruber et Sarmiento 1997).

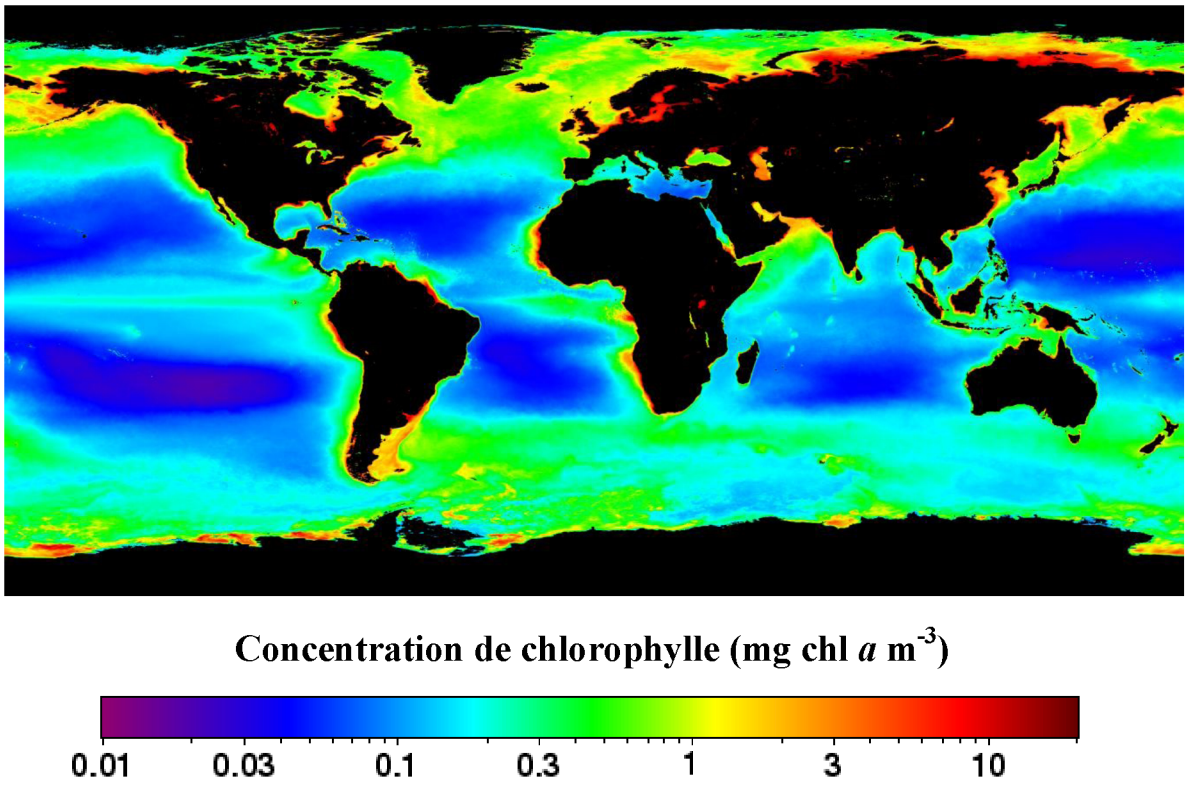

Figure 1.3 Distribution annuelle mondiale de la chlorophylle (chl *a*; mg m^{-3}) en milieu océanique. Composite satellitaire Aqua-MODIS L-3 entre juillet 2002 et décembre 2011. Résolution de 9 km. Source : http://oceancolor.gsfc.nasa.gov.

À long terme, ces processus sont équilibrés par la dénitrification et la séquestration du matériel organique dans les sédiments. La complexité de ces interactions mène à une distribution qui diffère, tant verticalement dans la colonne d'eau qu'entre les différents bassins océaniques, ce qui se traduit par une distribution hétérogène de la chlorophylle, principal indicateur de la biomasse phytoplanctonique (chl *a*; Fig. 1.3). Par exemple, en tenant compte de la circulation océanique et des processus physiques à moyenne échelle, on peut observer que dans les gyres centrales océaniques l'apport faible en nutriments provenant de l'océan profond mène à de faibles concentrations en chlorophylle dans la zone euphotique (en moyenne environ 0.2 mg chl *a* m^{-3}; Falkowski et al. 1998). Au contraire,

dans des zones de courants ascendants (ou, plus couramment appelé « upwelling » de l'anglais) induit par le vent, les régions où se produisent un mélange saisonnier (zones tempérées et boréales), les gyres subpolaires divergentes ou certaines zones de tourbillons (eddies), l'apport de nutriments en surface peut soutenir une production primaire plus importante (excédant 5 mg chl *a* m^{-3}; Falkowski et al. 1998).

1.3 Présence des maximums de chlorophylle dans l'océan mondial

Plusieurs études à travers le monde ont démontré que la distribution du phytoplancton dans les océans est hautement hétérogène tant horizontalement que verticalement. Parmi les structures verticales retrouvées, les maximums de chlorophylle subsuperficiels (SCM, de l'anglais « subsurface chlorophyll maximum » ou « deep chlorophyll maximum »; DCM) sont communs à la plupart des océans. Ces structures sont connues pour être induites par l'interaction de plusieurs mécanismes dont les apports en nutriments, la pression de broutage, la turbulence et la chute des cellules (Dolan et Marrasé 1995). On retrouve habituellement les SCM dans le milieu stratifié, lorsque la zone euphotique est plus profonde que la zone de mélange (Cullen 1982; Coon et al. 1987). La stabilité des conditions physiques et biologiques de ces milieux permet la formation de SCM en association avec la nitracline qualifié de « typical tropical structure » (TTS) par Herbland et Voituriez (1979) ce qui suggère l'importance des flux ascendants de nitrate dans la formation des SCM (Estrada et al. 1993). De cette façon, on retrouve les SCM de manière quasi permanente dans les eaux tropicales et subtropicales (Huisman et al. 2006; Mann et Lazier 2006). Dans les zones oligotrophiques des hautes latitudes, les SCM sont connus pour être sensibles aux variations saisonnières, particulièrement en Atlantique Nord où le mélange saisonnier permet de rompre la stabilité de la colonne d'eau et de renouveler les nutriments en automne et en hiver (Mann et Lazier 2006; Pommier et al. 2009).

Les SCM, lorsque biologiquement actifs, ont un impact important sur la productivité totale des écosystèmes. Ils peuvent représenter jusqu'à 90% de la biomasse retrouvée dans la colonne d'eau (Klausmeier et Litchman, 2001) et les concentrations de chlorophylle qu'on

retrouve au SCM peuvent être jusqu'à dix fois supérieures à celles de surface (Steele 1964; Anderson, 1969; Sharple et al. 2011).

En milieu océanique, le phytoplancton est limité en nutriments et principalement en azote (voir section 1.2). Puisque l'azote disponible se retrouve principalement en profondeur (près de la nitracline), les espèces favorisées sont celles avec les besoins en lumière sont les plus faibles. Généralement, une à quelques espèces contribuent à la plus grande partie de la biomasse des SCM (Coon et al. 1987; Huszar et al. 2003). En milieu extrêmement oligotrophique, les espèces fixatrices d'azote (par exemple, les cyanobactéries) sont de plus avantagées. Dans les zones tempérées comme en Atlantique Nord, le mélange annuel permet un rebrassage des éléments nutritifs dans la couche de mélange. Ce phénomène, jumelé à l'influence des changements d'intensité lumineuse, engendre une succession des espèces au SCM (Mann et Lazier 200; Pommier et al. 2009). Lorsque le milieu est riche en nutriments, on observe une dominance des diatomées, organismes ayant un taux de croissance rapide, qui mène à l'épuisement des concentrations de silice, composante essentielle de leurs frustules. Par la suite, la dominance passe, le plus souvent, aux prymnésiophycées, petites cellules flagellées pouvant utiliser le phosphate et le nitrate restant dans la colonne d'eau. Parallèlement, les stocks d'ultraplancton (aussi appelé picoplancton) soutiendront une plus petite partie de la production primaire, mais de façon plus constante. Ce phénomène est d'ailleurs observable un peu partout dans les océans (Miller 2004).

1.4 Utilisation de l'azote et production nouvelle versus régénérée

Puisque la majeure partie de l'azote se retrouve dans l'océan profond, isolé de la surface, la disponibilité en azote est connue pour limiter la production primaire pélagique dans plusieurs régions océaniques (DeVries et al. 2012). De ce fait, l'azote disponible dans les eaux de surface est grandement dépendant des apports ascendants dû à l'advection et à la diffusion du nitrate (Fig. 1.4, processus D) ou aux upwellings. Dans les eaux de surface, ce nitrate, une fois assimilé par le phytoplancton (transformé en azote organique particulaire; AOP), sera vraisemblablement recyclé en ammonium et en azote organique dissout (AOD)

par les hétérotrophes ou par la décomposition des cellules (Fig. 1.4, processus A et B; Zehr et Ward 2002). Parallèlement, une partie de l'AOP sera retirée des eaux de surface dû à la sédimentation (en milieu côtier; Fig. 1.4-I) ou enfoui puis nitrifié en eaux profondes (Fig. 1.4-IV). De leur côté, la fixation de l'azote gazeux (Fig. 1.4, processus C; possiblement limitée par les micronutriments, tels le molybdène et le fer, la destruction des zones anoxiques par la turbulence et la disponibilité de la lumière pour les cyanobactéries) ainsi que les apports en azote des rivières (dont l'effet est limité aux zones côtières; Fig. 1.4) sont des sources nettes d'azote pour le milieu. Cependant, leur effet sur la limitation en azote dans les eaux de surfaces est restreint puisque ces processus seraient insuffisants pour balancer les pertes d'azote fixé dues à la dénitrification et à l'oxydation anaérobique de l'ammonium (Fig. 1.4, processus E; DeVries et al. 2012).

Alimentée par l'azote allochtone (par exemple, le flux de nitrate ascendant qui résulte des processus de turbulence et/ou de diffusion, la fixation de l'azote gazeux, les apports par les fleuves ou les précipitations), la production nouvelle est dépendante des échanges avec l'atmosphère, du mélange et des processus d'advection verticale et horizontale associés à la circulation océanique (Eppley et Peterson 1979). À l'échelle locale, il a été démontré que la production régénérée (dépendante de l'azote recyclé *in situ* par les organismes hétérotrophes sous forme d'ammonium, d'urée ou de nitrite) peut représenter une partie non-négligeable de la production totale et même excéder la production nouvelle, par exemple lorsque la température augmente et favorise l'activité microbienne (Sambrotto et Mace 2000). Néanmoins, même si la production régénérée joue un rôle important lorsque les apports d'azote allochtone sont faibles, c'est la production nouvelle, additionnée à la pompe à solubilité, qui régule le transport de carbone biogénique vers l'océan profond. De plus, c'est aussi cette dernière qui empêche la production totale de décliner à cause des pertes d'azote hors du système semi-fermé qu'est la régénération évitant au système de s'épuiser (Dugdale et Goering 1967; Eppley et Peterson 1979).

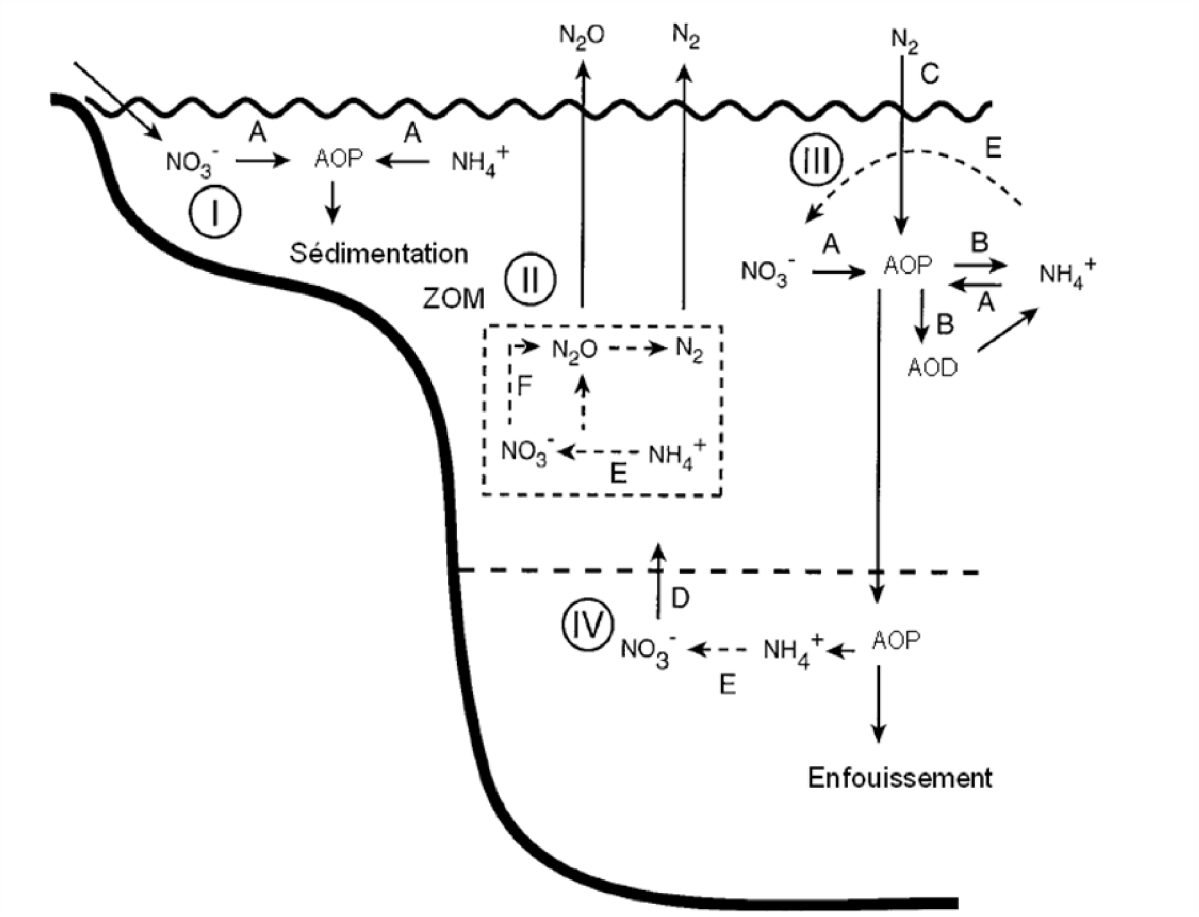

Figure 1.4 Schématisation des principaux processus du cycle de l'azote en milieu océanique pour différentes régions: (I) les zones côtières et d'upwelling, (II) la zone d'oxygène minimum (ZOM), (III) les eaux de surface et (IV) l'océan profond. L'azote organique particulaire et dissout sont respectivement représentés par AOP et AOD. Le nitrate (NO_3^-), l'ammonium (NH_4^+), l'oxyde nitreux (N_2O) et le diazote (N_2) sont présentés en tant que formes d'azote inorganique dissoutes (AID). Les flèches désignent les différents processus, soit l'assimilation de l'AID (A), la régénération de l'ammonium (B), la fixation de l'azote (C), la diffusion ou l'advection (D), la nitrification (E) et la dénitrification (F). Les lignes pointillées donnent les transformations nécessitant des étapes multiples. Adapté de Zehr et Ward 2002.

Il a été démontré que, lorsque présentes en quantité suffisante, les formes réduites d'azote (exemple l'ammonium et l'urée) sont préférées au nitrate (forme oxydée) puisque leur assimilation est énergétiquement plus favorable (Behrenfeld et al. 2008). Cependant, les différentes formes d'azote sont utilisées de façon proportionnelle à leur disponibilité lorsque la quantité d'azote totale devient moindre que la quantité requise pour soutenir la demande du phytoplancton (McCarthy et al. 1977; Harrison et al. 1982; Cochlan 1986).

La prise d'azote en milieu océanique n'étant pas nécessairement constitutive (ou assimilative, c'est-à-dire menant à la synthèse d'acides aminés), la production primaire phytoplanctonique peut se trouver partiellement découplée de la prise d'azote à court terme (Smith et Harrison 1991). Ce découplage peut être dû à des processus non-photosynthétiques comme la prise de luxe (alors que le nitrate peut être emmagasiné dans la cellule pour être assimilé lorsque les conditions lumineuses deviennent favorables ou relâché sous forme de nitrite après une réduction incomplète), à la prise bactérienne (Gilbert et al. 1982) ou à des différences de l'acclimatation à la lumière de la prise de carbone et d'azote (plus grande capacité à assimiler l'azote que le carbone dans le noir ou aux faibles intensités lumineuses; Smith et Harrison 1991; Probyn et al. 1996). Au noir, le transport de l'azote inorganique provient également potentiellement des processus de photosynthèse résiduelle (c'est-à-dire que l'azote peut être assimilé à partir d'un excès d'énergie accumulée par la cellule lors de son exposition à la lumière; le plus souvent aux hautes intensités lumineuses). Combinés, ces différents processus font en sorte que la prise au noir d'azote peut représenter une part significative de la prise d'azote totale et peut même être responsables de près de la moitié de la prise de nitrate et d'ammonium (Priscu 1989; Price et al. 1985; Cochlan et al. 1991).

1.5 Conditions de croissance du phytoplancton en Arctique

Dans l'océan Arctique, les conditions de croissance du phytoplancton sont particulièrement variables et souvent contraignantes. Le cycle solaire extrême (nuit polaire et soleil de minuit), la banquise permanente ainsi que la formation, la fonte et la dérive des glaces saisonnières exercent une influence majeure sur l'apport de lumière dans la colonne d'eau. Ces phénomènes limitent généralement la production primaire à quelques mois durant l'été

(Sakshaug 2004) et soumettent le phytoplancton à des fluctuations lumineuses extrêmes. De plus, dans cette région du monde, de faibles températures sont rencontrées tout au long de l'année sans toutefois que le phytoplancton ne démontre d'adaptation spécifique à cette condition (Platt et al. 1982; Smith et Harrison 1991), ce qui peut aussi potentiellement limiter la production primaire annuelle. De par sa position géographique et sa taille modeste, l'Arctique est fortement influencé par les rivières affluentes et les eaux de l'Atlantique et du Pacifique nord (Stein et Macdonald 2004). Ces masses d'eau ont des teneurs variables en nutriments lorsqu'elles pénètrent dans l'Arctique (Tremblay et al. 2002; Jones et al. 2003). Leur lente propagation fait en sorte que, durant le premier été, le phytoplancton épuise rapidement les nutriments dans la couche de surface. Le renouvellement des nutriments dans cette zone est ensuite limité par la forte stratification verticale due à l'eau douce des rivières, l'eau peu salée du Pacifique et la fonte des glaces saisonnières. Durant l'hiver, le couvert de glace limite le mélange éolien de sorte que le brassage vertical annuel observé dans d'autres océans est peu présent. La situation est différente en marge des grands plateaux continentaux peu profonds, où les upwellings induits par le vent peuvent renouveler les nutriments lorsque la glace se retire durant l'été (Tremblay et al. 2011). Afin de palier à ces conditions de croissance particulières, le phytoplancton arctique doit trouver un compromis entre la limitation en lumière (à la surface) et la limitation en nutriments (provenant des eaux profondes), ce qui conduit souvent à la formation de SCM.

1.6 Impact des changements climatiques sur la production primaire arctique

Depuis les années 90, on admet que les changements majeurs dans la configuration du couvert de glace arctique sont imputables à un réchauffement rapide du climat (ACIA 2005). Une réduction de 11.5% par décennie de la partie recouverte de glace (minimum estival) a été notée entre 1978 et 2010, alors que de 2007 à 2011 ont été répertoriés comme étant les 5 années records de minimum de glace. Il a aussi été observé qu'une grande partie de la glace pluriannuelle a été remplacée par de la glace saisonnière et que l'épaisseur générale de cette glace a diminué d'environ 1.75 m entre 1980 et 2008 (NSIDC 2011). Jumelé à la diminution de la durée de la saison des glaces, ces phénomènes mènent à

estimer que la glace estivale disparaîtrait en Arctique entre 2040 et 2100 (Serreze et al. 2007).

En altérant l'environnement nutritif et lumineux du phytoplancton, ces changements pourraient conduire à des floraisons précoces, modifier l'intensité de la production primaire annuelle et perturber les réseaux alimentaires et les cycles biogéochimiques. Une compilation des données de la chlorophylle estimées par télédétection dans différentes régions océaniques a mené à l'observation d'un déclin global de la moyenne du phytoplancton (dérivée des estimations de chlorophylle) de 1% par année (Boyce et al. 2010). Ces auteurs attribuent le phénomène à une augmentation de la température de surface et indirectement à une augmentation de la stratification, qui entraine une diminution de l'épaisseur de la couche de mélange et limite les apports de nutriments en surface. Cependant, ce mécanisme ne semble pas être la cause du déclin également observé en Arctique, où une corrélation positive est observée avec la température de surface. Ce phénomène pourrait être partiellement expliqué par l'augmentation de l'épaisseur de la couche de mélange ou de l'intensité des vents, mais une étude plus approfondie de cette région doit être effectuée afin de mieux comprendre les processus océanographiques qui y contrôlent le phytoplancton (Boyce et al. 2010). Une compilation de la littérature antérieure à 1998 suggère qu'une prolongation de la période libre de glace pourrait, en augmentant l'exposition du phytoplancton à la lumière, conduire à une augmentation proportionnelle de la production primaire annuelle (Rysgaard et al. 1999). Or, des études plus récentes suggèrent que la production primaire est plutôt limitée par les nutriments une fois les eaux affranchies du couvert de glace (Tremblay et Gagnon 2009). Dans les régions où la stratification est particulièrement forte et la couche de mélange peu profonde (ex. la baie d'Hudson, la mer de Beaufort), le renouvellement annuel des nutriments en surface est faible. Il pourrait toutefois y avoir suffisamment de lumière sous la mince couche de mélange pour permettre au phytoplancton d'exploiter le réservoir profond de nutriments. Dans un contexte de changements climatiques, la réduction du couvert de glace et l'augmentation du débit des fleuves pourraient causer le renforcement de la stratification et un amincissement de la couche de mélange (Peterson et al. 2002, IPCC 2001). De cette façon, l'essentiel de la production primaire s'effectuerait sous la couche de mélange dans

les SCM. Cependant, en présence de vents forts, l'upwelling et le mélange vertical épisodique pourraient être stimulés et provoquer des augmentations occasionnelles de la production primaire près de la surface (Carmack et Chapman 2003; Yang et al. 2004; Tremblay et al. 2011). Nos connaissances actuelles de l'écologie nutritive et photosynthétique ainsi que la répartition verticale de la production primaire étant nettement insuffisantes, un pronostique éclairé ne pourra être posé qu'après une étude approfondie.

1.7 Intensité et répartition verticale de la production primaire dans l'Arctique

Bien que l'océan Arctique demeure relativement peu étudié pour cause de contrainte logistique, il est possible de tracer une esquisse de la production primaire grâce à certains travaux récents (Fig. 1.5). Or, ces derniers présentent les résultats de façons différentes. Parfois exprimée en termes de flux (mg C m^{-2} j^{-1}) et parfois en termes de biomasse (mg chl *a* m^{-3}), la production imputable au phytoplancton n'est pas toujours comparable entre les différentes études et régions. Il ressort néanmoins que les SCM sont observés presque systématiquement dans la colonne d'eau (Tableau 1.1), SCM dont la profondeur et l'intensité semblent varier selon la topographie, la saison et la stratification verticale. Les mers côtières et leurs marges, étant sujettes au mélange et à l'upwelling, sont riches en éléments nutritifs limitant et, par le fait même, possèdent des SCM relativement peu profonds. Les différents bassins formant le centre de l'océan Arctique voient leur productivité diminuée par deux principaux facteurs : un fort pourcentage de surface recouverte de glace (peu de lumière) et un rebrassage annuel très limité des éléments nutritifs. Ces faits réunis en font des endroits peu propices à la croissance du phytoplancton, mais possédant tout de même des SCM et une production maximale appréciable.

Les SCM existent dans d'autres océans, comme dans les gyres subtropicales (Huisman et al. 2006), mais sont rarement aussi fréquents et intenses que dans l'Arctique. En Atlantique-Nord par exemple, on note une absence de stratification au printemps, cette dernière se développant tranquillement, à environ 50 mètres, au cours de l'été avec l'aide du rayonnement solaire menant à la formation d'un SCM temporaire (Mann et Lazier 2006).

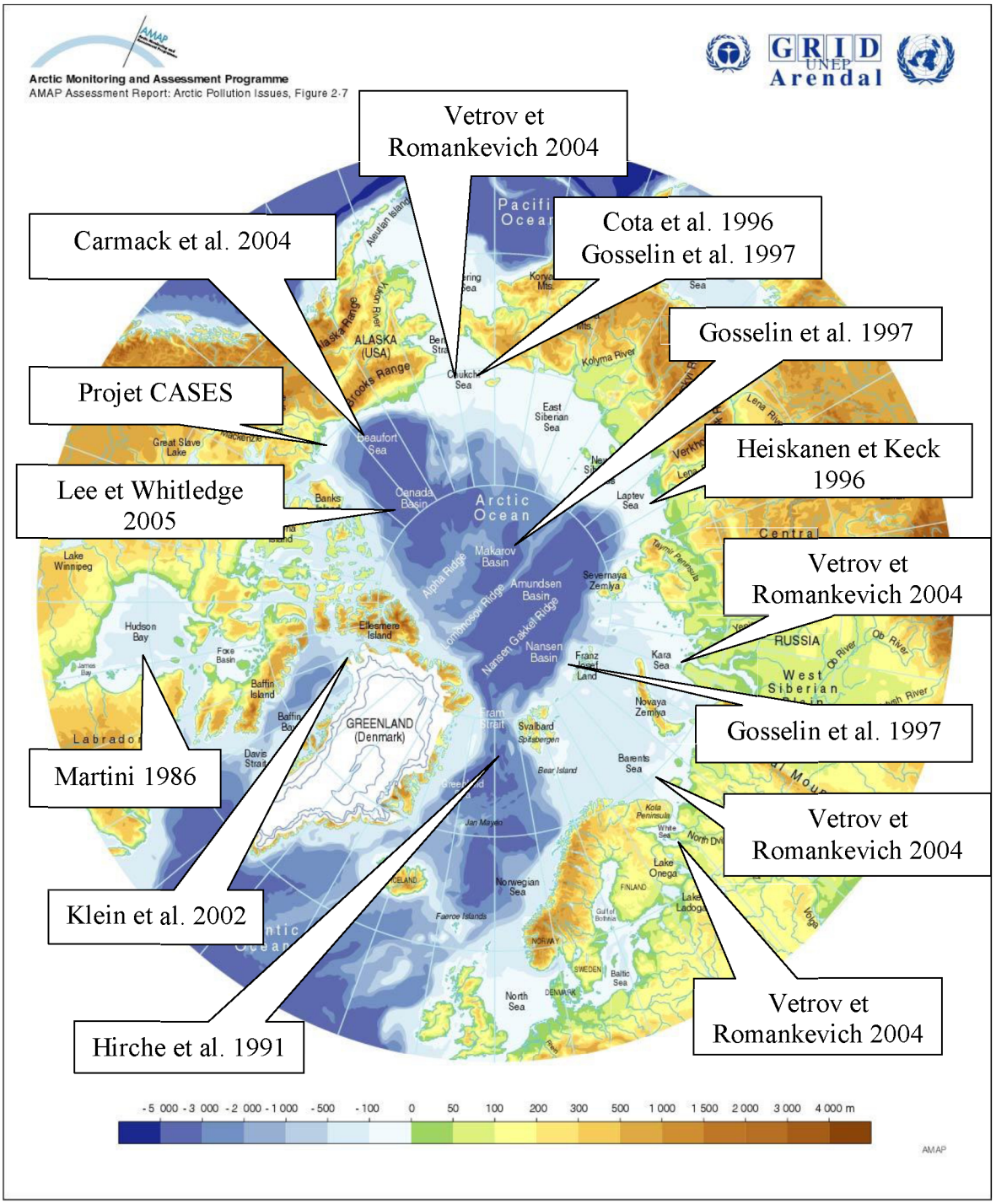

Figure 1.5 Publications antérieures à la présente étude portant sur la production primaire et faisant état de SCM dans l'océan Arctique.

Tableau 1.1 Synthèse des principales études portant sur la production primaire dans l'océan Arctique et publiées avant le début des travaux de cette thèse.

Localisation	Flux (mg C m^{-2} j^{-1})	Biomasse (mg chl *a* m^{-3})	Profondeur des SCM (m)	Publication
Mers côtières				
Baie d'Hudson	--	0.3-11	35-45	Martini, 1986
Golfe d'Amundsen	--	0.2-35	30-45	Projet CASES*
Mer de Baffin (nord)	--	1.4-19	0-35	Klein et al. 2002
Mer de Beaufort	10-200	--	20-50	Carmack et al. 2004
Mer Blanche	46	0.07-1.36	5-20	Vetrov et Romankevich, 2004
Mer de Barents	--	0.09-10	5-25	Vetrov et Romankevich, 2004
Mer de Kara	43	--	20-30	Vetrov et Romankevich, 2004
Mer de Laptev	--	5.8	30	Heiskanen et Keck, 1996
Mer de Chukchi (sud)	200-500	--	5, 10 et 15	Vetrov et Romankevich, 2004
Mer de Chukchi (centre)	162-445	0.1-1.0	30-40	Cota et al. 1996 Gosselin et al. 1997
Detroit de Fram	181.9-626.7	--	20, 30 et 50	Hirche et al. 1991
Zones profondes				
Basin du Canada	--	0.6	50-60	Lee et Whitledge, 2005
Basin de Marakov	1-27	--	20-85	Gosselin et al. 1997
Basin de Nansen	62	--	20-85	Gosselin et al. 1997

*** données non-publiées**

1.8 Présence des SCM en Arctique canadien

Bien que la présence de SCM soit notée dans la plupart des études portant sur le phytoplancton arctique, il s'agit d'observations ponctuelles dont le traitement est anecdotique. On ignore presque tout de la dynamique de production des algues constituantes ainsi que des mécanismes conduisant à leur formation et leur maintenance. Contrairement aux océans fortement mélangés où les floraisons ont d'abord lieu sur quelques dizaines de mètres en surface, une grande partie des floraisons arctiques semblent se dérouler dans une fine couche profonde qui pourrait constituer l'essentiel du carbone disponible pour le réseau alimentaire et l'exportation vers le fond. Des données obtenues durant le programme CASES suggèrent que les SCM se forment durant la débâcle des glaces et persistent tout l'été dans le sud-est de la mer de Beaufort (Fig. 1.6; Tremblay et al. 2008). On peut donc émettre l'hypothèse que le largage des algues de glace joue un rôle dans la formation initiale du SCM. Par ailleurs, de tels SCM sont susceptibles de ne pas contribuer à la pompe à CO_2, puisque leur photosynthèse est possiblement alimentée par les apports ascendants de carbone inorganique profond sans lien avec l'atmosphère. De par la nature hautement variable et dynamique de l'écosystème, estimer la production annuelle n'est pas aisée en Arctique. L'acquisition de séries temporelles de profils verticaux de la production primaire demande une logistique lourde. Les SCM arctiques, possiblement isolés de la surface par la forte stratification ou masqués par la présence de glace, pourraient aussi causer une sous-évaluation de la quantité de chlorophylle par télédétection puisque les observations satellitaires sont limitées à la couche de surface. Il est donc nécessaire d'échantillonner la colonne d'eau pour estimer la production primaire, en comprendre la dynamique et valider les modèles.

La plupart des études publiées rapportent des valeurs de chlorophylle à quelques profondeurs discrètes, sans égard à la structure détaillée des profils. Ainsi, il est probable que la valeur maximum rapportée soit moindre que le maximum réel et que le profil établi ne rende pas compte de la dispersion de la biomasse de part et d'autre du maximum. On ignore encore ce qui en détermine la profondeur, la structure, la biomasse, la productivité et la persistance. Est-ce qu'il s'agit d'algues performantes acclimatées aux conditions *in situ* ou d'algues peu productives en mauvais état physiologique (produites près de la surface ou

à la base de la glace pour ensuite chuter et s'accumuler passivement à la pycnocline)? Est-ce que le SCM représente aussi un maximum de biomasse ou est-ce le reflet de phénomènes physiologiques à l'intérieur des cellules phytoplanctoniques? Quelle est l'écologie nutritive de ces algues? Les algues du SCM dépendent-elles principalement de l'apport d'azote nouveau (nitrate injecté par mélange turbulent ou diffusion) ou recyclé *in situ* par l'activité des hétérotrophes? Dans quelle mesure la photosynthèse de ces algues est-elle limitée en lumière et en nutriments? Le rejet de nitrate sous forme de nitrite après une réduction incomplète des algues est-il responsables de la formation du maximum principal de nitrite dans la colonne d'eau? Est-il possible d'estimer la biomasse totale de la colonne d'eau en fonction de la chlorophylle de surface? Peut-on estimer et éventuellement prévoir la contribution des SCM à la production primaire totale (télédétection, modélisation)? Quel serait l'effet des changements climatiques sur l'intensité et la répartition verticale de la production primaire dans l'Arctique?

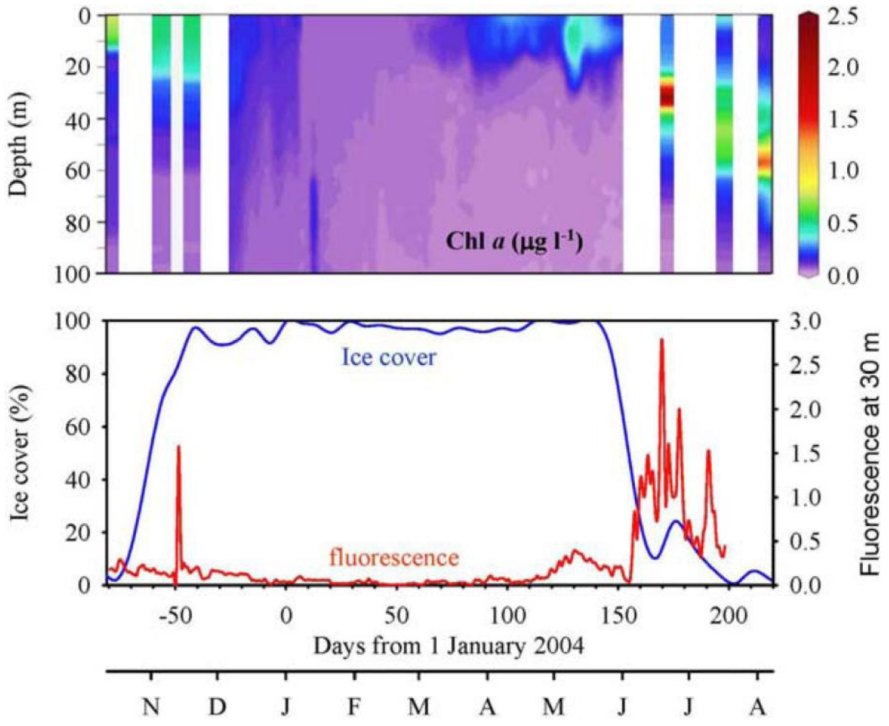

Figure 1.6 Série temporelle de la chlorophylle (chl *a*; en µg l^{-1} ou mg m^{-3}) en fonction de la profondeur (depth) ainsi que la fluorescence à une profondeur fixe de 30 m (ligne rouge : unité relative) et du pourcentage de couvert de glace en surface (ice cover; en bleu) en 2003-2004 dans la Baie de Franklin (sud-est de la mer de Beaufort). Tiré de Tremblay et al. 2008.

1.9 Objectifs spécifiques

Dans l'optique de répondre aux questions susmentionnées, les trois objectifs principaux de la présente étude sont (1) d'établir la quantité et la répartition verticale de la chlorophylle en fonction des conditions océanographiques physiques et chimiques dans les différentes régions de l'Arctique canadien, (2) d'évaluer de manière expérimentale les relations entre la lumière, les nutriments et la productivité au SCM et (3) de modéliser la production primaire en tenant compte de la contribution des SCM. Pour ce faire, plusieurs missions en mer ont été menées à bord du brise-glace NGCC *Amundsen* entre 2005 et 2008 (16 août – 16 octobre 2005, 4 septembre – 4 novembre 2006, 28 septembre – 6 novembre 2007 et 26 avril – 13 juillet 2008) lors des programmes scientifiques d'ArcticNet et de CFL. Ces missions ont permis l'étude d'un grand éventail de conditions océanographiques (Fig. 1.7) en couvrant la baie de Baffin (75.273 °N à 79.002 °N; 71.338 °O à 77.382 °O), le passage du Nord-Ouest (68.998 °N à 74.047 °N; 79.894 °O à 106.593 °O), la mer de Beaufort (69.091 °N à 71.564 °N; 114.805 °O à 139.992 °O), le bassin de Foxe (64.120 °N à 69.319 °N; 78.871 °O à 80.998 °O) et la baie d'Hudson (69.091 °N à 71.564 °N; 114.805 °O à 139.992 °O) ainsi que trois fjords du Labrador (56.397 °N à 59.092 °N; 61.217 °O à 63.826 °O). Les sites d'échantillonnage et d'expérimentation incluaient des régions encore recouvertes de glace (Passage), des régions où la glace était récemment disparue par fonte ou mouvement et des régions particulières où les eaux étaient libres de glace depuis plusieurs mois (polynie des Eaux-du-Nord et polynie du Cap Bathurst). La visite de ces sites a été effectuée à différents moments de l'année afin de pouvoir étudier l'effet des variations saisonnières sur les phénomènes étudiés (Fig. 1.8). Sur un total de 983 CTD, 265 stations ont été échantillonnées au cours des différentes expéditions et les paramètres photosynthétiques ont été estimés à 59 de ces stations (Fig. 1.7).

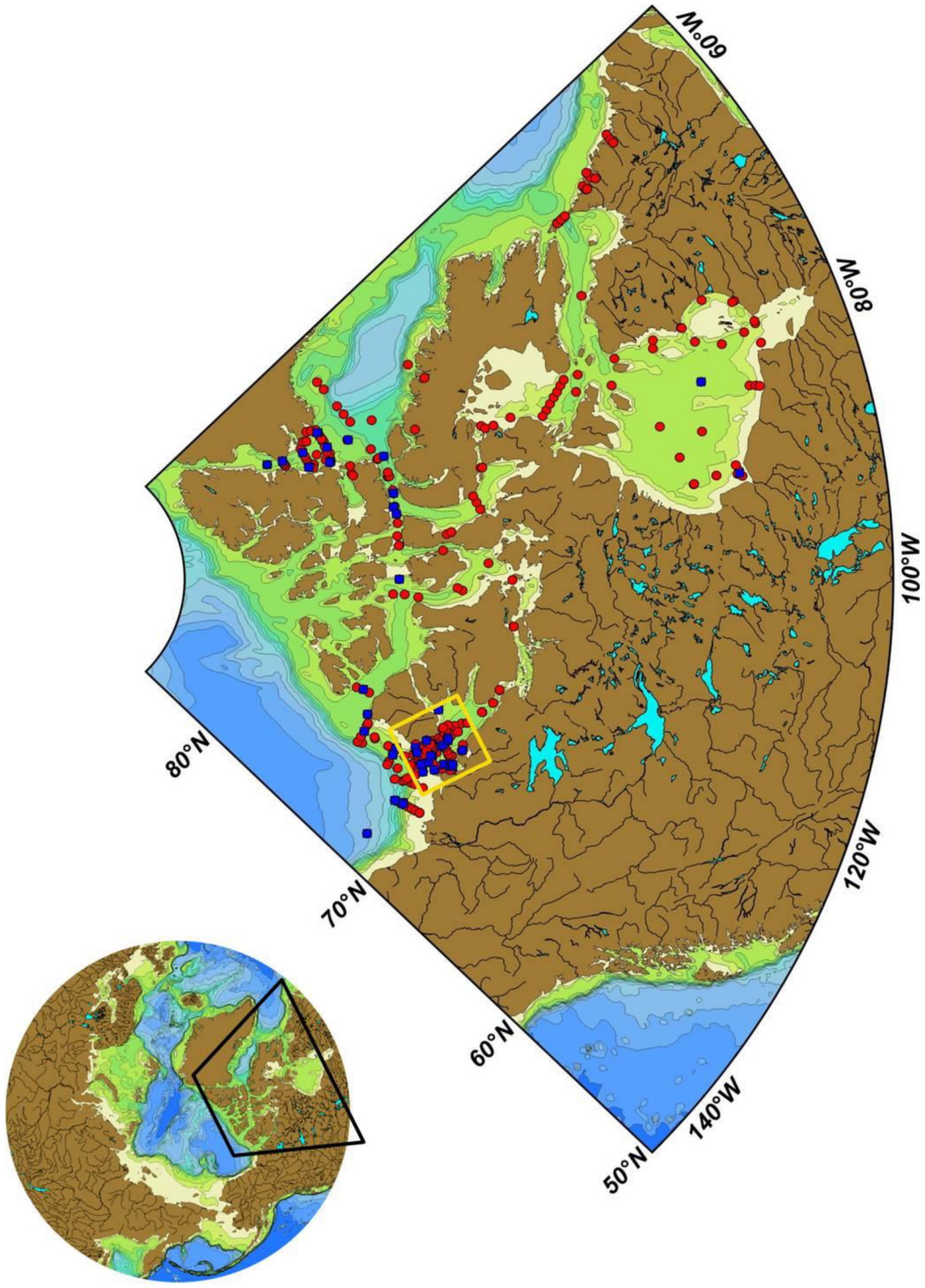

Figure 1.7 Emplacement de toutes les stations échantillonnées entre 2005 et 2008 (cercles rouges) et de celles où les paramètres photosynthétiques ont été estimés (carrés bleus). L'encadré jaune représente la zone sélectionnée pour l'étude de modélisation.

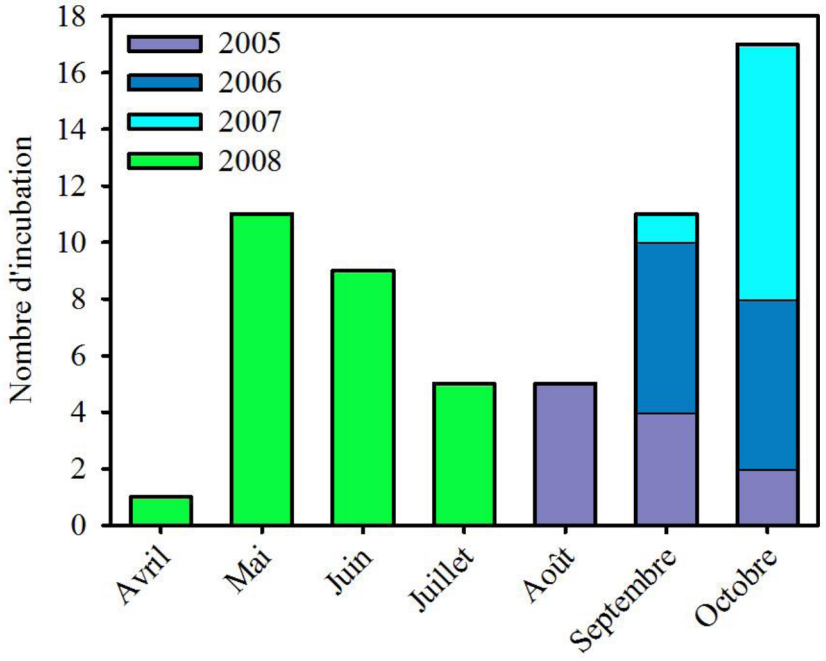

Figure 1.8 Répartition temporelle des stations où les paramètres photosynthétiques ont été estimés entre 2005 et 2008.

Le noyau scientifique de la thèse est donc divisé en trois chapitres qui reflètent les objectifs visés. Le premier chapitre s'intéresse à la distribution, la formation, la structure et la persistance des SCM dans les différentes régions de l'Arctique canadien. Pour ce faire, les caractéristiques intrinsèques des SCM (profondeur, intensité, compétences photosynthétiques) ont été comparées aux propriétés physiques et biochimiques de la colonne d'eau (ex. la stratification, la distribution des macronutriments, la disponibilité de la lumière). Le second chapitre a pour thème l'écologie nutritive et photosynthétique des algues recueillies aux SCM et, à des fins comparatives, dans la couche de mélange. Les mesures de prise simultanée de carbone et d'azote par le phytoplancton présentées dans ce chapitre facilitent la compréhension des phénomènes de formation et de maintien des structures observées au chapitre 1. De plus, ces données permettent de caractériser les stratégies d'acclimatation du phytoplancton ainsi que de faire la distinction entre la

production nouvelle et la production régénérée dans la colonne d'eau. Les résultats des deux premiers chapitres permettent d'encadrer le troisième objectif. Puisque toutes les conditions océanographiques ne peuvent être reproduites *in vitro*, une approche numérique peut s'avérer précieuse pour quantifier la production primaire et la réponse aux différents paramètres physiques et biologiques. Le troisième chapitre est donc consacré à la modélisation de la production primaire annuelle, en portant une attention particulière à la contribution des SCM à cette production. L'évolution des SCM et de la production nouvelle *versus* régénérée au cours d'une saison de croissance a ainsi pu être simulée et comparée avec des données de terrain. Le modèle permet aussi de donner des indications sur l'implication des modifications de la dynamique de la physique de la colonne d'eau en Arctique canadien sur la productivité des échelons inférieurs des réseaux alimentaires dans un contexte de changements climatiques.

Chapitre 2 Prevalence, structure and properties of subsurface chlorophyll maxima in Canadian Arctic waters

2.1 Résumé

Une étude approfondie des eaux libres de glace à la fin de l'été et au début de l'automne dans l'Arctique canadien a révélé la quasi omniprésence de maximums de chlorophylle subsuperficiels (SCM) persistants. La correspondance entre la position verticale du SCM et celle du maximum de biomasse suggère que ce dernier constitue une source importante de carbone pour le réseau alimentaire. La plupart des SCM étaient associés à la nitracline, ce qui indique que leur position verticale serait principalement déterminée par un manque d'azote inorganique dans la partie supérieure de la couche euphotique. Les rendements photosynthétiques élevés (F_v/F_m) tant à la surface qu'au SCM démontrent que le phytoplancton était photosynthétiquement compétent et bien acclimaté aux différentes conditions de disponibilité en lumière et en nutriments sur l'ensemble de la zone euphotique. La diversité de configuration verticale des SCM complique l'estimation de la chlorophylle et de la production primaire dans la couche euphotique à partir des propriétés de surface. Cette étude démontre que les SCM sont des structures dominantes qui devraient être prises en compte lors d'études de télédétection et de modélisation biogéochimique dans l'océan Arctique.

2.2 Abstract

Comprehensive investigations of the Canadian Arctic during late summer and early fall revealed the widespread occurrence of long-lived subsurface chlorophyll maxima (SCM) in seasonally ice-free waters. The vertical position of the SCM corresponded with the depth of the subsurface biomass maximum (SBM) suggesting that SCM could be an important source of carbon for the food web. Most of these SCM were in close association with the nitracline, implying that their vertical position was driven mainly by a shortage of inorganic nitrogen in the upper euphotic zone. The diversity of SCM configurations complicates the estimation of euphotic-zone chlorophyll and primary production from surface properties. High photosynthetic yields (F_v/F_m) showed the phytoplankton to be photosynthetically competent and well acclimated to conditions of irradiance and nutrient supply near the surface and at the SCM. This study demonstrates that the SCM, once regarded as anecdotal due to under-sampling, are a dominant feature of the Arctic Ocean that should be considered in remote sensing studies and biogeochemical models.

2.3 Introduction

The spatial distribution of marine phytoplankton is highly heterogeneous. On the vertical, subsurface maxima of chlorophyll (SCM) or biomass (SBM) are common under stratified conditions (Cullen 1982; Coon et al. 1987). Their vertical position is regarded as a compromise between nutrient limitation near the surface and light limitation at depth: a situation that should favor shade-adapted phytoplankton species with the lowest requirements for light (i.e. compensation irradiance; Huisman et al. 2006). The SCM have been found to harbor up to an order of magnitude the concentration of chlorophyll *a* (chl *a*) found at the surface (Steele 1964; Anderson 1969; Klausmeier and Litchman 2001; Sharples et al. 2001). Their existence poses a challenge to the remote-sensing estimation of primary production (e.g. Uitz et al. 2006).

Phytoplankton biomass at a given depth is the net result of local production, death by lysis or grazing and the gains and losses imparted by passive or active motion of the cells (e.g. Dolan and Marrasé 1995; Klausmeier and Litchman 2001; Fennel and Boss 2003; Hodges and Rudnick 2004; Holm-Hansen and Hewes 2004; Huisman et al. 2006; Beckmann and Hense 2007; Sharples et al. 2007). Vertical decoupling of the SBM and SCM is not rare and has been ascribed to photoacclimation, whereby the ratio of chl *a* to carbon increases with depth to optimize light harvesting (Steele 1964; Kiefer et al. 1976; Cullen 1982; Falkowski and Kiefer 1985; Fennel and Boss 2003). Most observational studies investigate only the SCM with high-resolution profiling of chlorophyll fluorescence and ignore the SBM since the visual estimation of biomass from microscopic enumeration and sizing of phytoplankton is tedious, and discrete sampling may miss the SBM altogether. Transmissometers can be used to pinpoint the SBM in clear waters where particulate beam attenuation (c_p) in the red part of the light spectrum is strongly influenced by microbial organisms (Chung et al. 1998), but the procedure is unreliable under the influence of river discharge or sediment resuspension in coastal waters.

SCM are persistent in perennially stratified tropical and subtropical waters (Huisman et al. 2006; Mann and Lazier 2006) and seasonal at high latitudes in the Southern Ocean (Holm-Hansen and Hewes 2004) and the boreal North Atlantic, where the extensive mixing of the water column during fall and winter replenishes the surface with nutrients (Mann and

Lazier 2006). This phenomenon permits the development of a spring bloom in the upper euphotic zone and a seasonal succession whereby a transient SCM community replaces the fast-growing bloomers once nutrients are exhausted from the surface (Mann and Lazier 2006; Pommier et al. 2009). In the High Arctic, the seasonal ice cover and extreme solar cycle restrict the productive period to a few months (Sakshaug 2004). Unlike the North Atlantic, the periodic renewal of nutrients in the upper euphotic zone is often tempered by the ice cover and the strong vertical stability imparted by seasonal melt and the horizontal inputs of freshwater from large rivers and low-salinity water from the Pacific Ocean (Jones et al. 2003; Stein and Macdonald 2004; Tremblay et al. 2008).

In the Beaufort Sea, convection and winds have a minor disrupting effect on stratification during fall and winter (Tremblay et al. 2008). Exceptions to this pattern are found in productive polynyas (e.g. the North Water; Tremblay et al. 2002) and along the margin of shallow continental shelves when upwelling-favorable winds blow under conditions of reduced ice cover (Williams and Carmack 2008). The low initial inventories of nitrate in the surface mixed layer are readily used in spring, which rapidly induces nitrogen limitation above the nutricline (e.g. Franklin Bay; Tremblay et al. 2008). The SCM form within days of the ice break-up and persist throughout summer, mediating a large portion of the annual nitrate drawdown. Despite their implications for food webs, biogeochemical fluxes and the accuracy of remote sensing estimates of primary production, SCM have only been briefly mentioned in observational studies of subarctic and Arctic primary production (e.g. Martini 1986; Hirche et al. 1991; Cota et al. 1996; Heiskanen and Keck 1996; Lee and Whitledge 2005), and their overall function, structure and significance have not been assessed.

Here we report on the large-scale incidence and properties of SCM in the Canadian High Arctic, the subarctic Hudson Bay and a few Labrador fjords. Surveys were conducted during late summer and early fall to ensure that all regions had lost their seasonal ice cover and the pelagic growth season was underway. Our working hypothesis is that SCM are photosynthetically competent and associated with favorable conditions of allochthonous nitrate supply, not merely a change in chl *a* content per unit of carbon. This hypothesis is validated here by a near-synoptic comparison of intrinsic SCM characteristics (i.e. vertical position, chl *a* concentration, taxonomic composition and photosynthetic competency) with

the physical structure of the water column and the vertical distribution of oxygen and macronutrients in contrasted environments. A second objective was to assess if the inventory of chl *a* in the euphotic zone can be predicted from surface values in the context of remote sensing.

2.4 Materials and methods

2.4.1 Sampling

The 2005 (16 August to 16 October) and 2006 (4 September to 4 November) expeditions of the CCGS Amundsen, covered the entire latitudinal and longitudinal swath of the Canadian Archipelago, including Baffin Bay, the Northwest Passage, the Beaufort Sea, Foxe Basin, Hudson Bay and 3 Labrador fjords (Fig. 2.1) at a total of 219 stations. Vertical profiles were obtained with a CTD rosette equipped with sensors to measure *in vivo* fluorescence (SeaPoint Chlorophyll Fluorometer), transmissivity (WET Labs CST671DR), dissolved oxygen (Sea-Bird SBE43), nitrate (SATLANTIC ISUS V1), photosynthetically active radiation (PAR; Biospherical QCP-2300 PAR), and temperature and salinity (Sea-Bird SBE-911plus).

At a subset of 140 stations (55 in 2005 and 85 in 2006), water samples for nutrient determinations (nitrate [NO_3^-] + nitrite [NO_2^-]), phosphate (PO_4^{3-}) and silicic acid ($Si(OH)_4$) were taken with 12 l Niskin type bottles attached to the CTD rosette at standard depths (5, 10, 20, 30, 40, 50, 60, 70, 80, 100, 125, 150, 175, 200, 250, 300 m and then every 100 m) unless the Arctic halocline was identified on the CTD downcast. In this case, sampling in the 100 – 200 m range occurred at every 20 m and at a salinity of 33.1 to capture the nutrient maximum. Out of those 140 stations, 64 (35 in 2005 and 29 in 2006) were also sampled for ammonium (NH_4^+), chl *a*, and photosynthetic yield. Samples for chl *a* and photosynthetic yield were taken at 5 depths: in the upper mixed layer (5 m), in the lower and upper trails of the SCM, at the SCM, and below the euphotic zone. Samples for phytoplankton identification and enumeration were collected at the depth of the SCM at 35 stations in 2005 (all regions) and at 15 stations in 2006 (Baffin Bay, Northwest Passage, and Beaufort Sea).

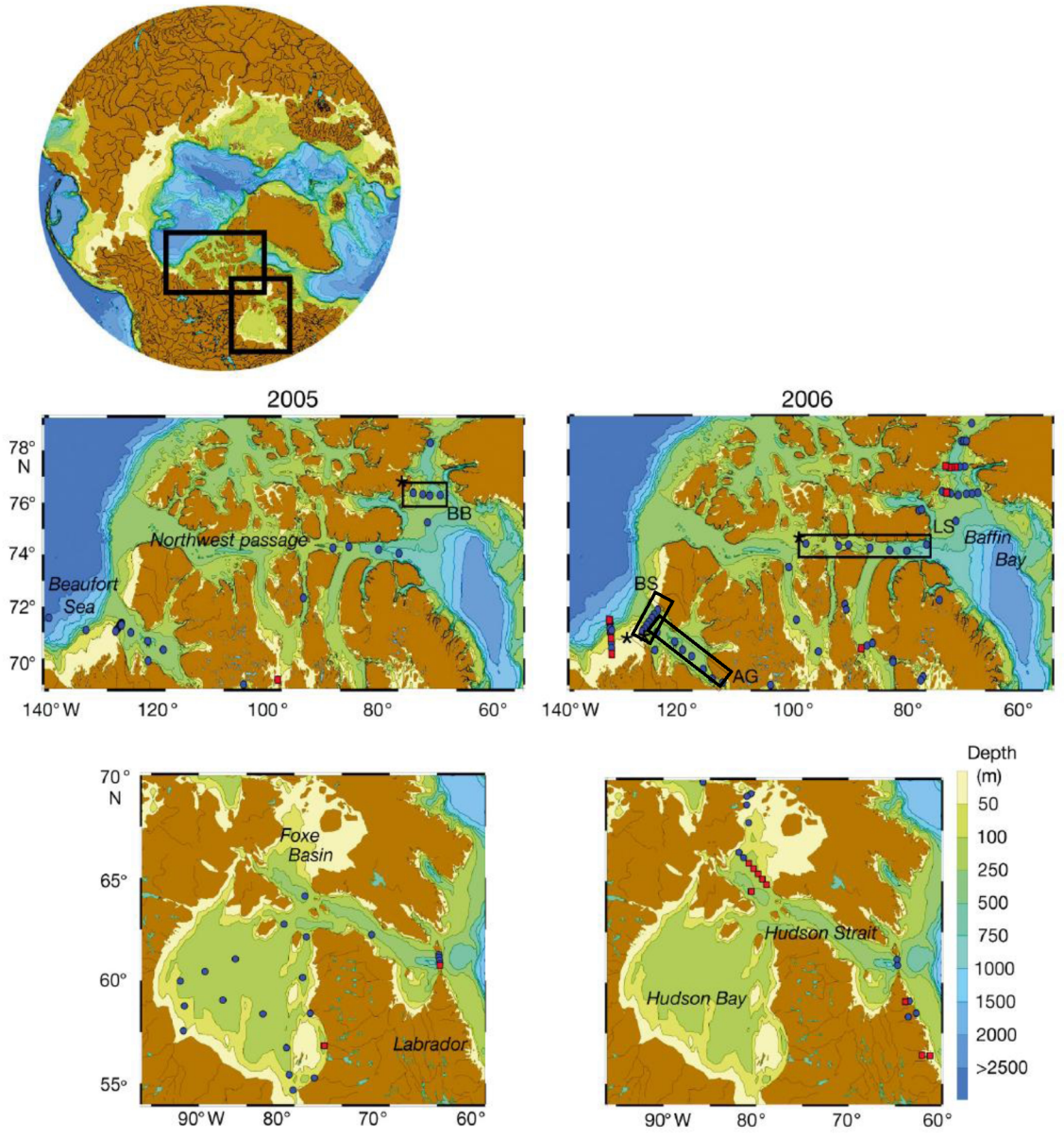

Figure 2.1 Location of sampling stations with the presence (blue circles) or absence (red squares) of a subsurface fluorescence maximum in the Canadian Arctic during 2005 (left-hand panels) and 2006 (right-hand panels). Four oceanographic sections are identified within boxes: southeast Beaufort Sea (BS; 5–6 Oct 2006), Amundsen Gulf (AG; 29 Sep–18 Oct 2006), Barrow Strait/Lancaster Sound (LS; 20–25 Sep 2006) and northern Baffin Bay (BB; 16–22 Aug 2005). Stars represent the starting point of the sections presented in Figs. 2.5 and 2.6

2.4.2 Nutrients

Samples for nutrient determinations were collected into acid-cleaned polyethylene tubes after thorough rinsing and filtration through a 5 µm polycarbonate filter inserted in a filter holder. This step insured the removal of the large particles (e.g. clay, mud) and organisms that may interfere with the analyses. Samples were stored at 4°C in the dark and analyzed within a few hours for NO_2^-, $NO_3^- + NO_2^-$, PO_4^{3-} and $Si(OH)_4$ using standard colorimetric methods (Grasshoff et al. 1999) adapted for the AutoAnalyzer 3 (Bran+Luebbe). NH_4^+ was determined manually with the sensitive fluorometric method of Holmes et al. (1999). The working reagent was added within minutes of sampling. The detection limit for NH_4^+ analysis was 0.02 µM or better.

2.4.3 Extracted chlorophyll and photosynthetic competency

Concentrations of chl *a* were determined using the fluorometric method described by Parsons et al. (1984). Samples were filtered onto Whatman GF/F filters and extracted with 90% acetone for 18 h at 4°C in the dark. The fluorescence was measured before and after acidification with a Turner Designs Model 10-AU fluorometer.

The photosynthetic competency (i.e. maximum photochemical quantum yield of photosystem II = F_v/F_m) of the algae was estimated by pulse-amplitude-modulated fluorometry (WALZ Phyto-PAM). This method is based on the induction and detection of chlorophyll fluorescence, which provides the minimum (Fo; near-darkness condition) and maximum (Fm; saturation pulse of 200 µs at 4000 µmol quanta m^{-2} s^{-1}) fluorescence required for the computation of variable fluorescence (Fv = Fm - Fo). Samples were dark-adapted for 30 min at ~4°C (Ban et al. 2006; no significant correlation was observed between F_v/F_m and *in situ* temperature at the depth of collection) to allow relaxation of fluorescence quenching. A blank was assessed at each station with SCM water filtered through a 0.2 µm syringe filter. To minimize the effect of taxonomic variability, fluorescence was measured at 3 specific wavelengths (470, 520, and 645 nm). Emissions at 645 nm (wavelength for allophycocyanin and phycocyanin: specific pigments of cyanobacteria) were close to background noise so that only the 470 and 520 nm emissions (wavelengths for chl *a*, *b* and *c*, flucoxanthin and carotenoids; specific pigments of diatoms,

dinoflagellates and green algae) were averaged for the calculation of F_v/F_m. There was no relationship between chl *a* concentration and F_v/F_m.

2.4.4 Phytoplankton abundance and taxonomic composition

For the identification and enumeration of phytoplankton, samples were preserved with acidic Lugol's solution (Parsons et al. 1984). Cells ≥4 µm were identified to the lowest possible taxonomic rank using an inverted microscope (WILD Heerbrugg) equipped with phase contrast optics (Lund et al. 1958). For each sample, a minimum of 300 cells was counted. The main references used for phytoplankton identification were Tomas (1997) and Bérard-Therriault et al. (1999).

2.4.5 Sensor calibrations and data transformations

Detailed vertical profiles of water temperature, salinity, transmissivity, PAR, oxygen and *in vivo* fluorescence were analyzed for 219 stations. The CTD and attached sensors were factory calibrated prior to each expedition. Analytically determined NO_3^- concentrations were used to post-calibrate the optical nitrate probe and generate high-resolution vertical profiles. Due to problems with the batteries of the probe and with problematic calibrations at a few stations, detailed NO_3^- profiles were only available for 147 stations. The output of the oxygen sensor was frequently calibrated against Winkler titrations (modified as in Carpenter 1965, and automated as described in WHOI technical report 90 - 35 by Knapp et al. 1990) and proved to be reliable and stable over time. The degree of oxygen saturation was calculated using *in situ* concentration and theoretical solubility based on temperature and salinity data (Weiss 1970). The Brunt-Väisälä (or buoyancy) frequency ($N^2 = \{[g/\rho\ d\rho/dz]^{½}\}^2$; in s^{-2}) was estimated from the difference in potential density (ρ) between consecutive depth (z) intervals. The pycnocline and nitracline were defined as the depth where N^2 and the vertical gradient in NO_3^- concentration (dNO_3^-/dz) were highest, respectively. The depth of the SCM was defined as the depth where the *in vivo* fluorescence was at a maximum, while its thickness was estimated as the zone of elevated fluorescence between areas where the mean vertical gradient in *in vivo* fluorescence (d(*in vivo* fluorescence)/dz) was zero over 5 consecutive depth bins.

Due to highly variable weather conditions (cloud cover) and because the ship did not stay at any station for more than a few hours, a comparison of sampling sites on the basis of absolute irradiance at the SCM was not practical. Instead, we made these comparisons using the coefficient of diffuse light attenuation (k), which is a more stable property of the water column over time scales of a few days at least. The percentage of incident PAR available at the SCM was calculated from the value of k determined between the surface and the SCM using vertical PAR profiles. In this paper, we arbitrarily define the base of the euphotic zone as the 1% of light level to facilitate comparisons with the literature.

Ordinary least-squares regressions (model I linear regression) were used to determine predictive relationships (e.g. equations used in the reconstruction of chl *a* profiles; post-calibrations) and geometric mean regressions (considering error on both variables; model II linear regression) were used to assess functional relationships between 2 variables (Laws and Archie 1981; Wallace et al. 1995; Calbet and Prairie 2003).

2.5 Results

Subsurface fluorescence maxima were widespread in the Canadian High Arctic, Hudson Bay and Labrador fjords during late summer 2005 and early fall 2006 (Fig. 2.1). Out of 140 stations, 85% clearly showed a subsurface maximum, which ranged broadly in vertical position (7 to 67 m; median: 29 m) and thickness (2 to 74 m; median: 18 m). The other stations (15%) showed vertically homogenous fluorescence (shallow Foxe Basin; 7 to147 m) or a surface maximum (western Baffin Bay, Mackenzie Shelf, inner Canadian Archipelago, Hudson Bay and Labrador fjords).

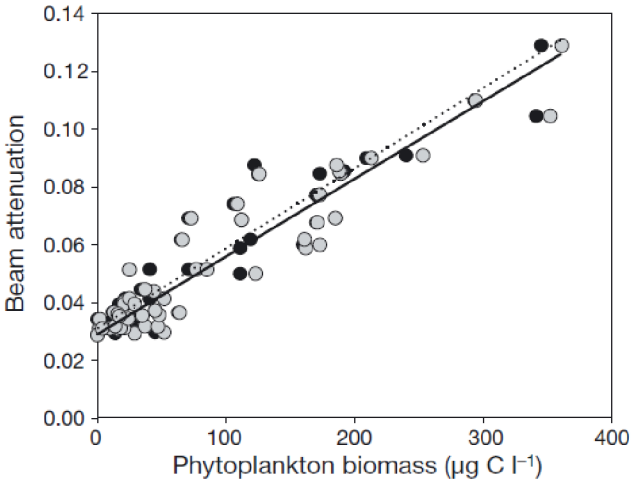

Figure 2.2 Relationships between beam attenuation and phytoplankton carbon estimates in northern Baffin Bay (data from late summer 1998; Booth et al. 2002). Model II linear regressions: $y = 0.0003x + 0.03$, $n = 53$, $r^2 = 0.88$ (diatom carbon; black circles, dotted line) and $y = 0.0002x + 0.03$, $n = 53$, $r^2 = 0.88$ (total autotrophic carbon; gray circles, solid line)

Using the average output of the fluorometer during bottle closure, the relationships between *in vivo* fluorescence and extracted chl *a* concentration were assessed separately for each region and expedition (e.g. for Baffin Bay in 2006: $y = 1.05x - 0.08$; $n = 39$, $r^2 = 0.92$, $p < 0.0001$). The small residuals of the regressions showed an even dispersal for concentrations ranging at least 2 orders of magnitude, and intercepts were statistically undistinguishable from zero, indicating negligible interferences or quenching near the surface. Region-specific relationships were used to construct high-resolution vertical profiles of chl *a*. To determine if c_p ($\lambda \approx 660$ nm) is an acceptable surrogate for phytoplankton biomass in Baffin Bay, the biovolume-based estimates of total autotrophic carbon biomass reported by Booth et al. (2002) (determined by epifluorescence microscopy enumeration and sizing) were compared with concomitant transmissometer data (Fig. 2.2). Strong linear relationships were observed between c_p and the carbon biomass of total phytoplankton and diatoms. This exercise was not attempted in the shallow Canadian Archipelago and the coastal Beaufort Sea due to the proximity of the Mackenzie River and resuspension on shallow shelves.

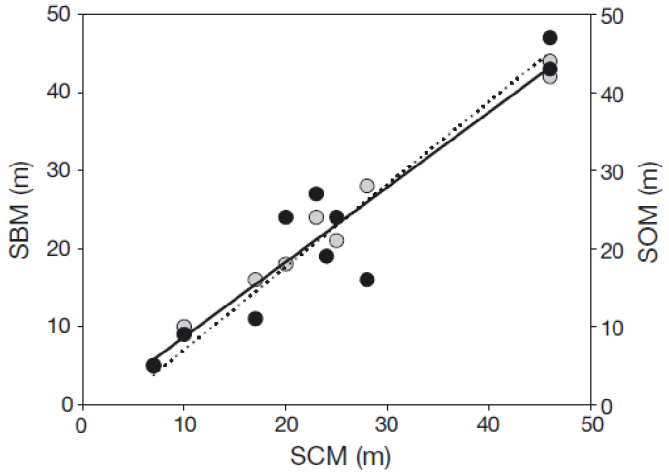

Figure 2.3 Relationships between the vertical positions of the subsurface chlorophyll maximum (SCM), beam attenuation maximum (SBM; gray circles) and oxygen saturation maximum (SOM; black circles) for northern Baffin Bay stations in 2006. Model II linear regressions between SBM and SCM depths (solid line: $y = 0.96x - 0.93$; $n = 10$, $r^2 = 0.98$) and between SOM and SCM depths (dotted line: $y = 1.06x - 3.57$; $n = 10$, $r^2 = 0.88$)

The depths of the SCM, the SBM and the oxygen saturation maximum (SOM) were compared in northern Baffin Bay (Fig. 2.3), where river runoff has a negligible influence on particle load. In 2006 (when the oxygen probe worked consistently and the spatial coverage of northern Baffin Bay was extensive), the vertical depth of the SCM closely matched those of the SBM (when detectable; i.e. when the particle load in surface waters was negligible) and of the SOM. A positive relationship between the depths of the SCM and SOM was also observed in the Beaufort Sea but was much weaker ($r^2 = 0.24$, $n = 61$) than in Baffin Bay.

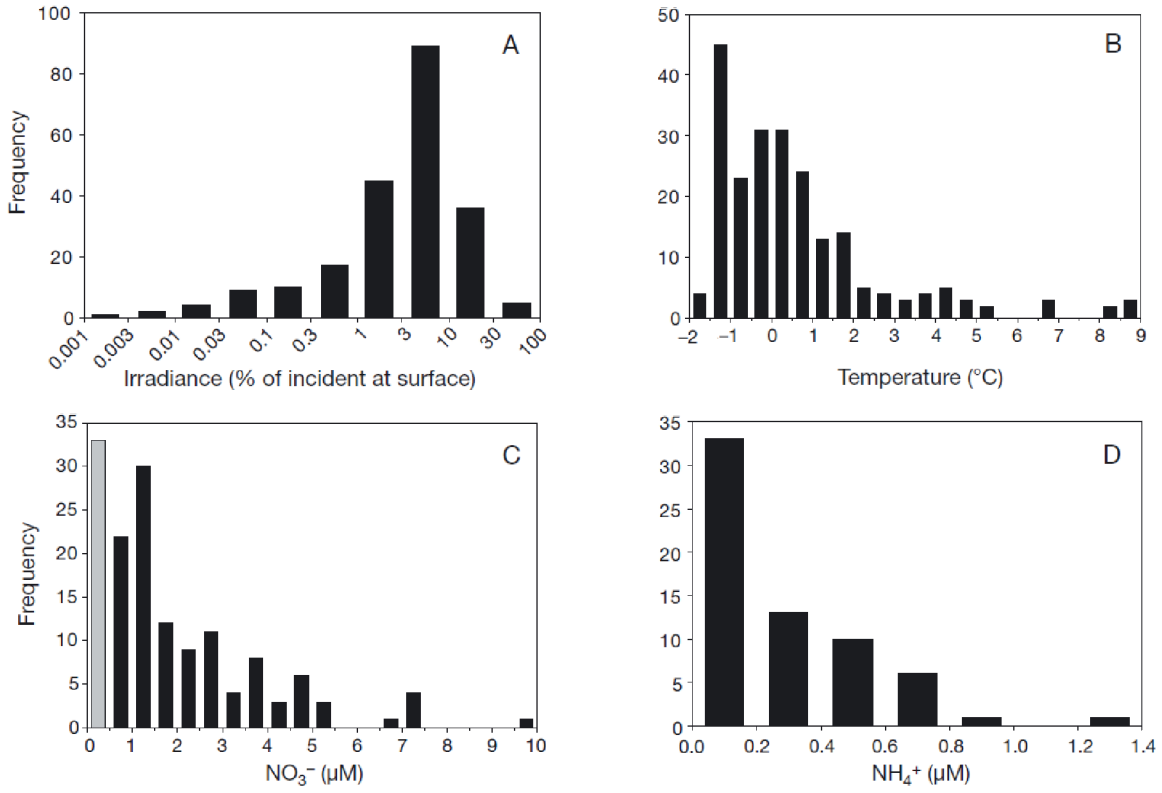

Figure 2.4 Frequency distributions of (A) percentage of surface irradiance, (B) water temperature, (C) NO_3^- and (D) NH_4^+ concentrations at the depth of the subsurface chlorophyll maximum (SCM). In (C), gray bar = samples below the analytical limit of detection (i.e. <0.05 µM). All sampling stations and years were pooled

2.5.1 General conditions at the SCM

The frequency distributions of physical properties and nitrogenous nutrient concentrations at the SCM depth are presented in Fig. 2.4. Although irradiance at the SCM ranged from 0.001 to 48% of surface values (daily mean absolute irradiance corresponding to 0.0006 - 75.12 µmol quanta m^{-2} s^{-1} assuming that the mean irradiance along the ship track during a day is representative of a given station), 83% (181 out of 219 CTD stations) of the SCM were located below the 10% light level and the mode of the distribution (52% of the stations) was in the 3 - 10% range (Fig. 2.4A). Water temperature ranged from -1.5 to 2.0°C at 83% of the stations (181 out of 219 CTD stations), with a mode between -1.5 and -1.0°C (at 21% of stations; Fig. 2.4B). Extreme values of -1.8 and 9°C were observed in isolated instances. Nitrate concentrations generally ranged from 0.5 to 3.0 µM with values

<0.5 µM or >3 µM at 22 and 20% of the stations, respectively (Fig. 2.4C). NH_4^+ concentrations varied between the detection limit (0.02 µM) and 1.40 µM with a mode of 0.20 µM at 52% of the stations (Fig. 2.4D).

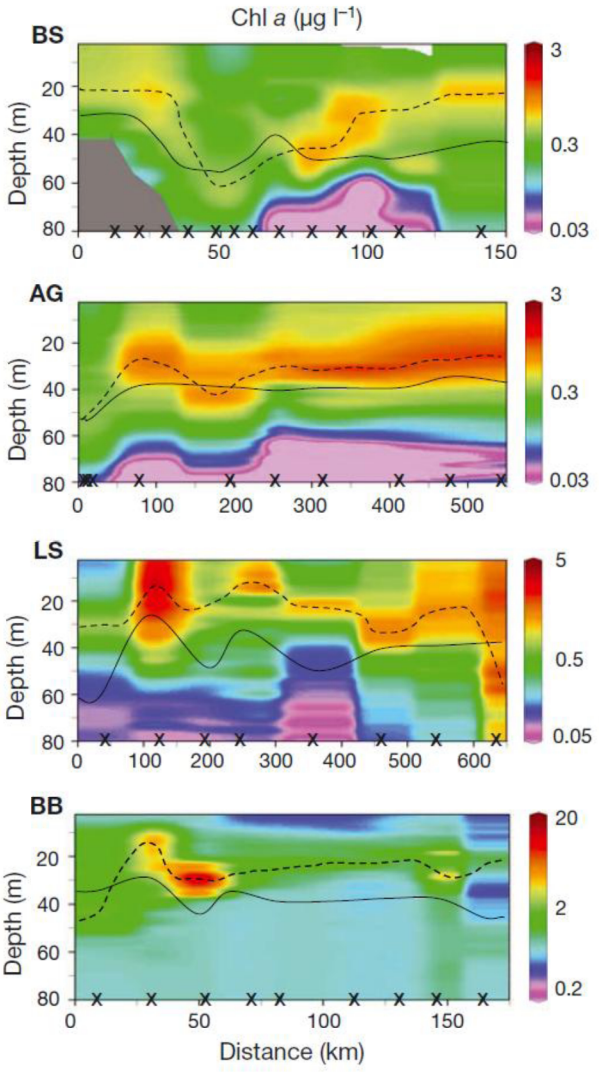

Figure 2.5 Vertical variations of calibrated chl *a* concentration (right-hand color key) along sections in BS, AG, LS and BB (see Fig. 2.1 for exact locations). Dashed and solid lines: depths of the subsurface chlorophyll maximum and of the euphotic zone (defined here as 1% of surface irradiance), respectively. Position of each sampling station: 'x' on the bottom axis.

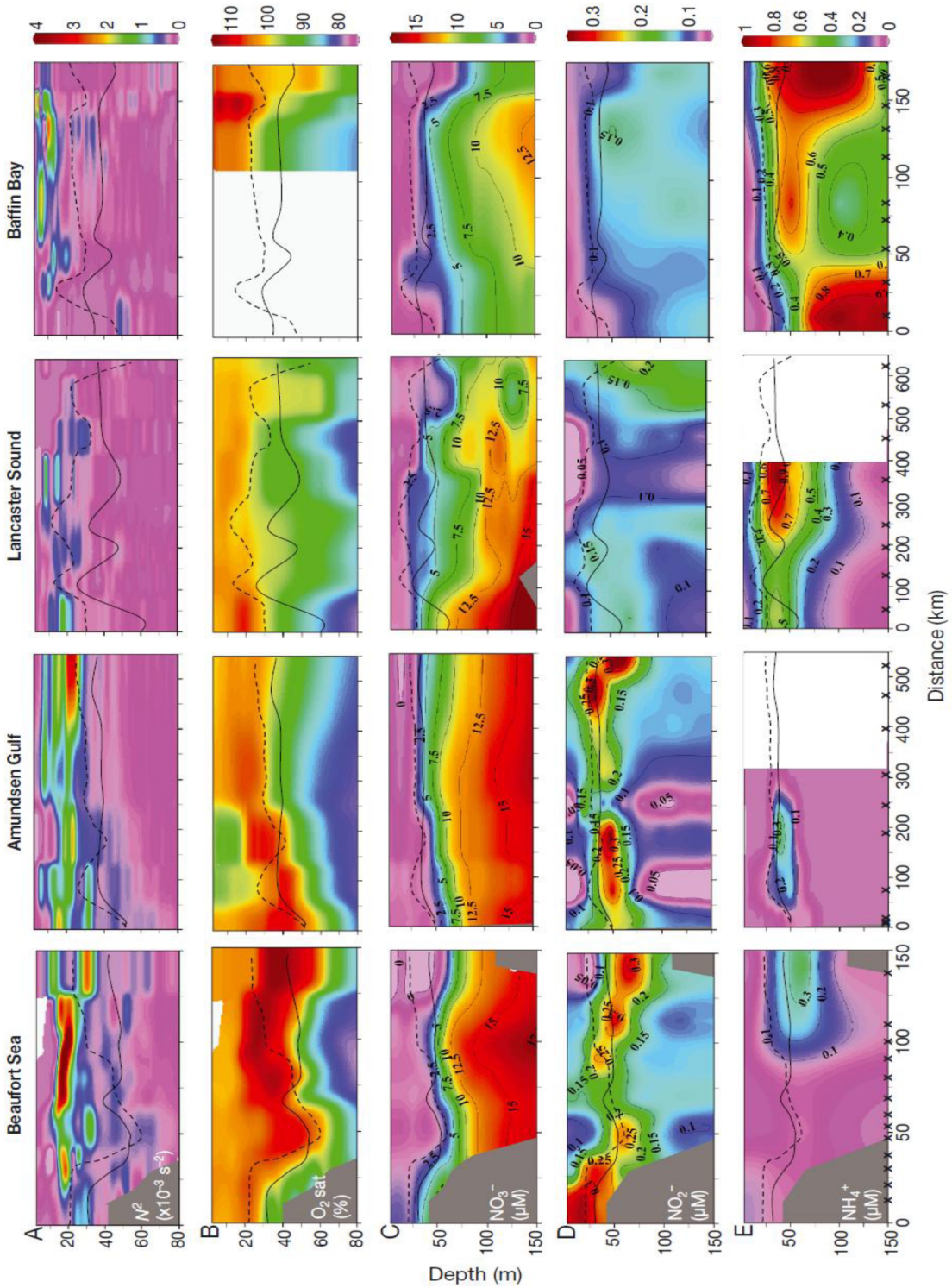

Figure 2.6 Vertical variations of (A) the Brunt-Väisälä frequency (N^2), (B) percent oxygen saturation (O_2 sat), (C) NO_3^-, (D) NO_2^- and (E) NH_4^+ concentrations along sections in Beaufort Sea, Amundsen Gulf, Lancaster Sound, and northern Baffin Bay. Note the different depth scale for N^2 and O_2 sat (0–80 m). See Fig. 2.5 for definition of lines and symbols

2.5.2 Oceanographic sections

The positioning of the SCM relative to vertical profiles of nutrients and the physical structure of the water column was explored in detail using 4 oceanographic sections (see Fig. 2.1 for locations). Concentrations of chl *a* at the SCM were generally lower in the western sections (Beaufort Sea [BS]: 0.32 - 0.74 $\mu g\, l^{-1}$; Amundsen Gulf [AG]: 0.34 - 2.50 $\mu g\, l^{-1}$) than in the eastern sections (Lancaster Sound [LS]: 0.53 - 4.52 $\mu g\, l^{-1}$; Baffin Bay [BB]: 1.39 - 16.65 $\mu g\, l^{-1}$) (Fig. 2.5). There was no consistent regional difference in the depth of the SCM, which most often occurred between 20 and 35 m. Conspicuous exceptions were noted off the shelf break on the BS section (40 – 62 m), at the entrance of LS (70 m) and at 3 stations on the LS and BB sections (12 - 15 m). The SCM was at or well above the 1% surface irradiance in all but 4 stations on the sections. Chl *a* concentration generally declined to very low values (<0.1 $\mu g\, l^{-1}$) below the SCM, except in northern BB where they remained moderate (>0.5 $\mu g\, l^{-1}$) in the upper 80 m of the water column.

The pycnocline (i.e. depth with the maximum value of N^2) was shallow nearly everywhere (14 - 32 m) but the stratification was stronger in the western sections (i.e. BS and AG) than in the eastern ones (i.e. LS and BB) (Fig. 2.6A). The pycnocline was systematically located in the upper euphotic zone and most often above the SCM. Oxygen saturation was generally >100% at the SCM, with maximum values generally observed at or close to the SCM (Fig. 2.6B). NO_3^- concentrations were generally near the analytical detection limit above the SCM, which was typically associated with the top of the nitracline (Fig. 2.6C). Note that $Si(OH)_4$ and PO_4^{3-} concentrations (not shown) followed the same vertical patterns as NO_3^-, but were not depleted in the surface layer. Maximum NO_2^- concentrations were much higher in the western sections than in the eastern ones (Fig. 2.6D). A well-defined primary NO_2^- maximum (PNM) was visible only in the western sections, where it generally tracked the SCM. In the eastern sections, the layer of elevated NO_2^- concentration was relatively diffuse and thick with no apparent relationship with the SCM. On all sections, NH_4^+ concentrations were uniformly low in surface waters and generally showed a subsurface maximum below the SCM (Fig. 2.6E). Subsurface concentrations were particularly high in the eastern sections (up to 1.24 μM) and elevated NH_4^+ concentrations extended far below the euphotic zone in northern BB.

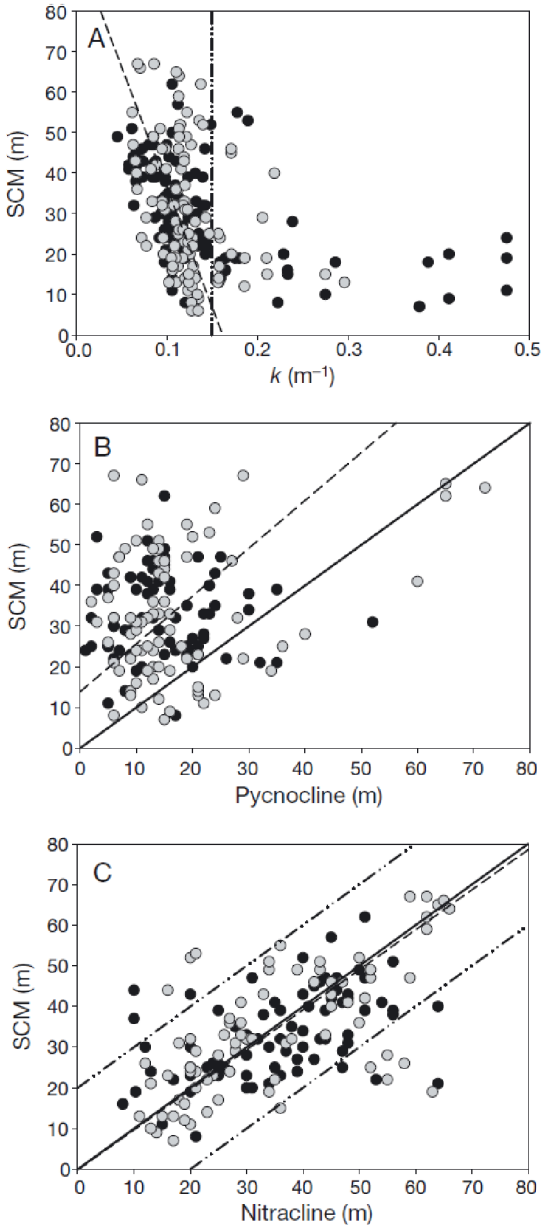

Figure 2.7 Relationships between the depth of the subsurface chlorophyll maximum (SCM) and (A) the coefficient of diffuse light attenuation (k), (B) the pycnocline, and (C) the nitracline in 2005 (solid black circles) and 2006 (solid gray circles). In (A), vertical dash-dotted line: $k = 0.15$ m^{-1} (see text for detail); and dashed line: model II linear regression for stations, where $k < 0.15$ m^{-1} ($y = -594.5x + 96.18$; $r^2 = 0.14$). In (B) and (C), solid line indicates 1:1 match; and dashed line: model II linear regression between SCM and pycnocline depths ($y = 1.18x + 13.86$; $r^2 = 0.04$) and between SCM and nitracline depths ($y = 0.98x - 0.16$; $r^2 = 0.66$ when excluding 16 outliers)

2.5.3 Light attenuation, nutrients and vertical position of the SCM

The relationship between the vertical position of the SCM and *k* for all stations is shown in Fig. 2.7A. The range of *k* went from a minimum of 0.046 m^{-1} at deep stations to a maximum of 0.475 m^{-1} at neritic stations influenced by large rivers (Fig. 2.7A). To remove this influence, a model II linear regression was adjusted for stations with $k < 0.15$ m^{-1} and showed a very weak ($r^2 = 0.14$), negative relationship between the 2 variables (Fig. 2.7A).

The SCM was deeper than the pycnocline at 86% of the stations and no significant correlation was observed between their respective vertical positions (Fig. 2.7B). However, 68% of the stations showed a vertical match between the depth of the SCM and the nitracline within a margin of ±10 m (Fig. 2.7C). This match extended to 90% of the stations for a margin of ±20 m. A linear regression fit trough all data evidenced 16 large residuals (standardized residuals ≥2; belonging to stations with poorly defined SCM or nitracline) that belonged to either very weakly stratified stations (maximum $N^2 \leq 0.0006$) or sites where the nitracline was more than 12 m below the 1% of surface irradiance (Fig. 2.7C). The regression was largely improved by removing the outliers from the analysis. To verify if light penetration through the upper water column improved the relationship, a multivariate linear regression model considering the depth of the SCM, *k* (x_1) and the depth of the nitracline (x_2) was adjusted to stations where $k < 0.15$ m^{-1} (minus the 16 outliers). A relationship was obtained ($y = -36.67x_1 + 0.775x_2 + 10.92$; $r^2 = 0.67$, $p_1 = 0.2260$, $p_2 < 0.0001$), but the regression coefficient for *k* was not significant.

2.5.4 Photosynthetic competency

Considering the entire sampling area, data from 2005 and 2006 generally displayed high F_v/F_m at the SCM (median = 0.56) although values varied between 0.32 and 0.70 (Fig. 2.8). At the surface, F_v/F_m ranged from 0.08 to 0.71 with a median value of 0.55 (Fig. 2.8). The scatter of values was much lower at the SCM than at the surface (where F_v/F_m was frequently <0.45) and there was no statistically significant difference between the 2 sampling depths (Wilcoxon signed rank test, $p = 0.542$).

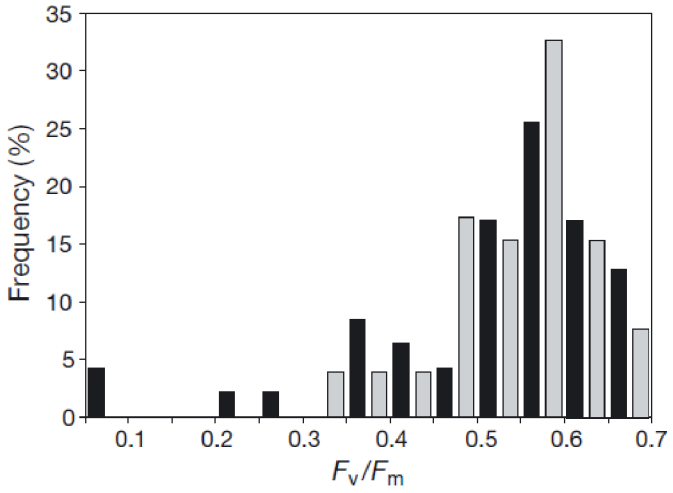

Figure 2.8 Frequency distribution of F_v/F_m at the surface (black) and at subsurface chlorophyll maximum (gray). All sampling stations and years were pooled

2.5.5 Taxonomic composition at the SCM

The taxonomic composition of the phytoplankton at the SCM was investigated for both sampling years (Fig. 2.9). The relative abundance of flagellates and dinoflagellates was 21 and 38% lower, respectively, in 2006 than in 2005 in all regions. During both years, the BS presented lower percentage of diatoms and higher percentages of flagellates and dinoflagellates than northern BB. Flagellates and dinoflagellates were numerically dominant in the Hudson Bay system in 2005 and made up, on average, 90% of the total phytoplankton abundance. In all regions, centric diatoms were, on average, 3 to 27 times more abundant than pennate diatoms. Except in the Hudson Bay system, *Chaetoceros* spp. were the most abundant centric diatoms at the SCM in 2005 and 2006 (76 to 99% of total centric diatoms on average). *Chaetoceros socialis* Lauder was present at 56% of the stations and represented up to 30% of the total *Chaetoceros* abundance. However, *C. socialis* was less abundant in 2006 than in 2005. Diatoms of the genus *Thalassiosira* were scarce throughout the Canadian Arctic (0 - 0.5%).

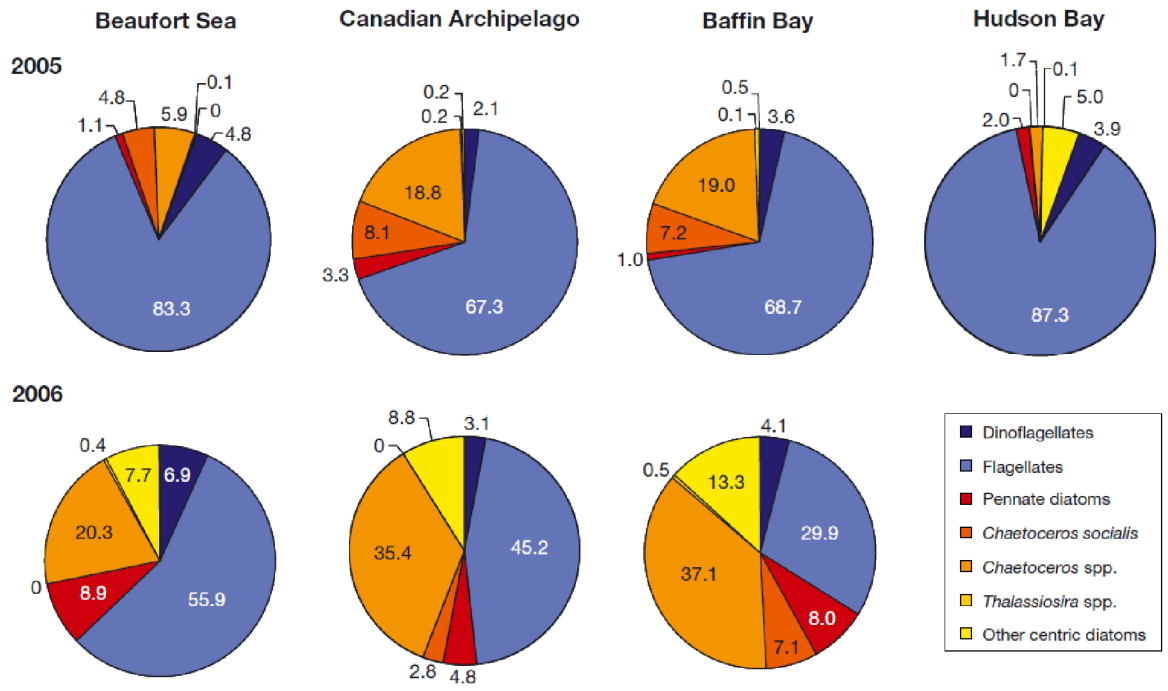

Figure 2.9 Mean percent abundance of the major phytoplankton groups observed at the depth of the subsurface chlorophyll maximum in the Beaufort Sea, inner Canadian Archipelago, northern Baffin Bay and Hudson Bay in 2005 and 2006. Hudson Bay was not sampled in 2006

Pearson's product moment correlations (PPMC) were used to evaluate relationships between environmental variables and the relative and absolute abundance data. Only the significant correlations are described here. At the SCM, the absolute abundance of flagellates increased with NH_4^+ concentration ($r = 0.48$, $p < 0.01$). The relative abundance of dinoflagellates increased with N^2 ($r = 0.32$, $p < 0.05$), whereas the relative abundance of pennate diatoms increased with NO_2^- concentration ($r = 0.39$, $p < 0.01$). The relative dominance of diatoms over flagellates decreased with water temperature ($r = -0.34$, $p < 0.05$) and increased with ambient NO_3^- concentration ($r = 0.31$, $p < 0.05$). NO_3^- concentration was positively correlated to NO_2^- concentration ($r = 0.52$, $p < 0.001$) and salinity ($r = 0.30$, $p < 0.05$).

2.6 Discussion

This study provides the first near-synoptic assessment of the incidence and properties of SCM through the Canadian Arctic, including the subarctic Hudson Bay and Labrador fjords, during late summer and early fall. Results show that SCM are almost ubiquitous and imply that they persist throughout the ice-free period since they are known to appear early in the growth season (Booth et al. 2002; Tremblay et al. 2008). Now that the prevalence of SCM is established, their characteristics will be discussed with respect to the physico-chemical structure of the water column, potential repercussions for the estimation of primary production by remote-sensing and biogeochemical implications.

The absence of SCM was noted only near rivers and at shallow locations (<100 m) where vertical mixing or upwelling is important (Fig. 2.1). For example, the shallow water column (<100 m) on the eastern side of Foxe Basin is completely mixed by 8 m tides (Prinsenberg 1986). Chl *a* was usually highest at the surface at very weakly stratified (western BB, Hudson Strait) and shallow (Canadian Archipelago, eastern Hudson Bay, Mackenzie Shelf and Labrador fjords) stations. Otherwise, chl *a* concentrations at the SCM were in agreement with sparse reports for the same regions or other sectors of the North-American Arctic (Cota et al. 1996; Vidussi et al. 2004; Lee and Whitledge 2005).

Concentrations of chl *a* at the SCM were relatively low (0.1 - 2.5 $\mu g\, l^{-1}$) in LS, AG and the southeast BS, where values generally increased from deep offshore waters to the shelf. The depth of the SCM was also quite variable. Off the shelf break, where NO_3^- was depleted in the upper euphotic zone, SCM were as deep as 62 m. This result can be explained by the strong stratification, which is not broken down during winter and limits the upward supply of nutrients all year long (Tremblay et al. 2008). Near the coast, some SCM were as shallow as 8 to 20 m where nutrient concentrations in the upper part of the water column were elevated due to enhanced local mixing (e.g. internal tidal waves; see Sharples et al. 2007) and mild shelf-break upwelling (Carmack and Chapman 2003) (Fig. 2.6). By contrast, chl *a* concentrations at the SCM in BB were generally high (1.4 $\mu g\, l^{-1}$ in the east to 16.7 $\mu g\, l^{-1}$ in the west), even over relatively deep waters. The most diffuse SCM on the vertical occurred in eastern BB where the stratification was weakest. A similar situation occurred at the eastern edge of LS, which received relatively well-mixed waters from the

north. Overall, the high variability in SCM characteristics was better explained by regional differences in stratification than by local properties (e.g. nutrient concentration, light availability) at the actual depth of the SCM on any given day. This result suggests that the mixing regime in the lower euphotic zone exerts a determinant influence on upward nutrient fluxes and the intensity and shape of SCM in the Canadian Arctic.

2.6.1 Implications of SCM for remote sensing

Using surface concentration to predict the shape of the vertical profile of chl *a* and its total stock in the euphotic zone is desirable for monitoring purposes and to estimate primary production from space. Algorithms for the remote-sensing estimation of primary production in the Arctic Ocean typically assume homogenous chl *a* in the upper mixed layer and an exponential decrease underneath (e.g. Arrigo et al. 2008). This assumption is adequate early in the growth season, especially in highly productive waters, but the biases it introduces where SCM prevail throughout most of summer and fall remain to be assessed. In first analysis, the coefficient of variation for chl *a* concentration was 2-fold higher at the SCM (143%) than at the surface (76%), implying that the high heterogeneity at depth was not well expressed at the surface. To investigate further, we compared our dataset with 2 predictive models established for other regions of the world ocean (Fig. 2.10; Morel and Berthon 1989; Uitz et al. 2006). These models describe the non-linear relationships between the mean concentration of chl *a* over the first penetration depth of orbiting sensors (depth of 1% irradiance ÷ 4.6) in Case I waters with (1) the total chl *a* inventory in the euphotic zone and (2) the shape of the standardized vertical chl *a* profile.

Surface chl *a* explained 65% ($p < 0.0001$) of integrated chl *a* in the euphotic zone, and the weak, significant relationship shown in Fig. 2.10A agrees broadly with Morel and Berthon (1989) and Uitz et al. (2006). However, applying these general regressions indiscriminately to the Arctic can (1) overestimate chl *a* inventories by 2- to 3-fold at neritic stations (Fig. 2.10B) or (2) underestimate it by a factor of 3 to 5 in relatively clear, stratified waters with a pronounced SCM (Fig. 2.10C). The overestimation (Fig. 2.10B) is not surprising since it occurs in turbid waters not considered by these regressions, i.e. where river runoff and shallow bathymetry severely restrict the thickness of the euphotic zone (Fig. 2.10A:

black circles outside of the lower 95% confidence line). The underestimation (Fig. 2.10A,C: circles outside the upper 95% confidence line) is explained by the relationships shown in Figs. 2.6A & 2.7B,C as the SCM seasonally lowers the nitracline well beneath the thin upper mixed layer in clear waters. It becomes physically disconnected from the surface and resides in the upper halocline, where a moderate density gradient limits turbulent dispersion.

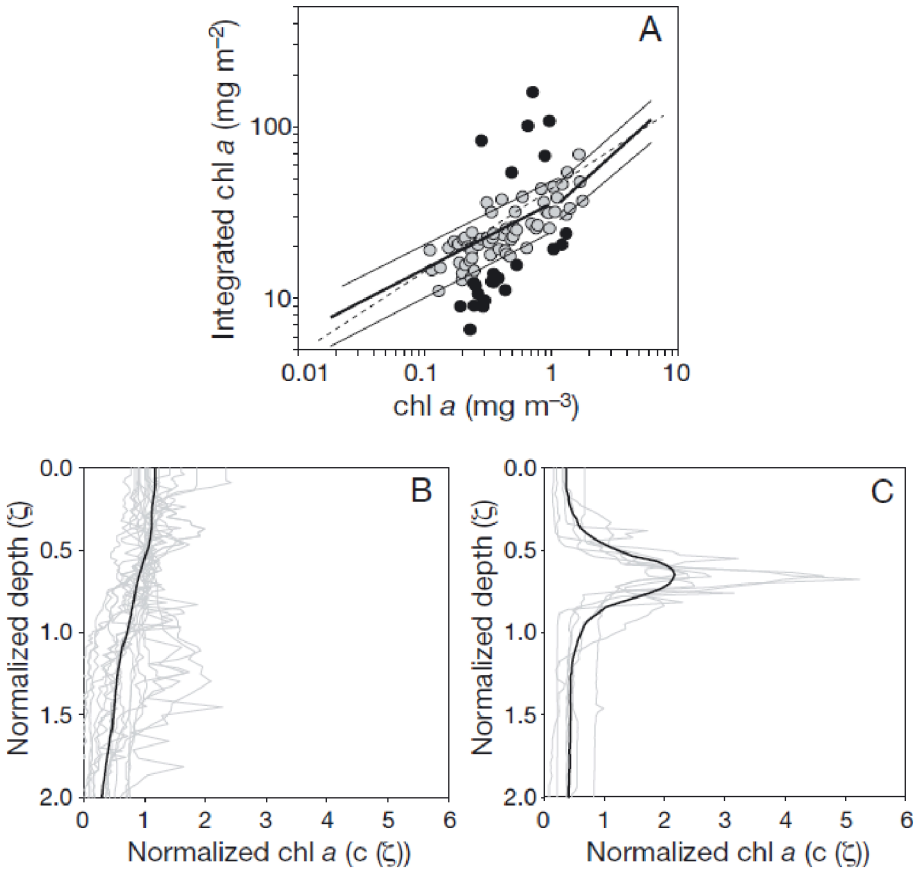

Figure 2.10 Relationships between (A) chl *a* concentration at the surface (depth of euphotic zone ÷ 4.6) and chl *a* concentration integrated over the euphotic zone, showing the present data set (gray circles) relative to global regression lines for stratified Case I waters (Morel and Berthon 1989 = dashed line; Uitz et al. 2006 = thick solid lines with 95% confidence interval provided as thin solid lines). Vertical profiles of normalized (following Uitz et al. 2006) chl *a* concentration (c(ζ) = chl *a* at depth z / mean chl *a* in euphotic zone) and depth (ζ = depth [m] / depth of the 1% irradiance level) presented for groups of stations (black circles in A) (B) below and (C) above the 95% confidence interval determined by Uitz et al. (2006). Thick black lines in (B) and (C): average of all profiles shown

2.6.2 Implications of SCM for primary production in the Arctic

Because SCM usually occur in the lower euphotic zone, errors in the assumed vertical distribution of chlorophyll are likely to translate into lesser errors for the estimation of primary production. Pending the detailed results of our ongoing process-oriented investigation into the matter, 3 large-scale emergent properties suggest that SCM are important for primary production (see also Cullen 1982 and Lee and Whitledge 2005) in seasonally ice-free waters of the Arctic Ocean.

First, the frequency distribution of relative irradiance (Fig. 2.4A) and the detailed sections (Fig. 2.5) and dimensionless profiles (Fig. 2.10C) of chl *a* show that Arctic SCM are more pronounced and thrive higher in the euphotic zone (3 to 10% light level) than their counterparts for stratified oceanic waters of the world ocean (≤1% light level; Uitz et al. 2006; Pommier et al. 2009). Under the assumption phytoplankton in the SCM are light limited, then photosynthesis would respond linearly to light at low irradiance (e.g. in the lower euphotic zone; near 1% light level). As such, the relative share of the SCM in total water column primary production in the Canadian Arctic could possibly be an order of magnitude higher than at lower latitudes (e.g. primary production estimated between 12 and 60 mg C m^{-3} d^{-1} at the SCM depth in Arctic and subarctic regions and between 1.5 and <15 mg C m^{-3} d^{-1} in North Atlantic Ocean and North Pacific subtropical gyre; Steele and Yentsch 1960; Steele 1964; Rysgaard et al. 1999; Miller 2004; Mundy et al. 2009; Pommier et al. 2009). This distinction arises because the upper mixed layer is relatively thin and stable in the former, allowing SCM to form in the upper euphotic zone early in the growth season (Tremblay et al. 2008; Mundy et al. 2009).

Second, in a companion study, Tremblay et al. (2009) observed that the numerical contribution of diatoms was up to 10 times higher in the lower euphotic zone (i.e. at the SCM depth) than in the upper mixed layer at stations where a SCM was well defined. Booth et al. (2002) also reported a strong dominance of the SCM by *Chaetoceros socialis* in northern BB during July. In our study, spatial and inter-annual differences in assemblage composition were related to nutrients and physical properties at the SCM (Fig. 2.9). Centric diatoms, especially of the genus *Chaetoceros*, tended to dominate at high NO_3^- concentrations, whereas flagellates and dinoflagellates tended to take over when water

temperature, NH_4^+ concentration and the strength of the pycnocline were high (see also Tremblay et al. 2009). Moreover, other study show that eukaryotic picoplankton *Micromonas* (a flagellate not detected by the inverted microscopy method that allow identification of cells ≥4 μm) is abundant and widely distributed in the Canadian Arctic, even in low light conditions as observed at SCM depth (Lovejoy et al. 2007). Nevertheless, the large size of SCM diatoms (cells > 20 μm; Lee and Whitledge 2005; Tremblay et al. 2009) relative to other taxa, that dominate higher up in the water column (cells < 10 μm; Lee and Whitledge 2005; Tremblay et al. 2009), contributes to the coincidence between the SCM and the SBM in northern BB. Because these communities also thrive higher in the euphotic zone than their counterparts in oligotrophic gyres, they can accumulate enough carbon to maintain a SBM.

Last, the maximum quantum yield of photochemistry for photosystem II (F_v/F_m) was generally high (median = 0.56) in the SCM, implying that the local phytoplankton communities were photosynthetically competent. The good vertical correspondence between the SCM and the degree of O_2 supersaturation (Figs. 2.3 & 2.6) implies that oxygenic photosynthesis at or in the vicinity of the SCM was sufficiently high to offset total community respiration, even at low irradiances.

The conceptual model that emerges from our findings and previous ones is that phytoplankton initially develop in the surface layer, where mineralization and mixing processes during winter replenish the inventory of NO_3^-. The size of this inventory, however, differs greatly between the various regions. In northern BB, surface concentrations at the end of winter are relatively high (up to 10 μM; Tremblay et al. 2002), whereas they are much lower in the BS (3 to 4 μM). In the latter, a marked nutricline is already present at ~25 m prior to the onset of the growth season. Nitrate is readily consumed in the upper mixed layer and the SCM forms very early at the time of ice breakup, after which diatoms lower the nutricline deeper into the upper halocline (Tremblay et al. 2008, Mundy et al. 2009) until light is insufficient to support net growth (i.e. compensation depth; Klausmeier and Litchman 2001).

The mechanism(s) controlling the vertical position, thickness and seasonal persistence of the SCM in the Arctic Ocean remain to be elucidated, but previous studies demonstrated

the importance of turbulent mixing (Zakardjian et al. 2000; Huisman et al. 2006) and variations in the buoyancy of diatoms (physiologically induced changes in response to nutrient supply and decrease of irradiance at the bottom of the euphotic zone: Steele and Yentsch 1960; Cullen 1982). The latter is presumably important in the strongly stratified BS. Surface communities composed largely of nano- and picophytoplankton (Tremblay et al. 2009) with some degree of motility presumably thrive reasonably well on recycled nitrogen, consistent with the generally high F_v/F_m near the surface (Fig. 2.8).

2.6.3 Biogeochemical significance of the SCM

The nitrogen initially taken up as NO_3^- by phytoplankton at the SCM may follow several paths, including (1) release as NO_2^- by diatoms, (2) assimilation into organic matter followed by vertical export or local recycling as NH_4^+ or dissolved organic nitrogen. The latter occurs via exudation or waste production by consumers and can be taken up again to fuel the "regenerated" component of primary production. Given the highly productive nature of the North Water in BB (Tremblay et al. 2002), the relatively large inventories of NH_4^+ beneath the SCM are also consistent with a progressive build up during the growth season, a result of export and ammonification during the microbial degradation of particulate organic matter and zooplankton excretion (Tremblay et al. 2006).

The positive relationship between the depth of the nitracline and the depth of the SCM at the synoptic scale (Figs. 2.6C & 2.7C) and throughout the growth season (Tremblay et al. 2008) suggests that NO_3^- accounts for a significant share of their nitrogen demand. The SCM more or less acts as a boundary, effectively preventing the upward diffusion of NO_3^- into the upper euphotic zone (Fig. 2.6C). This is consistent with previous reports that the SCM progressively lowers the nitracline during the growth season, accounting for at least half of the NO_3^- drawdown after ice break-up (Tremblay et al. 2008; Mundy et al. 2009). On a daily basis, however, local recycling may contribute a significant part of the nitrogen demand, which is consistent with the very low concentrations of NH_4^+ at and above the SCM throughout the Canadian Arctic.

The oxidation of NH_4^+ to NO_2^- by ammonia-oxydizing bacteria or, most likely, archea and to NO_3^- by nitrite oxydizers also supplies "recycled" nitrogen to phytoplankton (Ward

2002; Konneke et al. 2005). Nitrification can account for a substantial share of the NO_3^- demand in other stratified waters (e.g. Raimbault et al. 1999; Yool et al. 2007) and is hypothesized to supply a third of the NO_3^- renewal in the upper mixed layer of the coastal BS during winter (Tremblay et al. 2008). These issues have important implications for the operational estimation of new production (sensu Dugdale and Goering 1967) and the biogeochemical significance of the SCM. Striking spatial contrasts in the accumulation of NH_4^+ and NO_2^- at the base of the euphotic zone (Fig. 2.6D,E), which necessarily arises from imbalances between inputs and losses, provide additional insights into the ecology of Arctic SCM.

The well-defined maxima of NH_4^+ and NO_2^- at or immediately below the SCM in the southeast BS and AG were conspicuously absent in the eastern Canadian Arctic, which can be explained by physical and biological processes.

In the western Canadian Arctic, N^2 at and underneath the pycnocline is higher than in northern BB (Fig. 2.6A). This distinction is well rendered by NO_3^-, whose concentrations jump from 2 to 10 μM over a distance of 15 m in the AG versus 100 m in northern BB. In the former, the strong stratification limits the turbulent diffusion of solutes away from the SCM. In BB and the Atlantic end of LS, mixing is more likely to produce diffuse vertical structures such as those observed for NH_4^+ and NO_2^- (i.e. biological rates are presumably low relative to physical diffusion). The midnight sun may also have contributed to the absence of a PNM during August 2005 in northern BB, since previous experimental work showed nitrification to be completely inhibited at light:dark cycles exceeding 16:8 h (Horrigan et al. 1981). Under an 8 h light:16 h dark cycle similar to what prevailed in the Beaufort Sea during fall 2006, Horrigan et al. (1981) observed low but measurable daily rates of NH_4^+ oxidation in the euphotic zone. In that study, nitrite oxidizers were particularly sensitive to light and were active only under 24 h of darkness (Horrigan et al. 1981), which is consistent with the accumulation of NO_2^- we observed in the euphotic zone.

That NO_2^- concentrations were high and similar despite a 4-fold variation in NH_4^+ across the BS section suggests that PNMs were maintained mostly by light-limited phytoplankton in the lower trail of the SCM. The PNM was located at the base of the euphotic zone where phytoplankton can take up more NO_3^- than they can assimilate into organic matter, the

rationale being that reducing NO_3^- to NO_2^- is energetically cheap compared to reducing NO_2^- to NH_4^+ (Kiefer et al. 1976; Lomas and Lipschultz 2006). The NO_2^- trapped at the physiological bottleneck is released into the water. This scenario is consistent with the positive correlation observed between the concentrations of NO_2^- and NO_3^- ($r = 0.52$, $p < 0.001$), which is not likely to be driven mainly by NO_2^- oxidation since NO_3^- concentrations were primarily explained by salinity (implying physical processes; $r = 0.30$, $p < 0.05$).

2.7 Conclusion

Our observations confirm that photosynthetically-competent SCM are widespread in stratified oceanic waters of the Canadian Arctic and Subarctic during late summer and early fall. Since SCM also correspond to maxima of phytoplankton biomass, at least in northern BB, they presumably represent an important source of carbon for the food web and the sediment. In contrast with those of other oceans, Arctic SCM (1) are located relatively high in the euphotic zone, (2) are generally disconnected from the upper mixed layer and, at times, (3) contain a disproportionately high and poorly predictable portion of total biomass in the euphotic zone. These conditions present a unique set of challenges for the estimation of biomass and primary production with orbiting sensors that scrutinize the upper mixed layer. Although previously published global, statistical relationships between surface chl *a*, integrated chl *a* and the shape of the vertical chl *a* profile hold reasonably well for the Canadian Arctic, they can lead to severe underestimation when the SCM is sharp and intense in clear oceanic waters. Given their prevalence, the repercussions of SCM for the accuracy of remote-sensing estimations of primary production in the Arctic Ocean should be quantified.

By virtue of their longevity and widespread occurrence, SCM in the BS share common traits with those of subtropical oceanic gyres. Prompt depletion of the modest NO_3^- inventories present in the upper mixed layer at the onset of the productive period drives the early appearance of SCM, whose longevity currently depends on the duration of the ice-free season. The September minimum extent of sea-ice extent decreased at the mean rate of 9% between 1978 and 2006 and reached dramatic record lows in 2007 and 2008 as the

multiyear ice was largely replaced by seasonal ice (NSIDC 2009). It is likely that a protracted ice-free season will allow SCM to lower the nitracline further and make an increased contribution to annual primary production, except where mixing or upwelling replenish nutrients at the surface.

The relative importance of SCM for water-column primary production and the food web is also likely to increase as freshwater deliveries by rivers, precipitation and glacier melt rise (Wu et al. 2005). Due to the ensuing increase in vertical stability and decrease in convection during seasonal cooling and ice growth, phytoplankton communities in the interior of the Arctic Ocean may come to rely even more on the availability of nutrients at the base of the euphotic zone. The importance of allochthonous versus locally recycled nitrogen for the nutrition of SCM communities remains largely unknown, although our results suggest that nitrification plays a lesser role in the Arctic than in warm oceans. Ongoing investigations into the roles that physical (e.g. mixing, diffusion) and biological (e.g. nitrogen cycling, photo-acclimation, functional diversity and buoyancy-regulation) processes play in the persistence and productivity of SCM will help elucidate their biogeochemical significance in an era of drastic environmental changes.

Chapitre 3 Nutritive and photosynthetic ecology of subsurface chlorophyll maxima in Canadian Arctic waters

3.1 Résumé

L'estimation des taux d'assimilation de carbone et d'azote (N) dans les eaux de l'Arctique canadien a confirmé l'importante contribution des maximums de chlorophylle subsuperficiels (SCM) à la production de matière organique dans la colonne d'eau durant toute la saison de production. Bien que les communautés retrouvées au SCM ont démontré une capacité d'acclimatation à la pénombre et à la disponibilité accrue du nitrate (NO_3^-), leur productivité était généralement limitée par la lumière et la température. Pendant le printemps et le début de l'été, la majeure partie de la production primaire au SCM était soutenue par la prise de NO_3^- avec un *f*-ratio moyen (i.e. contribution de la prise de NO_3^- à la prise totale de N) de 0.74 ± 0.26. La diminution de la disponibilité du NO_3^- et de la lumière au cours de la période de production, couplée à l'augmentation des concentrations en ammonium (NH_4^+) ont favorisé une transition vers un système dominé par le recyclage et la production régénérée (*f*-ratio = 0.37 ± 0.20). Ces résultats soulignent l'importance de tenir compte des SCM de manière réaliste lors de l'estimation de la production primaire et d'actualiser les paramètres utilisés dans les modèles écosystémiques appliqués aux environnements fortement stratifiés tels que l'Arctique canadien.

3.2 Abstract

Assessments of carbon and nitrogen (N) assimilation in Canadian Arctic waters confirmed the large contribution of subsurface chlorophyll maxima (SCM) to total water-column production from spring to late fall. Although SCM communities showed acclimation to low irradiance and greater nitrate (NO_3^-) availability, their productivity was generally constrained by light and temperature. During spring-early summer, most of the primary production at the SCM was sustained by NO_3^-, with an average *f*-ratio (i.e., relative contribution of NO_3^- uptake to total N uptake) of 0.74 ± 0.26. The seasonal decrease in NO_3^- availability and irradiance, coupled to the build up of ammonium (NH_4^+), favoured a transition toward a predominantly regenerative system (*f*-ratio = 0.37 ± 0.20) during late summer and fall. Results emphasize the need to adequately consider SCM when estimating primary production and to revisit ecosystem model parameters in highly stratified Arctic waters.

3.3 Introduction

In the Arctic Ocean, the extreme solar cycle and the formation, ablation and motion of sea ice exert a major influence on light availability in the water column (Smith and Harrison 1991; Sakshaug 2004). While these processes constrain the timing of algal production and impose large, short-term light fluctuations during the growth period, first-order differences in the annual primary production of seasonally-open waters ultimately depend on mixing regime, which modulates the supply of nitrogen (N) to the upper euphotic zone (Tremblay and Gagnon 2009; Ardyna et al. 2011)

In peripheral Arctic seas (e.g., Bering Sea, Barents Sea, eastern Baffin Bay) the relatively weak vertical stratification allows for vertical mixing that recharges the euphotic zone with nutrients at least once a year (Tremblay et al. 2002). In the interior (e.g., Chuckchi and Beaufort seas), however, low-salinity waters entering through Bering Strait and the freshwater supplied by rivers impart strong vertical stratification. Although large quantities of nutrients are supplied by the Bering Sea, N is depleted in the surface waters of the Chukchi Sea and weakly replenished downstream in the Beaufort Sea (Tremblay et al. 2008). In the coastal Canadian Arctic, the pycnocline is shallow nearly everywhere (between 14 and 32 m) but is stronger in the west (where the Brunt-Väisälä or buoyancy frequency, N^2, reaches up to 0.004 s^{-2} in Amundsen Gulf) than in the east (where N^2 generally ranges from 0.0006 to 0.002 s^{-2} in Baffin Bay and Lancaster Sound; Martin et al. 2010).

Recent work showed that strongly opposing vertical gradients of irradiance and inorganic N in the coastal Canadian Arctic result in the widespread occurrence of subsurface chlorophyll maxima (SCM). These SCM are located relatively high in the euphotic zone and show a strong association with the nitracline by comparison with those observed in other oceans (e.g., SCM in tropical oceans are located at the base of or below the euphotic zone, above the nitracline and do not correspond to a biomass or productivity maximum; Martin et al. 2010). Arctic SCM communities are numerically dominated by flagellates with important contributions of large-sized diatoms (Ardyna et al. 2011; Palmer et al. 2011; Martin et al. 2010) that presumably account for a disproportionate share of the carbon biomass and productivity.

Since the Canadian Arctic represents a large portion of the Arctic (ca. 27%) and because SCM there are seasonally persistent, highly photosynthetically-competent and closely associated with the nitracline, Martin et al. (2010) hypothesized that SCM mediate a large share of new production, i.e., the portion of total primary production based on the uptake of allochthonous N (e.g., nitrate, NO_3^-). Due to their positioning in the water column, SCM probably act as a "nutrient trap" that further weakens N renewal and new production in the upper euphotic zone (see also Taylor et al. 1986 and Harrison 1990). However, Martin et al. (2010) also found that most SCM in the Canadian Arctic operate at very cold temperatures (< 1°C), which possibly limits their contribution to water-column productivity since phytoplankton do not exhibit specific adaptations to low temperature in the Arctic (Platt et al. 1982; Smith and Harrison 1991).

In the study of Martin et al. (2010), the combination of low levels of ammonium (NH_4^+) at and above the SCM with rapidly increasing concentrations underneath suggested that local N recycling is important for SCM communities. It follows that regenerated production possibly fuels a substantial part of total primary production on a daily basis. When abundant, reduced N (i.e., NH_4^+ and urea) is generally preferred over NO_3^-, whereas all N forms tend to be used in proportion to their availability when total N is lower than phytoplankton demand (McCarthy et al. 1977; Harrison et al. 1982). Whether SCM communities are predominantly regenerative or efficient vectors of export toward top predators or the deep ocean remains to be assessed.

The main objective of this study was to evaluate how the uptake of carbon (C) and N by primary producers responds to the availability of light and nutrients at the SCM. Secondary goals were to generate uptake-irradiance parameters to inform ecosystem models or remote-sensing algorithms, and to produce a preliminary assessment of the relative contribution of SCM layers to water-column production, based on a limited comparison of surface and SCM samples. In selecting a methodological approach, we also considered previous studies showing that C and N uptake can be partly decoupled in the short-term (i.e. may not lead to primary organic synthesis), especially at low irradiances such as observed at the SCM (Price et al. 1985; Cochlan et al. 1991; Smith and Harrison 1991). This decoupling can be caused by luxury uptake, whereby algae store NO_3^- or release NO_2^-

after incomplete reduction, bacterial N uptake (Kirchman and Wheeler 1998, Allen et al. 2002), or a greater capacity for algal N uptake (relative to C) under low irradiance (Smith and Harrison 1991; Probyn et al. 1996). For all these reasons, we elected to measure C and N uptake simultaneously, using short-term incubations in light-gradient, laboratory modules, instead of classical 24-hr incubations on deck (e.g., Simpson et al. 2013; Brugel et al. 2009; Fouilland et al. 2007; Smith et Harrison 1991; Harrison et al. 1982; Platt et al. 1982). The latter are useful to provide daily rates and biogeochemical snapshots at a given location, but do not provide dynamical parameters (e.g., maximum uptake at light saturation, initial slope of the uptake-irradiance relationship) to quantify and model physiological state, acclimation, and responses to experimental or natural changes in growth conditions.

3.4 Materials and methods

3.4.1 Sampling

During 2005 (16 August to 16 October), 2006 (4 September to 4 November), 2007 (28 September to 6 November) and 2008 (26 April to 13 July) expeditions of the *CCGS Amundsen*, 983 vertical profiles were obtained with a CTD-Rosette equipped with sensors to measure *in vivo* fluorescence (SeaPoint Chlorophyll Fluorometer), transmissivity (WET Labs CST-671DR), dissolved oxygen (Sea-Bird SBE43), NO_3^- (SATLANTIC ISUS V1), photosynthetically active radiation (PAR; Biospherical QCP-2300), temperature and salinity (Sea-Bird SBE-911*plus*). Our sampling covered the entire latitudinal and longitudinal swath of the Canadian Archipelago, including Baffin Bay, the Northwest Passage, the Beaufort Sea, Foxe Basin, Hudson Bay and three Labrador fjords (Fig. 3.1).

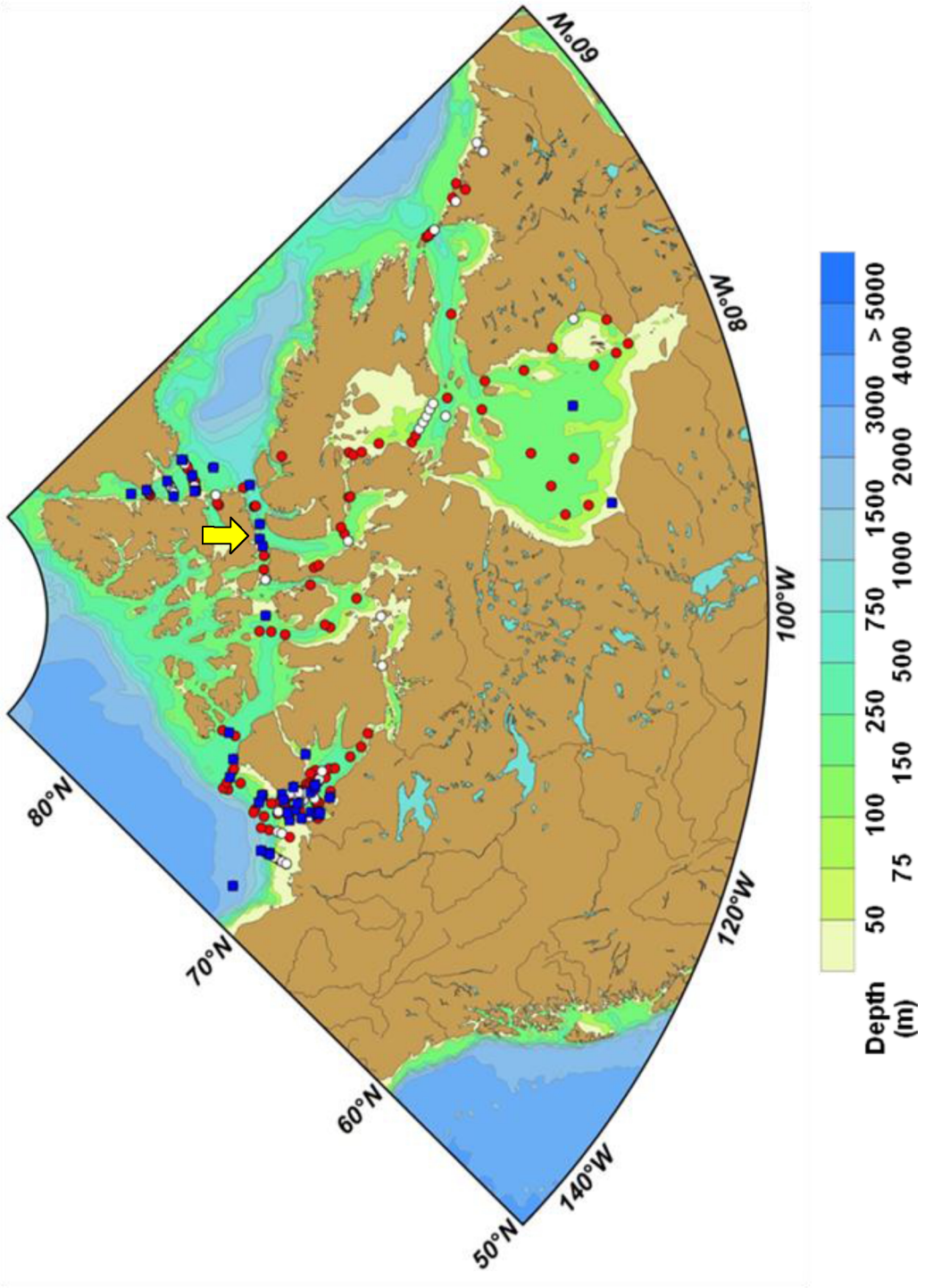

Figure 3.1 Location of all sampling stations (red circles) and those where incubation were performed (blue squares). Open symbols represent stations with no visible SCM and the yellow arrow points to station 303, which is analyzed separately in the text.

Table 3.1 Characteristics of the SCM at experimental stations located in the coastal Beaufort Sea (CBS), offshore Beaufort Sea (OBS), North-West Passage (NWP), western, central and eastern Baffin Bay (WBB, CBB and EBB, respectively) and Hudson Bay (HB) for spring-early summer and late summer-fall. Stations where incubations were also performed with surface samples are marked with an asterisk, "n/d" indicates that no data were available and "-" stands for values below the limit of detection. Averages (AVG) and standard deviations (SD) are presented for each season.

Region	Station	Date	Day of year	Depth (m)	[chl *a*] (µg/L)	$[NO_3^-]$ (µM)	$[NO_2^-]$ (µM)	$[NH_4^+]$ (µM)	[Urea] (µM)	Total N (µM)	*T* (°C)	% of *E* at surface	E_{SCM} (µmol quanta m^{-2} s^{-1})
CBS	D43[1]	28-04-2008	119	30	0.73	3.63	0.09	0.02	-	3.77	-1.7	6.4	0.3
CBS	1020A	06-05-2008	127	44	0.46	6.21	0.26	0.02	-	6.54	-1.7	8.8	44
CBS	405b	19-05-2008	140	16	8.31	0.00	0.10	0.05	-	0.15	-1.0	16	62
CBS	1011	21-05-2008	142	63	0.88	6.53	0.11	1.01	-	7.66	-1.5	1.7	5.8
CBS	1806	23-05-2008	144	50	4.47	7.53	0.11	-	-	7.65	-1.4	4.3	18
CBS	9008	27-05-2008	148	37	12.10	1.34	0.08	-	-	1.42	-1.2	6.8	31
CBS	405	01-06-2008	153	37	0.53	4.02	0.16	0.20	-	4.38	-1.7	11	36
CBS	F7[1]	08-06-2008	160	12	2.98	1.87	0.18	0.25	0.1	2.42	-1.4	44	30
CBS	405b	10-06-2008	162	37	0.84	2.32	0.19	0.10	0.1	2.75	-1.2	4.8	30
CBS	F7[1]	19-06-2008	171	33	9.57	5.00	0.16	0.35	-	5.52	-1.4	4.7	1.6
CBS	FB07[1]	21-06-2008	173	37	4.42	1.16	0.14	0.16	-	1.53	-1.3	2.7	9
CBS	1216	23-06-2008	175	33	1.27	3.44	0.12	0.18	-	3.74	-1.4	2.2	15
CBS	F7[1]	24-06-2008	176	33	4.80	1.61	0.08	0.63	-	2.34	-1.3	6.7	25
CBS	1200	27-06-2008	179	36	1.52	0.80	0.16	0.09	0.1	1.18	-1.2	2.7	17
CBS	1208	28-06-2008	180	35	1.64	0.10	0.00	-	0.2	0.27	-1.1	1.7	11
OBS	421	01-07-2008	183	62	3.55	0.79	0.08	0.08	-	0.96	-1.2	2.8	20
CBS	6006	04-07-2008	186	54	7.55	4.55	0.20	0.06	0.2	5.05	-1.3	2.0	12
CBS	2010	06-07-2008	188	29	0.37	3.89	0.14	0.04	0.2	4.25	-1.5	5.9	30
CBS	410	08-07-2008	190	54	1.25	3.54	n/d	0.26	-	3.80	-1.5	4.6	28
CBS	416	10-07-2008	192	73	4.52	6.77	0.14	0.19	-	7.10	-1.4	0.9	5.4
			AVG	40	3.59	3.26	0.13	0.22	0.15	3.62	-1.4	7.0	23
			(SD)	(15)	(3.42)	(2.32)	(0.06)	(0.25)	(0.05)	(2.40)	(0.2)	(9.3)	(15)

[1] E_{SCM} corrected for the presence of ice-covered.

Region	Station	Date	Day of year	Depth (m)	[chl *a*] (µg/L)	[NO_3^-] (µM)	[NO_2^-] (µM)	[NH_4^+] (µM)	[Urea] (µM)	Total N (µM)	*T* (°C)	% of *E* at surface	E_{SCM} (µmol quanta $m^{-2}s^{-1}$)
EBB	BA01-05	16-08-2005	228	24	0.88	0.28	0.08	0.05	n/d	0.41	0.0	9.2	12
WBB	BA03-05	18-08-2005	230	42	2.14	0.07	0.06	-	n/d	0.13	1.9	0.5	1.3
CBB	BA04-05	22-08-2005	234	25	1.05	5.34	0.30	-	n/d	5.64	-1.4	10	24
NWP	S3	23-08-2005	235	33	3.45	2.73	0.12	0.33	n/d	3.18	-0.7	4.8	4.0
NWP	S4	24-08-2005	236	29	6.38	0.49	0.09	0.39	n/d	0.97	-1.1	4.4	7.9
CBS	S201	02-09-2005	245	19	0.79	1.13	0.10	0.41	n/d	1.64	0.4	3.6	7.9
OBS	S10	05-09-2005	248	52	0.41	2.34	0.12	0.14	n/d	2.60	-1.0	9.3	20
CBS	CA08-05	09-09-2005	252	43	0.41	0.70	0.10	-	n/d	0.80	-0.2	8.1	12
CBS	CA18-05	12-09-2005	255	30	2.70	4.82	0.22	0.11	n/d	5.15	-1.1	4.4	8.0
HB	S22	06-10-2005	279	35	0.83	0.70	0.09	0.04	n/d	0.83	-1.4	2.5	1.3
HB	NR24	10-10-2005	283	17	1.35	1.03	0.08	0.25	n/d	1.36	5.1	0.8	1.9
CBB	132*	09-09-2006	252	34	0.32	4.03	0.09	0.34	n/d	4.46	-1.4	2.4	1.2
EBB	131*	11-09-2006	254	35	0.62	4.84	0.23	0.47	n/d	5.54	-0.2	1.3	2.4
WBB	118	14-09-2006	257	50	1.84	1.23	0.07	0.12	n/d	1.42	-1.2	0.1	0.1
CBB	108*	17-09-2006	260	40	1.50	2.32	0.11	0.34	n/d	2.77	0.7	0.9	1.4
NWP	303*	21-09-2006	264	22	1.36	2.34	0.06	0.64	n/d	3.04	0.2	12	20
NWP	307*	23-09-2006	266	31	0.16	5.47	0.12	0.63	n/d	6.22	-1.3	9.1	12
CBS	405*	01-10-2006	274	48	0.67	8.30	0.47	0.30	n/d	9.07	-1.3	0.8	0.8
CBS	408*	03-10-2006	276	67	0.32	7.13	0.27	0.09	n/d	7.49	-1.3	2.1	2.1
CBS	SH (409)*	04-10-2006	277	35	0.47	0.19	0.09	0.25	n/d	0.53	0.4	2.2	2.4
CBS	436	09-10-2006	282	18	0.65	0.03	0.07	0.04	n/d	0.14	0.4	11	3.0
CBS	435*	12-10-2006	285	55	0.16	3.69	0.20	0.03	n/d	3.92	-1.2	3.3	1.5
CBS	407	18-10-2006	291	30	0.70	0.88	0.15	0.13	n/d	1.16	-0.5	2.6	0.9
WBB	101	29-09-2007	272	41	0.31	1.66	0.00	0.79	n/d	2.45	-1.6	1.4	n/d
EBB	115	01-10-2007	274	80	0.13	10.6	0.12	-	-	10.73	-0.8	0.001	n/d
CBB	108	03-10-2007	276	30	5.62	2.22	0.03	0.35	-	2.61	-0.6	3.4	n/d
NWP	302	07-10-2007	280	37	0.24	0.63	0.03	0.51	-	1.17	0.4	6.1	n/d
CBS	435	17-10-2007	290	16	0.24	1.85	0.02	0.29	-	2.16	-0.9	24	6.1
CBS	1806	19-10-2007	292	22	0.33	0.00	0.02	0.02	-	0.04	-0.8	17	1.7
CBS	408	22-10-2007	295	12	0.65	0.51	0.15	0.32	n/d	0.98	-1.1	22	3.3
CBS	407	23-10-2007	296	34	0.70	2.28	0.14	0.34	n/d	2.76	-1.3	4.1	0.4
CBS	405	25-10-2007	298	31	0.23	0.47	0.06	0.17	n/d	0.70	-0.7	6.0	0.8
CBS	1116	28-10-2007	301	7	0.23	7.10	0.31	0.46	-	7.89	-1.5	47	12
			AVG	34	1.15	2.65	0.13	0.29	-	3.03	-0.5	7.2	5.9
			(SD)	(15)	(1.47)	(2.70)	(0.10)	(0.20)	(-)	(2.79)	(1.3)	(9.3)	(6.6)

3.4.2 Nutrients

Nutrient determinations were performed at subsets of 265 stations for NO_3^- and NO_2^- (55 in 2005, 85 in 2006, 52 in 2007 and 73 in 2008) and 129 stations for NH_4^+ (35 in 2005, 29 in 2006, 22 in 2007 and 43 in 2008). Samples were taken at the SCM and at standard depths (5, 10, 20, 30, 40, 50, 60, 70, 80, 100, 125, 150, 175, 200, 250, 300 m and then every 100 m where the Arctic halocline was not present. Otherwise, sampling in the 100–200 m range occurred at every 20 m and at a salinity of 33.1 to capture the nutrient maximum; see Martin et al., 2010 for details). Samples were collected in acid-cleaned tubes (stored with 10% HCl) and stored in the dark at 4°C. Concentrations of $NO_3^- + NO_2^-$ and NO_2^- were determined within a few hours using standard colorimetric methods (Grasshoff et al., 1999) adapted for the AutoAnalyzer 3 (Bran + Luebbe) and NH_4^+ was measured manually with the sensitive fluorometric method (Holmes et al., 1999). For the latter, reagents were added within minutes of sample collection. Urea samples were either frozen or analyzed fresh using the method of Mulveena and Savidge (1992) and Goeyens et al. (1998). The analytical detection limits for NH_4^+ and urea were 0.02 µM and 0.1 µM, respectively.

3.4.3 Chlorophyll and F_v/F_m

Chlorophyll *a* (chl *a*) concentration and photosynthetic competency (F_v/F_m) at the surface (5 m) and the SCM depth were analysed at the 129 stations where NH_4^+ determinations were also performed (see section 2.2). Concentrations of chl *a* were determined using the fluorescence method (Parsons et al. 1984) and F_v/F_m by Pulse-Amplitude-Modulated fluorometry (WALZ Phyto-PAM; see details in Martin et al. 2010). F_v/F_m measurements were also used to assess the response of SCM and surface communities to experimental treatments. Samples were obtained from bottles after their incubation and dark adapted for 30 minutes before analysis.

3.4.4 Incubations

Of the 129 stations sampled for chl *a* concentrations and F_v/F_m, 59 were selected for light-gradient incubations with water collected at SCM depth (11 in 2005, 12 in 2006, 10 in 2007 and 26 in 2008). In 2006, 9 of the 12 incubations examined NO_3^- uptake simultaneously for surface (5 m) and SCM communities (Table 3.1). Most samples were

taken during the local morning. Relationships between PAR (E; estimated with a Biospherical QSL-2101 light sensor) and the uptake of C and N by phytoplankton from the SCM were assessed in four, ten-position light-gradient incubators designed to minimize spectral shift and accurately resolve photosynthetic parameters, especially in oligotrophic waters (Babin et al. 1994). Full-spectrum, 400-W Optimarc metal-halide lamps mimicking solar irradiance were used in combination with a blue filter (118 Light Blue Lee Filters Ltd.) and optically-neutral filters (Lee Filters) to simulate the coastal underwater light spectrum (Hill and Cota 2005; Carmack et al. 2004; Harrison et al. 1977). Actual PAR values in the incubators were kept in the low range to reproduce conditions near the SCM (from 664.2 to 0.3 μmol quanta^{-1} m^{-2} s^{-1} in 2005, with 6 of the 10 light intensities below 100 μmol quanta m^{-2} s^{-1} and from 309.1 to 1.8 μmol quanta^{-1} m^{-2} s^{-1} in 2006, 358.0 to 3.0 μmol quanta^{-1} m^{-2} s^{-1} in 2007 and 281.0 to 1.8 μmol quanta^{-1} m^{-2} s^{-1} in 2008, with 8 or 9 of the 10 light intensities below 100 μmol quanta m^{-2} s^{-1}). Temperature was maintained at *in situ* levels with a chilling circulator.

Samples from all incubators were spiked with ^{13}C-bicarbonate; one incubator was enriched with $^{15}NO_3^-$ (10 μM) and another with either $^{15}NH_4^+$ (4 μM) or $^{15}NO_2^-$ (2 μM). The other two incubators received trace additions (10% of ambient concentrations) of the same N substrates in order to match *in situ* conditions. Experiments that compared surface and SCM communities were performed with enriched and trace additions of $^{15}NO_3^-$ only. Incubations were kept short (5 – 6 h) to minimize isotopic dilution and were terminated by filtration onto 24-mm glass microfibre filters (Whatman GF/F; vacuum pressure < 250 mmHg). All filters were desiccated at 60°C and stored dry for post-cruise analysis. An elemental analyzer (ECS 4010, Costech Analytical Technologies Inc.) coupled to a mass spectrometer (Delta V Advantage, Thermo-Finnigan) was used to determine isotopic enrichment and particulate organic carbon and nitrogen using a modified Dumas method (for details see Blais et al. 2012). Specific C and N uptake was calculated using Equation 3 of Collos (1987).

3.4.5 Sensor calibrations and data transformations

Detailed vertical profiles were obtained with a CTD and attached sensors (see Martin et al. 2010 for detailed post-calibration procedures). The depths (Z) of the pycnocline and nitracline were identified as those where the vertical gradients of the Brunt-Väisälä (or buoyancy) frequency (N^2; s^{-2}) and NO_3^- had the highest values, respectively. The depth of the SCM was defined as the depth where the *in vivo* fluorescence was at a maximum. Daily-averaged PAR at the SCM (E_{SCM}) and at other sampling depths was calculated using the coefficient of diffuse light attenuation (k; see Martin et al. 2010 for calculation method) and a continuous record of incident PAR above the sea surface (Kipp and Zonen; PARLite) to estimate E_0. Values of E_0 were corrected for surface reflectance based on the work of Sakshaug and Slagstad (1991) and assuming a mean loss of 7.5% for the high Canadian Arctic (Mei et al. 2002).

Chl *a* normalized (superscript B) photosynthesis-irradiance parameters (and standard errors on these parameters) were calculated using the empirical exponential models that provided the best fit to the data. The model of Platt et al. (1980) was used when photoinhibition occurred:

$$P^B = P_s^B[1\text{-}\exp(-\alpha E/P_s^B)][\exp(-\beta E/P_s^B)] \quad (1)$$

with

$$P_m^B = P_s^B[\alpha/(\alpha+\beta)][\beta/(\alpha+\beta)]^{\beta/\alpha} \quad (2)$$

and the model of Webb et al. (1974) when photoinhibition was not apparent

$$P^B = P_m^B[1\text{-}\exp(-\alpha E/P_m^B)] \quad (3)$$

where P_m^B is the maximum observed uptake rate [µg C (µg chl a)$^{-1}$ h^{-1}], E is the incubation irradiance (PAR, µmol quanta m^{-2} s^{-1}), and α and β in units of [µg C (µg chl a)$^{-1}$ h^{-1} (µmol quanta m^{-2} s^{-1})$^{-1}$] are the photosynthetic efficiency at low irradiance (initial slope of the relationship) and the photoinhibition parameter, respectively. The models of Platt et al. (1980) and Webb et al. (1974) were previously shown to give

similar results (Frenette et al. 1993). The photoacclimatation index (E_k; µmol quanta m^{-2} s^{-1}) was calculated as:

$$E_k = P_m^B/\alpha \quad (4)$$

The same model parameters were estimated for nitrogen uptake (in which case the letter N substitutes for P in Eqs. (1) to (3) and N form identified with subscript $_{NO3}$, $_{NO2}$ and $_{NH4}$), with the inclusion of a term for dark uptake (D^B in [µg N (µg chl a)$^{-1}$ h^{-1}] on the right hand side of equations 1 and 3 (Priscu 1989). While some studies also include a dark term for C uptake, here the intercept of the initial slope of the photosynthesis-irradiance relationship never differed significantly from zero. A more robust estimation of D^B for N uptake was done *a posteriori* by taking the y-intercept ($E = 0$) of the linear portion of the relationship at low irradiance. On average, standard errors were 8 ± 7%, 11 ± 8% and 15 ± 9% for the photosynthetic parameters P_m^B, α and E_k, respectively, and 21 ± 36%, 31 ± 27%, 54 ± 70% and 41 ± 44% for the N uptake parameters $N_m{}^B{}_{(NO3\ and\ NH4)}$, $\alpha_{(NO3\ and\ NH4)}$, $D^B{}_{(NO3\ and\ NH4)}$ and $E_{k\ (NO3\ and\ NH4)}$, respectively. For consistency with all other Arctic studies reporting uptake-irradiance parameters obtained with artificial light sources (Gallegos et al. 1983; Lewis and Smith 1983; Gosselin et al. 1986; Harrison 1986; Hirche et al. 1991; Kristiansen and Lund 1989; Kristiansen and Farbrot 1991; Kristiansen et al. 1994; Cota et al. 1996; Carmack et al. 2004; Palmer et al. 2011) and due to our need to compared photosynthesis and N uptake (whose coupling with photochemistry is not as straightforward as for C fixation), we did not perform a posteriori corrections of α for differences in light spectrum between the incubators and the water column.

Since irradiance varied between incubators, the *f*-ratio ($N^B{}_{NO3}$ / [$N^B{}_{NO3}$ + $N^B{}_{NH4}$]) at a given irradiance was calculated using uptake values predicted from individual N^B-E curves for NO_3^- and NH_4^+. The resulting *f*-ratio-E curves were used to assess the *f*-ratio and the relative preference index (RPI) for NO_3^- uptake at E_{SCM}. The RPI was calculated by dividing the *f*-ratio by the relative contribution of NO_3^- to total inorganic N concentration (NO_3^- + NH_4^+) and represented the degree to which NO_3^- was selected (RPI > 1) or discriminated (RPI < 1) over NH_4^+ (McCarthy et al. 1977).

3.4.6 Statistical analyses

The geometric mean regression (model II linear regression; considering error on both variables) was used to assess functional relationships between variables. Relationships between environmental variables and uptake-irradiance parameters for C and N were determined with the Pearson's product moment correlation (PPMC) and differences between treatments were evaluated with a paired t-test when data were distributed normally or the Wilcoxon's signed-rank test otherwise (SigmaPlot 11, Systat Software). When relevant, descriptive statistics were calculated separately for the spring-early summer period and late summer-fall period (see Table 3.1).

3.5 Results

3.5.1 General conditions in the sampling area

Unless stated otherwise, the descriptions below refer to all data from 2005 to 2008. When appropriate, separate results are reported for the subset of stations where C and N uptake rates were measured (hereafter termed "experimental stations") in order to demonstrate that sub-sampling was representative of the whole data set. Distinct SCM were present at 81% of the 465 stations analyzed (Fig. 3.1; see Martin et al. (2010) for a discussion of the other stations where chl *a* was maximum at the surface or vertically homogenous). The depth of the SCM ranged from 4 to 114 m with a mean of 35 ± 16 m (at experimental stations the range was 11 - 75 m and the mean 36 ± 15 m). The vertical position of the SCM matched the depth of the nitracline (mean = 38 ± 16 m for all stations and 40 ±17 m for experimental ones) within ± 10 m in 79% (67% for experimental stations) of the cases and within ± 20 m in 89% (88% for experimental stations) of cases ($Z_{SCM} = 1.00 \times Z_{nitracline} - 2.57$, $r^2 = 0.46$, $p < 0.0001$ for all stations; $Z_{SCM} = 1.12 \times Z_{nitracline} - 9.24$, $r^2 = 0.41$, $p < 0.0001$ for experimental stations). Primary maxima of NO_2^- (PNM) and NH_4^+ (PAmM) were widespread (not shown but see Martin et al., 2010) and their vertical positions were significantly correlated with the SCM ($Z_{PNM} = 0.50 \times Z_{SCM} + 39.23$, $r^2 = 0.12$, $p < 0.0001$, $n = 201$; $Z_{PAmM} = 0.72 \times Z_{SCM} + 25.75$, $r^2 = 0.20$, $p < 0.0001$, $n = 96$).

F_v/F_m was generally high at the surface and the SCM (not shown), with median values of 0.55 and 0.58, respectively (see Martin et al., 2010). Although the overall data distribution

was similar for the two sampling depths, a comparison of locally paired samples showed F_v/F_m to be significantly higher at the SCM during spring-early summer (2008 expedition; Wilcoxon's signed-rank test, $p < 0.001$). This difference was not apparent during late summer-fall (2005, 2006 and 2007 expeditions; $p = 0.76$).

Table 3.1 provides the details of physical and chemical properties at Z_{SCM} for experimental stations. Temperature ranged from -1.7 to 5.1°C and exceeded 0°C in only 17% of cases. Daily averaged irradiance varied between 0.1 and 62 µmol quanta m^{-2} s^{-1} across stations (overall mean of 13 ± 13 µmol quanta m^{-2} s^{-1}), representing 0.001 to 47% of incident irradiance at the surface (mode in the 1 - 10% range for 68% of stations). Concentrations of NO_3^- ranged from the limit of detection to 10.6 µM but were generally lower than 2 µM (47% of stations), whereas NH_4^+ concentrations ranged from the limit of detection to 1.0 µM, with values below 0.2 µM at 55% of stations. The concentrations of NO_2^- and urea remained relatively low. Overall, 99% of the variability in the concentration and 78 ± 24% of the total amount of inorganic N (i.e., $NO_3^- + NO_2^- + NH_4^+$) at the SCM were due to NO_3^-.

3.5.2 Difference in uptake-irradiance parameters between surface and SCM communities

At stations where incubations were performed simultaneously (see Table 3.1) with surface and SCM samples, P_m^B did not differ significantly between the two communities (Fig. 3.2; $n = 9$, paired t-test $p = 0.212$; all results are presented in Appendix C), whose mean values were 0.82 ± 0.35 and 0.64 ± 0.46 µg C (µg chl *a*)$^{-1}$ h^{-1}, respectively. However, α was significantly lower at surface than at the SCM (Fig. 3.2; mean of 0.026 ± 0.013 *versus* 0.033 ± 0.015 µg C (µg chl *a*)$^{-1}$ h^{-1} (µmol quanta m^{-2} s^{-1})$^{-1}$; Wilcoxon's signed-rank test $p < 0.01$), driving a decrease in E_k between surface and SCM depth (Fig. 3.2; mean of 33 ± 7 µmol quanta m^{-2} s^{-1} at the surface and 19 ± 9 µmol quanta m^{-2} s^{-1} at the SCM; paired t-test $p < 0.01$). Photoinhibition was observed only at the SCM, for which β varied between 0 and 0.0006 µg C (µg chl *a*)$^{-1}$ h^{-1} (µmol quanta m^{-2} s^{-1})$^{-1}$ (data not shown).

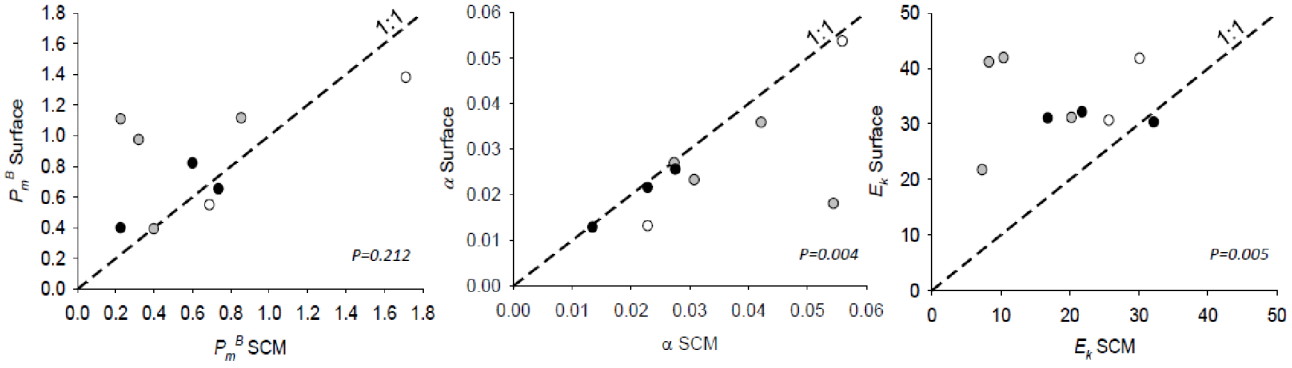

Figure 3.2 Comparison of photosynthesis-irradiance parameters (P_m^B, α and E_k) between the surface and the SCM in Baffin Bay (black), the Canadian Archipelago (white) and the Beaufort Sea (gray). The level of significance (p) for the difference between paired samples is given in each panel.

The $N_m^B{}_{(NO3)}$ (not shown) was clearly lower at the surface than at the SCM (mean of 0.018 ± 0.022 and 0.031 ± 0.021 µg N (µg chl *a*)$^{-1}$ h^{-1}, respectively; n = 8; paired t-test $p < 0.05$). However, $\alpha_{(NO3)}$ (mean of 0.001 ± 0.002 *versus* 0.003 ± 0.003 µg N (µg chl *a*)$^{-1}$ h^{-1} (µmol quanta m^{-2} s^{-1})$^{-1}$) and $E_{k(NO3)}$ (mean of 18 ± 14 *versus* 15 ± 9 µmol quanta m^{-2} s^{-1}) were not significantly different (Wilcoxon's signed-rank test $p = 0.578$ and 0.844, respectively).

In order to assess the contribution of the SCM layer (defined as the zone between the top of the SCM – i.e. the first depth where the mean vertical gradient of *in vivo* fluorescence was zero over 5 consecutive depth bins – and the bottom of the euphotic zone, set here as the depth of the 0.1% of surface irradiance) to daily primary production and NO_3^- uptake during 2006, we combined uptake-irradiance parameters with measurements of daily mean irradiance and detailed vertical profiles of chl *a* reconstructed from calibrated *in vivo* fluorescence. A specific example is given in Figure 3.3 for station 303, which is representative of mean conditions for this data set (see yellow arrow in Fig. 3.1). In this case, we prescribed the uptake-irradiance parameters of the surface community between 0 and 14 m (which coincidentally matched the depth of the pycnocline at this station) and those of the SCM from 14 to 71 m (based on the fact that $N_m^B{}_{(NO3)}$ neither varied with ambient NO_3^- concentrations nor experimental enrichment; see section 3.7 and Table A2).

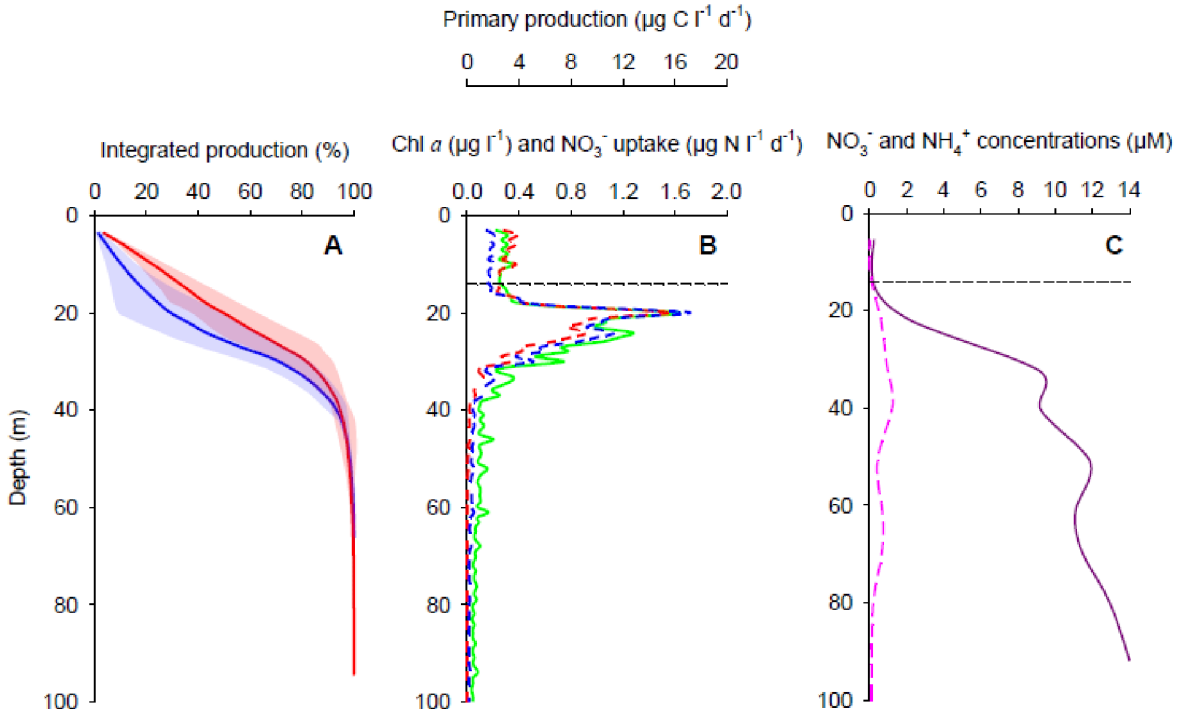

Figure 3.3 Reconstructed profiles of (A) averaged integrated production (% of total water-column production; standard deviation delimited by the shaded areas) for C uptake (red) and N uptake (blue) for incubations performed simultaneously with surface and SCM samples, (B) chl *a* concentration estimated from post-calibrated *in vivo* fluorescence (µg l^{-1}; solid green line) and primary production (µg C l^{-1} d^{-1}; red dashed line) and NO_3^- uptake (µg N l^{-1} d^{-1}; blue dashed line) estimated from uptake-irradiance parameters and (C) NO_3^- (solid purple line) and NH_4^+ (pink dashed line) concentrations (µM) for station 303 in 2006 (yellow arrow in Fig. 3.1; left-hand side). The black dashed line marks the depth of the pycnocline (14 m).

We observed that the SCM layer mediated 43 to 76% of C uptake (mean = 62 ± 11%) and 64 to 98% of NO_3^- uptake (mean = 80 ± 12%) in the euphotic zone. For instance, at station 303 (a station representative of mean conditions for the entire data set; yellow arrow in Fig. 3.1), maximum primary production (15.67 µg C l^{-1} d^{-1}) and NO_3^- uptake (1.55 µg N l^{-1} d^{-1}) occurred at 20 m and coincided with the SCM (1.64 µg chl *a* l^{-1}; Fig. 3.3). Vertical integration over the two vertical horizons gave a production of

36.35 µg C l^{-1} d^{-1} and a NO_3^- uptake of 2.00 µg N l^{-1} d^{-1} for the surface layer (representing 24% and 13% of the total, respectively) and C production and NO_3^- uptake of 112.40 µg C l^{-1} d^{-1} (76% of the total) and 13.44 µg N l^{-1} d^{-1} (87% of the total) for the SCM layer.

3.5.3 Photosynthetic parameters at the SCM under trace ^{15}N additions

A larger set of experiments was performed with water from the SCM only (excluding results obtained from incubations performed simultaneously with surface and SCM; see Table 3.1) collected during late summer-fall (2005 to 2007) and spring-early summer (2008). For a given station, photosynthetic parameters were derived using data from all incubators since no significant effect of N substrate on C uptake was observed. The P_m^B in units of µg C (µg chl *a*)$^{-1}$ h^{-1} ranged from 0.07 to 2.77 (mean = 0.65 ± 0.45; Fig. 3.4; all results are presented in Appendix C). The parameter α in units of µg C (µg chl *a*)$^{-1}$ h^{-1} (µmol quanta m^{-2} s^{-1})$^{-1}$ ranged from 0.006 to 0.078 (mean = 0.027 ± 0.014; Fig. 3.4). Corresponding E_k values in units of µmol quanta m^{-2} s^{-1} varied between 7 and 97 (mean = 24 ± 13; Fig. 3.4). The β parameter (same units as α) was significant at only 12% of the stations, with values ranging from 0.00002 to 0.0032 (mean = 0.0010 ± 0.0008; data not shown).

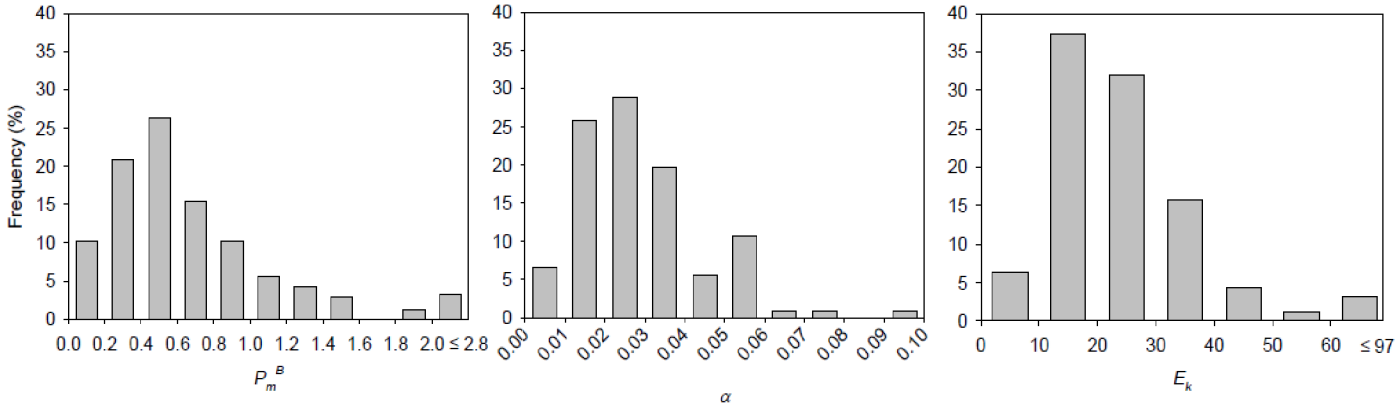

Figure 3.4 Relative frequency distribution of photosynthesis-irradiance parameters at the SCM.

3.5.4 Nitrogen uptake by SCM communities under trace ^{15}N additions

Nitrate uptake was highly variable among stations (n = 53; Appendix B). The mean values for uptake-irradiance parameters was 0.042 ± 0.043 µg N (µg chl *a*)$^{-1}$ h^{-1} for $N_m^B{}_{(NO3)}$, 0.004 ± 0.007 (µg N (µg chl *a*)$^{-1}$ h^{-1} (µmol quanta m^{-2} s^{-1})$^{-1}$) for $\alpha_{(NO3)}$, 18 ± 12 µmol quanta m^{-2} s^{-1} for $E_{k(NO3)}$ and 0.010 ± 0.030 for $D^B{}_{(NO3)}$ (same unit as N_m^B) representing $14 \pm 17\%$ of the total uptake ($N_m^B + D^B$). Nitrite uptake was an order of magnitude lower (mean $N_m^B{}_{(NO2)} = 0.005$; mean $\alpha_{(NO2)} = 0.0007$; mean $E_{k(NO2)} = 11$; mean $D^B{}_{(NO2)} = 0.001$; n = 3). For NH_4^+ uptake (n = 32; Appendix B), $N_m^B{}_{(NH4)} = 0.016 \pm 0.017$, $\alpha_{(NH4)} = 0.005 \pm 0.008$ and $E_{k(NH4)} = 7 \pm 8$. Dark uptake $_{(NH4)} = 0.008 \pm 0.009$ and accounted for $26 \pm 24\%$ of the total uptake. Urea uptake-irradiance incubations were also performed, but data will not be shown here since only 2 out of 8 stations had detectable responses and *in situ* urea concentrations were most often below the limit of detection. All results are presented in Appendix C.

3.5.5 Relationships between environmental factors and uptake-irradiance parameters under trace ^{15}N additions

The PPMC analysis showed a strong correlation between P_m^B, E_k and *in situ* temperature at SCM depth (correlation coefficient for P_m^B between 0.62 and 0.97 across incubation sets, $p < 0.0001$ and for E_k between 0.72 and 0.88, $p < 0.0001$; Appendix A). Note that for the SCM this correlation was strongly influenced by station NR24, which was near the Nelson River and showed anomalously high temperature (5.1°C). The day of year (DY) was significantly related to $N_m^B{}_{(NO3)}$ uptake. No correlation was observed between E_k and daily-averaged irradiance at the SCM (E_{SCM}). For surface samples, the E_k and α for C and N uptake showed a strong correlation with both NH_4^+ and total inorganic N concentrations (Table A2). A weak negative correlation was observed between α of C uptake and NO_2^- concentrations and positive between α and NH_4^+ concentrations. At the SCM, strong positive relationships were observed between $N_m^B{}_{(NO3 \text{ and } NH4)}$, $\alpha_{(NO3 \text{ and } NH4)}$ and the concentrations of NO_3^- and total dissolved N (Table A1). The only relationship observed with dark uptake (not shown) was a weak positive correlation between E_{SCM} and $D^B{}_{(NO3)}$ uptake (0.40, $p < 0.05$).

When excluding outlying station NR24 (see above), a detailed analysis of P_m^B versus *in situ* temperature (T) showed a significant, positive linear relationship during late summer-fall (Fig. 3.5; $P_m^B = 0.178\ T + 0.538$, $r^2 = 0.64$, $p < 0.0001$). No significant relationship with temperature was observed during spring-early summer when the temperature range was very narrow at the SCM (between -1.7 and -1.0°C). The predictive power of the relationship for the spring-early summer was increased by including both T and DY in a multiple linear regression ($P_m^B = 8.417 - 0.0229\ DY + 2.742\ T$, $r^2 = 0.77$, $p < 0.001$; not shown).

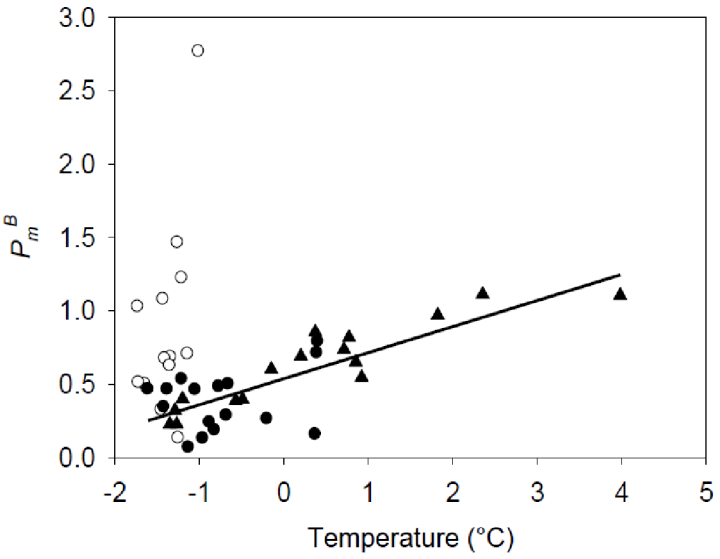

Figure 3.5 Relationships between P_m^B and *in situ* temperature for spring-early summer (open symbols) and late summer-fall (solid symbols) for surface (triangles) and SCM (circles) communities. The line represents the linear regression for late summer-fall dataset.

Estimates of E_{SCM} were lower than E_k for C uptake at 47% of the experimental stations during spring-early summer and 85% of the stations during late summer-fall (Fig. 3.6). The same percentage (85%) was observed for NO_3^- uptake during late summer-fall, but not during spring-early summer when only 21% of E_{SCM} were lower than $E_{k(NO3)}$. For NH_4^+

uptake, E_{SCM} was lower than $E_{k(NH4)}$ in only 11% and 29% of cases during the spring-early summer and late summer-fall periods, respectively.

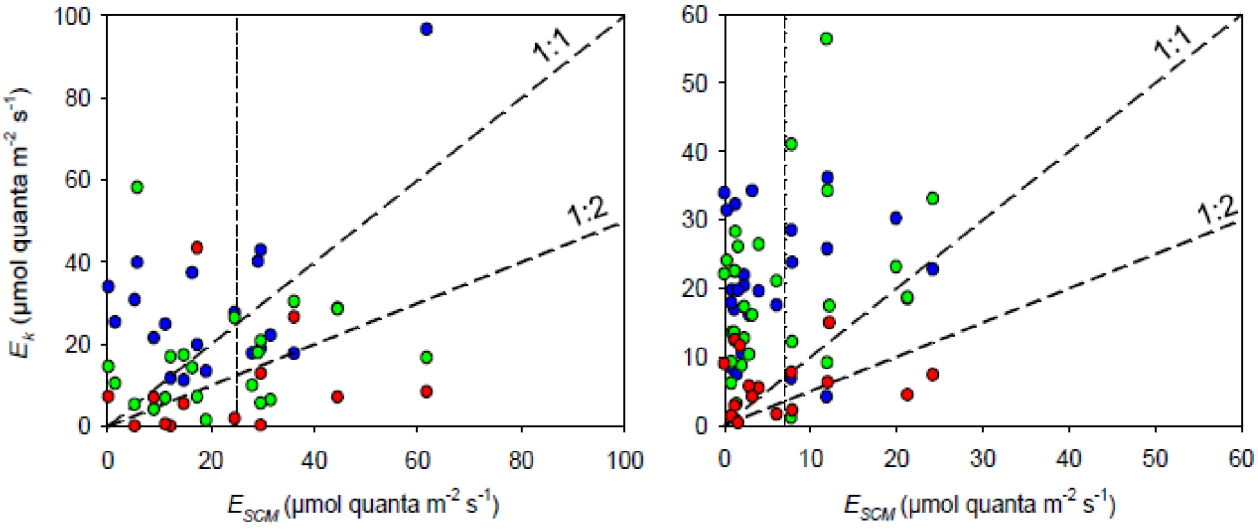

Figure 3.6 Relationship between E_k and E_{SCM} for photosynthesis (blue circles) and the uptake of NO_3^- (green circles) and NH_4^+ (red circles) during spring-early summer (left-hand side) and late summer-fall (right-hand side). The dashed vertical lines represent the mean E_{SCM} for each season and the dashed lines provide visual reference for 1:1 and 1:2 ratios.

3.5.6 Contribution of NO_3^- uptake to inorganic N uptake (*f*-ratio) at the SCM

When excluding dark uptake (D^B) from calculations, the average *f*-ratio estimated for the mean E_{SCM} during spring-early summer (23 µmol quanta m^{-2} s^{-1}) was 0.74 ± 0.26 (Fig. 3.7). During late summer-fall, the average *f*-ratio estimate was 0.37 ± 0.20 for a mean E_{SCM} of 6 µmol quanta m^{-2} s^{-1} (Fig. 3.7). Despite the wide range of observed E_{SCM} during spring-early summer (0.3 to 62 µmol quanta m^{-2} s^{-1}) the mean *f*-ratio estimated from individual *f*-ratio-irradiance curves for all stations only varies from 0.65 ± 0.31 to 0.76 ± 0.24 (Fig. 3.7). For late summer-fall, the E_{SCM} varied between 0.1 and 24 µmol quanta m^{-2} s^{-1}, with corresponding *f*-ratios ranging from 0.28 ± 0.18 to 0.48 ± 0.21 (Fig. 3.7). The *f*-ratio did not covary with E_{SCM} but was positively related to ambient NO_3^-concentation

(*f*-ratio = 0.1 NO_3^- + 0.3; $r^2 = 0.61$, $p < 0.0001$). Adding D^B to the calculation produced a modest but significant decrease ($p < 0.001$) of 9% in the mean *f*-ratio for both seasons (Fig. 3.7; 0.65 ± 0.24 and 0.28 ± 0.16). Over the range of incubation irradiances, the decrease in mean *f*-ratio imparted by the inclusion of D^B in calculations varied from 17 to 8% (values for minimum and maximum irradiances, respectively) for spring-early summer and between 4 and 11% for late summer-fall (Fig. 3.7).

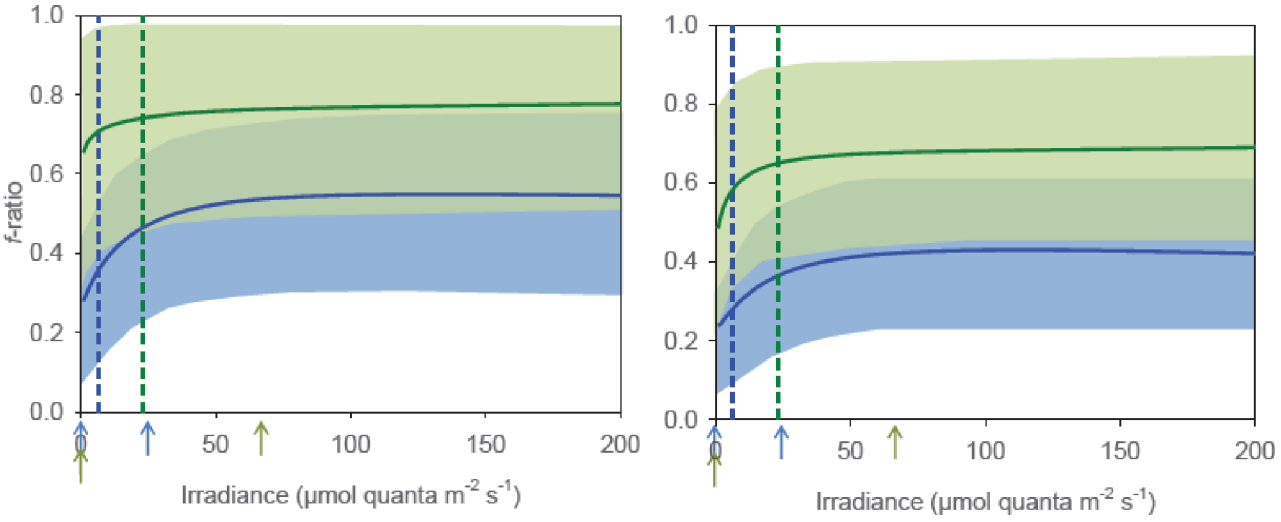

Figure 3.7 Averages (solid lines) and ranges (shaded areas) of the *f*-ratio at the SCM as a function of incubation irradiance during spring-early summer (green) and late summer and early fall (blue), calculated with (right-hand side) or without (left-hand side) dark uptake (D^B). Arrows and dashed lines give the range and mean of E_{SCM}, respectively.

Most SCM showed a RPI for NO_3^- below unity (range 0.14 - 0.95 with D^B and 0.16 - 1.03 without D^B; Fig. 3.8). The RPI was strongly correlated to NO_3^- concentration (PPMC; correlation coefficient = 0.80 and $p < 0.0001$ with D^B included and correlation coefficient = 0.76 and $p < 0.0001$ without D^B). Weak correlations were also observed between E_{SCM} and the *f*-ratio (correlation coefficient = 0.40, $p < 0.05$ with or without D^B) and the RPI (correlation coefficient = 0.40, $p < 0.05$ with or without D^B).

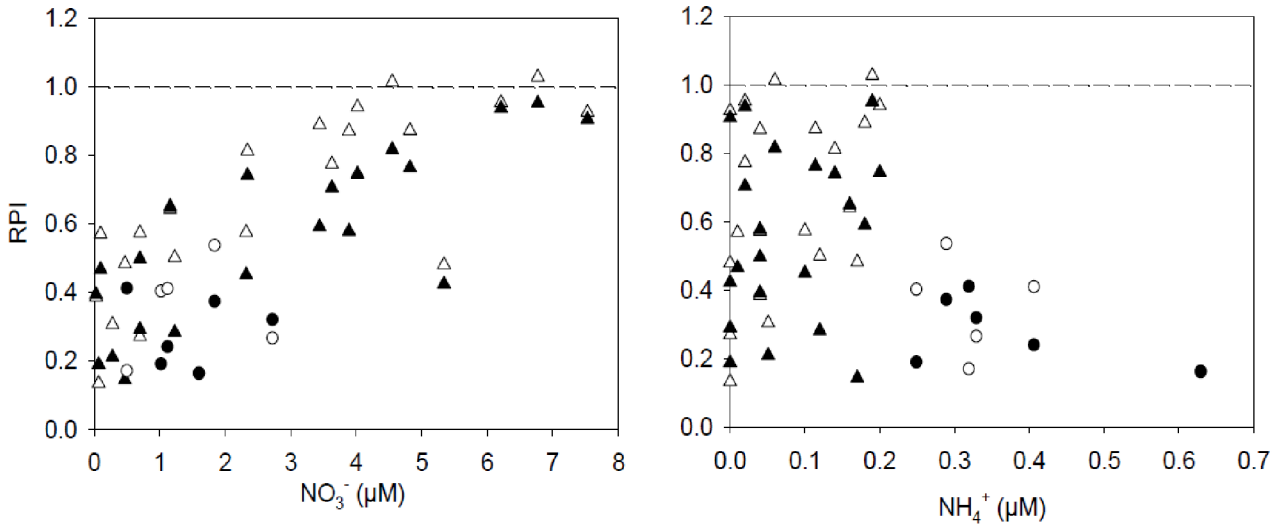

Figure 3.8 Relationships between the ambient concentrations of NO_3^- (left-hand side) or NH_4^+ (right-hand side) and the relative preference index (RPI) for NO_3^- calculated with D^B included (solid symbols) or not (open symbols) for NH_4^+ concentrations above (circles) and below or equal to (triangles) 0.2 µM.

3.5.7 Effect of N enrichment on uptake-irradiance parameters and their relationships with environmental variables

Apart from a few anomalous data points, N enrichment had no significant overall effect ($p > 0.05$) on uptake-irradiance parameters for C (not shown), NO_3^- and NO_2^- (Fig. 3.9). Most of the apparent effects at individual stations (i.e., points away from the 1:1 line) disappeared when taking into account the standard error of the parameter estimates (errors bars were omitted to keep the graph legible). Only the ${N_m}^B_{(NH4)}$ and $E_{k(NH4)}$ uptake were higher ($p < 0.001$) under enriched conditions. Most relationships observed between environmental variables and uptake parameters under trace ^{15}N additions (Sect. 3.5) also held for the enriched treatments. Exceptions included the disappearance of relationships between ${N_m}^B_{(NO3 \text{ and } NH4)}$, $\alpha_{(NO3 \text{ and } NH4)}$ and the concentrations of NO_3^- and total dissolved N and the appearance of positive relationships between chl *a* concentration and ${N_m}^B_{(NO3 \text{ and } NH4)}$ and $\alpha_{(NO3 \text{ and } NH4)}$ and between E_{SCM} and ${N_m}^B_{(NO3 \text{ and } NH4)}$ and $E_{k(NH4)}$ (Table A1).

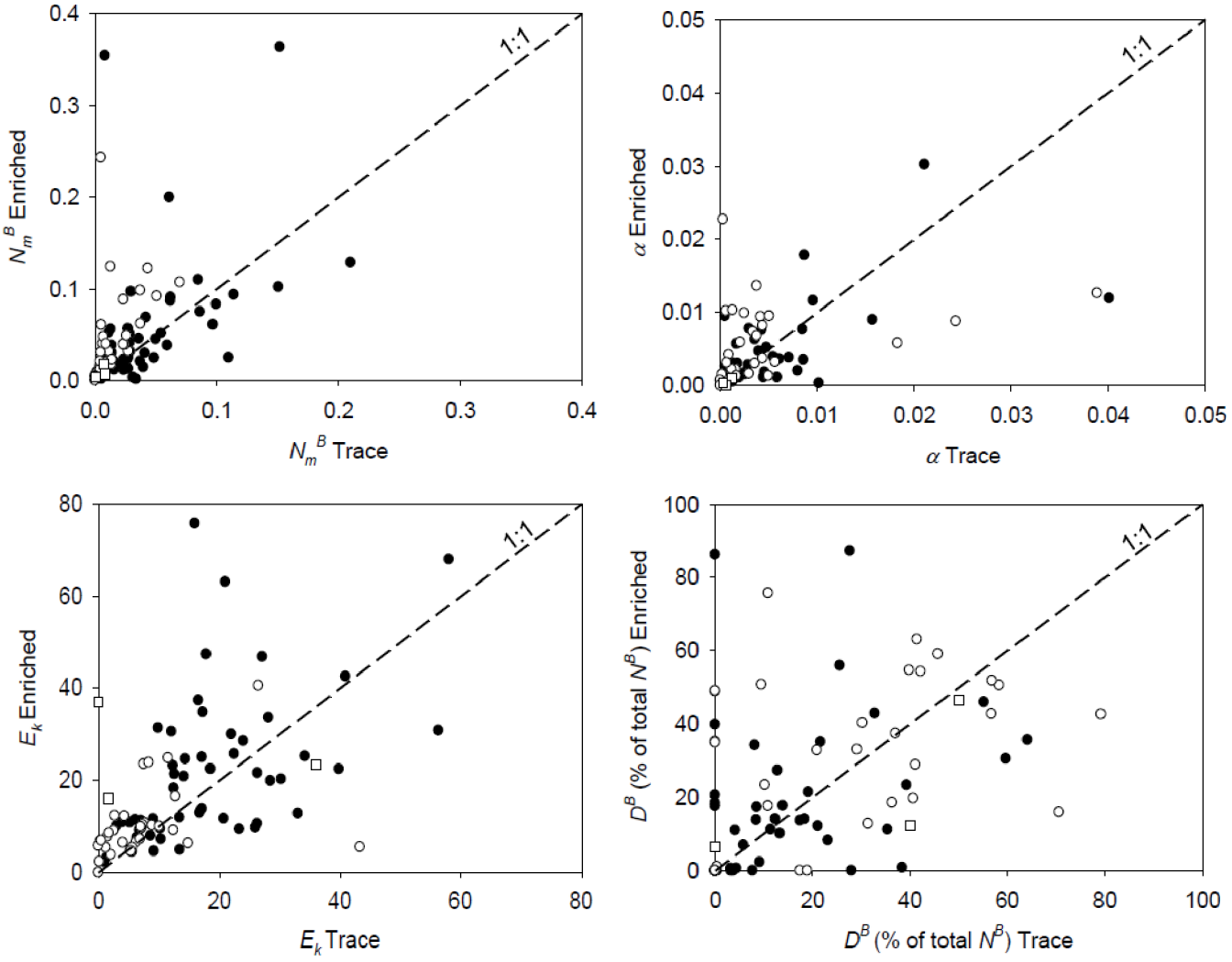

Figure 3.9 Response of N_m^B, α, E_k and D^B for NO_3^- (solid circles), NH_4^+ (open circles), and NO_2^- (open squares) uptake to experimental N enrichment during incubations (see Methods). The dashed 1:1 line represents a lack of response and is provided for visual reference. To ease the comprehension, the standard error is not presented in the graph (refer to "Sensor calibrations and data transformations" section).

3.5.8 C:N stoichiometry at the SCM

The C:N uptake ratios (where N is the sum of NH_4^+ and NO_3^- uptake) showed a general decrease with increasing inorganic N concentration (Fig. 3.10). The ratios at E_{SCM} (P^B:N^B) were lower than at light-saturation (P_m^B:N_m^B) and generally close to the Redfield value (6.625; Redfield et al. 1963). The negative effect of N enrichment on the C:N uptake ratio was strongest under experimental light saturation and rapidly vanished when N concentrations rose above 2 µM (Fig. 3.10).

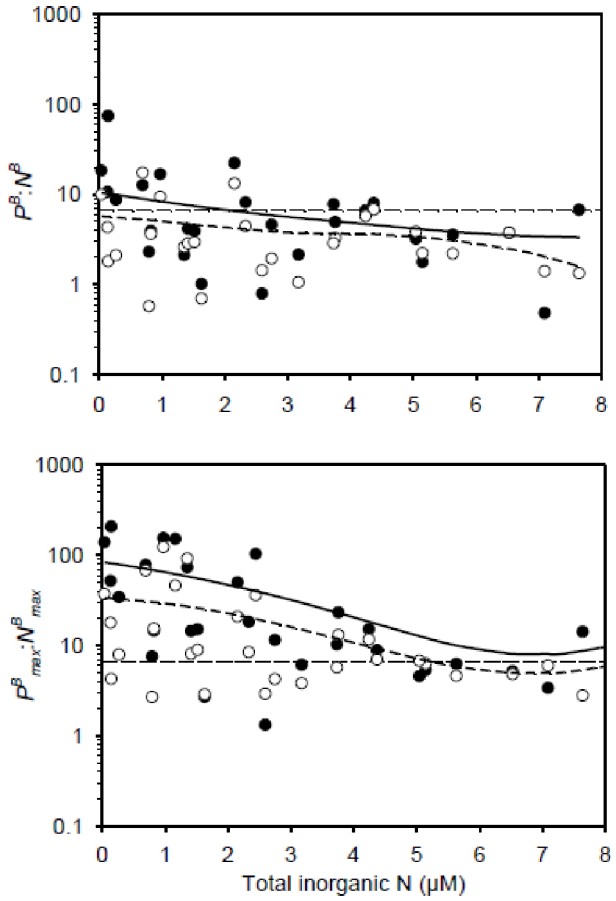

Figure 3.10 Relationships between total inorganic N and C:N uptake ratios under trace (closed symbols) and enriched (open symbols) N additions at E_{SCM} (upper panel) and under saturating light conditions (bottom panel). Lines indicate the Redfield ratio (fine dashed) and moving averages (5 points) for trace (solid) and enriched (dashed) conditions.

3.5.9 Post-incubation F_v/F_m

For SCM phytoplankton, a significant negative correlation was observed between post-incubation F_v/F_m and irradiance during the incubation (Fig. 3.11; $r = -0.64$, $p < 0.0001$, $n = 553$). F_v/F_m was stable (mean = 0.62) up to *ca.* 30 µmol quanta m^{-2} s^{-1} and then declined with irradiance. All extreme low values (F_v/F_m below 0.3) were measured in samples exposed to irradiance greater than 85 µmol quanta m^{-2} s^{-1} (representing on average 27% of incident irradiance at the surface). Post-incubation F_v/F_m of surface phytoplankton (5 m; mean of 62% of incident irradiance measured at surface) also showed a significant negative correlation (Fig. 3.11; $r = -0.73$, $p < 0.0001$, $n = 48$), but extremely low values were not observed in the range of simulated irradiance.

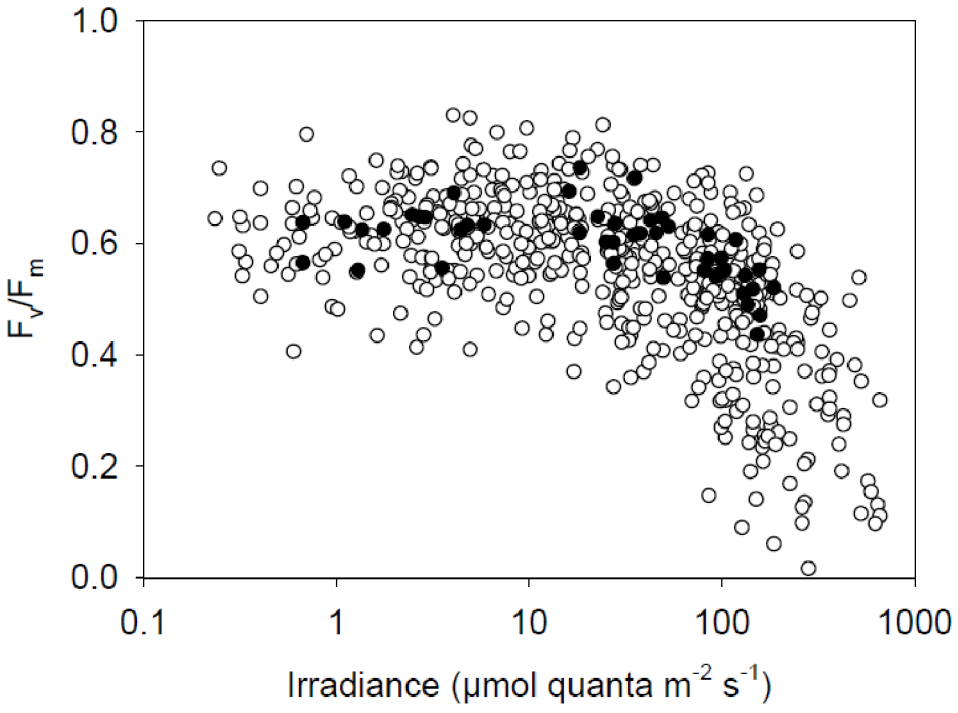

Figure 3.11 Changes in F_v/F_m after light-gradient incubations of SCM algae (open symbols) and surface algae (solid symbols).

3.6 Discussion

This study provides the first assessment of combined C and N uptake by SCM communities over the entire swath of the Canadian Arctic and the full extent of the growth period (April to early November). It also extends recent observations showing that SCM are thriving, photosynthetically-competent communities in the Arctic Ocean (Martin et al. 2010) and provides contemporary uptake-irradiance parameters to better tune models and remote-sensing algorithms of primary production. By distinguishing between the new and regenerated components of total primary production, our study also addresses the biogeochemical significance of SCM communities for the food web and the biological CO_2 pump.

Martin et al. (2010) hypothesized that the primary productivity of SCM communities was limited by irradiance due to their position in the lower euphotic zone near the nitracline. As a corollary, they further hypothesized that SCM depend principally on NO_3^- and mediate a large share of water-column new production. Here we examine these hypotheses through a discussion of 1) the relative importance of dark versus light-dependent uptake for different N sources, 2) the photo-acclimation and stoichiometry of C and N uptake at low irradiance, and 3) the response of C and N uptake to environmental conditions in Canadian Arctic waters. The discussion ends with a strategy for selecting uptake-irradiance parameters for models and remote-sensing algorithms.

3.6.1 N nutrition and the significance of dark versus light-driven N uptake

Light-independent N uptake ($D^B_{(NO3\ and\ NH4)}$) is known to occur during daytime or at night when samples taken in the euphotic zone are incubated. In the short term (i.e. a few hours), $D^B_{(NO3\ and\ NH4)}$ cannot be assumed to support short-term photosynthetic primary production because it can be mediated by heterotrophic bacteria (Kirchman and Wheeler 1998; Allen et al., 2002) and the portion taken up by phytoplankton is not necessarily constitutive (i.e., not assimilated or, more precisely, not leading to amino acid synthesis; Dortch 1982) since photosynthesis does not occur in the dark but N may be stored in cell vacuoles. In our study, adding $D^B_{(NO3\ or\ NH4)}$ to ${N_m}^B_{(NO3\ or\ NH4)}$ generally had a modest impact on the *f*-ratio,

translating in potential errors of only 4 – 17% (9% on average) in new production estimates. However, $D^B_{(NO3\ and\ NH4)}$ represented a variable and sometime high proportion of total N uptake and its role in nutrition and N cycling needs to be discussed.

Using antibiotics and 0.2 µm filters, Berrouard (2011) estimated absolute bacterial uptake rates in our study area to be 0.0017 ± 0.0019 µg N l^{-1} h^{-1} for NO_3^- and 0.0032 ± 0.0061 µg N l^{-1} h^{-1} for NH_4^+, on average. Those numbers are close to the median absolute dark uptake ($D^B_{(NO3\ or\ NH4)}$ x chl *a*) values obtained here using GF/F filters (0.0014 µg N l^{-1} h^{-1} for NO_3^-; 0.0029 µg N l^{-1} h^{-1} for NH_4^+). Since over half the bacteria present in the water are retained by GF/F filters in the coastal Beaufort Sea (Simpson et al. 2013), we estimate that at least 61 and 55% of $D^B_{(NO3)}$ and $D^B_{(NH4)}$ was mediated by heterotrophs, respectively. Given this, up to 39 and 45% of $D^B_{(NO3)}$ and $D^B_{(NH4)}$, respectively, can be attributed to assimilation or non-constitutive uptake by autotrophs.

Assimilatory algal $D^B_{(NO3\ and\ NH4)}$ requires excess C and energy acquired in the light prior to incubation, which is likely to be near the surface but is unlikely to occur under low light at SCM depth (where biomass is generated primarily by local growth instead of the accumulation of cells sinking from above; Martin et al. 2010). For this reason, the lack of correlation between $D^B_{(NH4)}$ and E_{SCM} points to a low occurrence of light-independent NH_4^+ assimilatory uptake by phytoplankton at the SCM, which is probably masked by the contribution of bacteria that use NH_4^+ preferentially. This scenario is compatible with the low ratio of $D^B_{(NO3\ and\ NH4)}$ to total N uptake at light saturation in our study compared to previous ones (Price et al., 1985; Cochlan et al. 1991; Smith and Harrison 1991; Probyn et al. 1996). This ratio was also much lower for NO_3^- than for reduced N sources, as expected from the relatively high energy cost of NO_3^- reduction (Behrenfeld et al. 2008), which is consistent with the positive correlation between $D^B_{(NO3)}$ and E_{SCM}. However, the algae there probably lack energy to perform both photosynthesis and the full reduction of all the NO_3^- taken up, leading to the release of NO_2^- (Kiefer et al. 1976; Lomas et al. 2006) and widespread presence of a PNM near or at the SCM (see also Tremblay et al. 2008 and Martin et al. 2010). It is advantageous to use reduced N in this situation, which explains the negligible contribution of NO_2^- to total N uptake and the positive effects of NH_4^+ enrichment on NH_4^+ uptake (Fig. 3.9) and of incubation irradiance on the *f*-ratio (Fig. 3.7).

Since N enrichment or elevated ambient N concentrations did not stimulate P_m^B in our study, we surmise that $D^B_{(NO3\ and\ NH4)}$ was mediated mostly by bacteria during incubations, with a secondary contribution of non-constitutive uptake by phytoplankton. Without $D^B_{(NO3\ and\ NH4)}$, P^B:N^B ratios at E_{SCM} hovered near the Redfield ratio, implying that phytoplankton did not need $D^B_{(NO3\ and\ NH4)}$ to fulfill their N demand (Fig. 3.10). If anything, the autotrophic component of $D^B_{(NO3\ and\ NH4)}$ could result from the storage of inorganic N in the vacuoles of diatoms, which are numerically important at the SCM (Martin et al. 2010), and would explain decreasing P_m^B:N_m^B ratios under N enrichment (Fig. 3.10). Whether this storage actually occurs or eventually fuels PON synthesis before the cells sink or die is unknown. For these reasons, only the light-driven component of N uptake will be considered for further analysis.

Based on the above considerations, our working hypothesis that NO_3^- was the main form of N consumed by phytoplankton at the SCM is supported during spring-early summer (the mean *f*-ratio estimated for this period = 0.74 ± 0.26). However, our hypothesis is not supported for later summer and fall, when the mean *f*-ratio declined to 0.37 ± 0.20 due to decreasing NO_3^- availability and irradiance at the SCM, which was then often lower than the $E_{k(NO3)}$. While recent studies indicate that nitrification may cause the overestimation of new production in stratified waters (Raimbault et al. 1999; Yool et al. 2007), the SCM considered here were generally exposed to 24-hr sunlight and located high in the euphotic zone relative to those of other oceans (Martin et al. 2010). These conditions should strongly inhibit bacterial nitrification (Horrigan et al. 1981).

3.6.2 Acclimation and vertical coupling of C and N uptake

The following discussion assumes that α (and thus E_k) estimates are reliable despite the absence of correction for possible shifts in light absorption with depth. While these shifts are known to occur, Shakshaug and Slagstad (1991) reported only small differences in α (ca. $\pm < 0.001$ µg C (µg chl *a*)$^{-1}$ h^{-1} (µmol quanta m^{-2} s^{-1})$^{-1}$) over the depth interval that separates surface and SCM samples in our study. Such a shift is similar to the statistical error attached to α estimates obtained with the ^{13}C method (here ±11% for a mean value of

0.027) and one order of magnitude smaller than the observed range of α values (0.027 ± 0.014; see also Brunelle et al. 2012)

SCM communities located in a strongly stratified environment would benefit by acclimating to low irradiance. For C uptake, this expectation is consistent with the contrast between the data of Platt et al. (1982), who found no vertical differences in uptake-irradiance parameters in weakly-stratified waters (Baffin Bay), and our data set, where α was higher at the SCM than at the surface. Here, uncoupled changes in P_m^B and α resulted in lower E_k values for SCM communities, which maintained very high photosynthetic performance (F_v/F_m). This pattern is entirely consistent with photochemical acclimation to low light instead of a physiological response to nutrient stress, senescence or the influence of taxonomic composition (i.e., E_k-independency, *sensu* Behrenfeld et al. 2008). The low E_k values (24 ± 13 µmol quanta m^{-2} s^{-1}) observed during all years and seasons at the SCM and the continuous and rapid acclimation (within 4 to 10 days) of phytoplankton to changing light conditions during the ice - open water transition in the coastal Beaufort Sea (Palmer et al. 2011) imply widespread and persistent shade acclimation. This interpretation is supported by the sharp drop (photoinhibition) in post-incubatory F_v/F_m for SCM phytoplankton exposed to irradiances greater than 70 µmol quanta m^{-2} s^{-1} (irrespective of season or region) while surface phytoplankton were able to manage higher irradiance (Fig. 3.11). Similar patterns were previously observed in Baffin Bay and Lancaster Sound, where samples from the surface demonstrated negligible photoinhibition relative to deeper ones under stratified conditions (Platt et al. 1982; Gallegos et al. 1983).

The photochemical acclimation observed for C uptake was not observed for NO_3^- uptake, for which $N_m^B{}_{(NO3)}$ but not $\alpha_{(NO3)}$ was significantly higher at the SCM than at the surface (E_k-independency). Since $N_m^B{}_{(NO3)}$ was also positively related to ambient NO_3^- concentration (Table A1), SCM communities near the nitracline physiologically adjusted to higher N concentrations presumably by increasing their enzymatic capacity to reduce NO_3^-. The general lack of increase in $N_m^B{}_{(NO3)}$ with experimental enrichment suggests that acclimation occurred on time scales of days rather than hours. The inhibition of NO_3^- uptake by NH_4^+ observed in other regions (e.g., Glibert et al. 1982; Price et al. 1985;

Cochlan 1986) was not manifest in the Canadian Arctic (no significant negative correlation between the *f*-ratio and NH_4^+ concentration as observed by Smith and Harrison 1991 nor between the $N_m^B{}_{(NO3)}$ and *in situ* NH_4^+ concentration), probably due to the fact that ambient NH_4^+ concentrations were generally low. Inhibition is typically observed at concentration exceeding 0.5-1.0 µM (McCarthy et al. 1977).

For NH_4^+, the absence of correlation between $N_m^B{}_{(NH4)}$ and ambient concentration was probably due to the highly dynamic nature of this N pool, which defeats the purpose of acclimation. However, the clear response of $N_m^B{}_{(NH4)}$ to experimental enrichment indicates that phytoplankton can exploit sudden inputs, in accord with the minimal energy and enzymatic requirements of NH_4^+ assimilation. Despite this advantage, low ambient NH_4^+ availability forced the phytoplankton to rely strongly on NO_3^- to fulfill their N demand when irradiance and NO_3^- at the SCM were relatively high during spring-early summer (Fig. 3.7). This reliance decreased toward late summer-fall with declining irradiance and NO_3^- availability. The synoptic manifestation of this phenomenon is well rendered by the RPI for NO_3^- uptake and the relationship between the *f*-ratio and NO_3^- concentrations, which indicated strong "discrimination" against this N source at relatively low ambient concentrations (Fig. 3.8).

Overall, the acclimation of C uptake to low light and of NO_3^- uptake to high concentrations, as well as the low cost of NH_4^+ uptake, favoured efficient C and N nutrition at the SCM. However, the different E_k values (µmol quanta m^{-2} s^{-1}) obtained for C (24 ± 13), NO_3^- (18 ± 12), and NH_4^+ (7 ± 8) uptake imply a measure of vertical decoupling between total, new and regenerated production. For example, using these mean E_k values with the irradiance data of station 303 (Table 3.1) yields the onset of light-saturation at depths of 34, 24 and 21 m, for NH_4^+, NO_3^- and C uptake, respectively. However, we did not observe differences in the vertical position of absolute maxima between total and new production (both occurred at 22 m: Fig. 3.3) because 1) the strong concentration of chl *a* biomass at the SCM overrides the vertical separation that different E_k values would cause (Fig. 3.3) and 2) N_m^B for NO_3^- uptake was twice as high as for NH_4^+ uptake at the SCM.

Recent attempts to assess the impact of SCM on water-column primary production and remote-sensing estimates at the pan-Arctic scale reached different conclusions. While

Arrigo et al. (2011) propose that SCM play a modest role and account for ca. 8% of annual production, Hill et al. (2013) assess their contribution to be 53%. This apparent discrepancy is caused by the different averaging techniques applied to *in situ* profiles obtained from the ARCSS-PP database and to the different methods used to estimate water-column production from remotely-sensed surface variables. It is also noteworthy that 1) the extent to which the studies used for ground truthing specifically targeted and sampled the SCM is unknown, 2) the database includes profiles dating back to 1957 and may not fully represent actual conditions, and 3) spatial coverage is very patchy, especially during the spring-summer transition for which little data is available. The true contribution of SCM to primary production thus remains a matter of debate and there is a dire need to obtain contemporary estimates based on field data.

In the reconstructed profiles (Fig. 3.3), the depth of maximum productivity occurred at the SCM and the "classical" decrease in primary productivity with depth was not observed (Cullen 1982; Harrison 1990). The SCM layer mediated up to 76% of total production and up to 98% of NO_3^- uptake in the water column across the Canadian archipelago during early fall. These estimates apply to one sector of the Arctic Ocean, but underscore the need to consider this structure in remote-sensing estimations of productivity in regions where strong vertical stratification prevails (e.g., the Chuckchi Sea; Arrigo et al. 2011) and/or where NO_3^- is perennially low at the surface (e.g., the Beaufort Sea).

3.6.3 Environmental control of SCM productivity

Although SCM communities were shade-adapted, several if not most (47% for spring-early summer and 85% for late summer-fall) were exposed to E_{SCM} lower than the E_k for C uptake (Fig. 3.6). Light conditions were more favorable at the remaining stations where irradiance equaled or slightly exceeded E_k (mostly during spring-early summer) but even if E_{SCM} had been 2 times higher than E_k (a condition met at only 2 out of 48 stations), P^B would not exceed 87% of ${P_m}^B$ (based on Eq. 3). Primary production in the SCM layer thus operated at sub-optimal irradiance throughout most of the growth period.

Despite sub-optimal irradiance at the SCM, ${P_m}^B$ may have been constrained by nutrient availability or temperature, which would negatively affect P^B even when E_{SCM} exceeds E_k.

Because the E_k for N uptake was lower than for C uptake, we surmise that low light levels had a much lower impact on nutrition than on photosynthesis. The independency of P_m^B from ambient N concentrations further suggests that total primary production was not nutrient-limited at the SCM and the C:N uptake ratios at E_{SCM} (P^B:N^B) showed no clear sign of N stress under trace additions, except perhaps when ambient N reached the lowest values (Fig. 3.10). This pattern is expected in a situation where SCM communities push the nitracline downward or benefit from upward N fluxes in its vicinity, as long as E_{SCM} remains above the compensation irradiance (e.g., ca. 0.16 ± 0.02 µmol quanta m^{-2} s^{-1}; Tremblay et al. 2006). The much greater uptake ratios at light saturation (P_m^B:N_m^B; Fig. 3.10) suggest the possibility of N stress at light levels greatly exceeding what is realistic for the SCM, consistent with the effect of NH_4^+ enrichment on P_m^B:N_m^B.

In polar regions, phytoplankton experience low temperatures throughout the year but uptake-irradiance parameters do not reveal specific adaptations to this condition (Platt et al. 1982; Smith and Harrison 1991). Given that optimum temperatures for phytoplankton growth (> 10°C; Li 1985) are greater than those observed during our study, the positive correlation between P_m^B and temperature during late summer-fall (Fig. 3.5) is expected and consistent with previous Arctic data sets (Harrison et al. 1982; Harrison and Platt 1986 and Harrison and Cota, 1991) and experimental studies (Subba Rao and Platt 1984; Smith and Harrison 1991). Such a correlation was not observed when excluding surface data, which was expected since the range of observed temperatures was very narrow at the SCM. The lower envelope of P_m^B values at the SCM was nevertheless consistent with the temperature relationship established with surface data, especially for late summer-fall (Fig. 3.5). During spring and early summer, cold stations with high P_m^B values at the SCM were presumably associated with fast-growing, blooming diatoms (pigment analysis indicated diatom dominance at the SCM during the ice-open water transition in the Beaufort Sea during 2008; Palmer et al. 2011). A similar temperature-independent, transient increase in P_m^B was previously observed during an intense diatom bloom in northern Baffin Bay (Tremblay et al. 2006).

3.6.4 Strategy and rationale for the selection of uptake-irradiance parameters

The extensive spatial and regional coverage of our data set permits to update some of the parameters used in ecosystem models and remote sensing algorithms for the Arctic (Table 3.2). Although the uptake-irradiance parameters reported here showed no obvious regional or seasonal patterns, the typical P_m^B constant of 2 µg C (µg chl *a*)$^{-1}$ h^{-1}) based on previous studies (Harrison and Platt 1980; Subba Rao and Platt 1984; Harrison and Cota 1991; Smith and Harrison 1991; Weston et al. 2005) clearly needs to be reconsidered.

When considering spring-early summer only, P_m^B can be approximated as a function of day of the year (which integrates a complex set of interaction between environmental parameters; e.g., surface irradiance, SCM depth, nutrient availability, stratification) and temperature (e.g., $P_m^B = 8.417 - 0.0229\ \mathrm{DY} + 2.742\ T$). Otherwise P_m^B can be estimated as a function of temperature only (e.g., $P_m^B = 0.178\ T + 0.538$; Fig. 3.5) for post-bloom situations spanning spring, summer and fall (since P_m^B after the spring bloom apparently obeys the relationship obtained for late summer and fall). The difference in photosynthetic parameters observed between the upper mixed layer and the SCM suggests that algorithms should consider acclimation of the phytoplankton to the vertical light gradient in strongly stratified Arctic waters (e.g., implement models with at least 2 sets of parameters and ideally several that cover the vertical extent of the SCM layer).

While our data set contains few early spring data, a companion study performed in 2008 during the ice-open water transition by Palmer et al. (2011) found mean P_m^B values of 1.25 and 0.82 in Franklin Bay and Darnley Bay (Beaufort Sea), respectively, similar to those reported here for spring to late fall, i.e. $P_m^B = 0.65 \pm 0.45$. At the very beginning of the season, the phytoplankton seems to show a continuous and rapid acclimation (within 4 to 10 days) to changing conditions at the time of the SCM development (Palmer et al. 2011). Given this fact, the E_k values used after that rapid early-spring acclimation by algorithms below the upper mixed layer should be lower (e.g., $E_k = 24 \pm 13$ µmol quanta m^{-2} s^{-1}) than those prescribed for surface waters (e.g., E_k of ca. 60 µmol quanta m^{-2} s^{-1}; Arrigo et al. 2011; Palmer et al. 2011).

Table 3.2 Summary of the parameterization proposed for different case scenarios.

	Spring-early summer	Late-summer fall
P_m^B	0.65 ± 0.45 µg C (µg chl a)$^{-1}$ h^{-1}	
P_m^B *vs* T	P_m^B = 8.417 - 0.0229 DY + 2.742 T	P_m^B = 0.178 T + 0.538*
E_k suface	ca. 60 µmol quanta m^{-2} s^{-1}**	
E_k SCM	24 ± 13 µmol quanta m^{-2} s^{-1}	
N_m^B (NO3)	N_m^B (NO3) = -0.0005 DY + 0.16	
f-ratio surface	0.74	0.30
f-ratio SCM	0.74	0.37
f-ratio vs NO_3^-	0.1 NO_3^- + 0.3	

*Also applicable to post-bloom estimations.

** Arrigo et al. 2011; Palmer et al. 2011

By contrast with C uptake, the *f*-ratio showed a relatively weak dependence on irradiance during spring-early summer. A vertically constant value of 0.74 could thus be assumed for this period. The situation was different in late summer-fall, where the *f*-ratio was relatively low even at light saturation. Considering that the SCM acts as a "nutrient trap", limiting upward NO_3^- diffusion to the surface, we would advocate using a maximum *f*-ratio of 0.3 in the upper mixed layer (derived from the relationship observed at SCM where *f*-ratio = 0.1 NO_3^- + 0.3; see also Harrison 1990). In the SCM layer, a *f*-ratio of 0.37 could be used to convert remote sensing estimations of total P into new production. In models using N as a currency (Fasham et al. 1990 and Kuhn and Radach 1997), a more dynamic parameterization of N_m^B according to the day of year could be achieved (e.g., N_m^B (NO3) = -0.0005 DY + 0.16).

3.7 Conclusion

Data collected over the full extent of the growth season in the Canadian Arctic revealed that primary production at the SCM is generally co-limited by light and temperature. Nevertheless, SCM communities 1) show high photosynthetic competence, 2) are well acclimated to low light conditions and 3) can be photoinhibited by irradiance levels typical of those prevailing in the upper mixed layer. These communities consume predominately NO_3^- during spring-early summer but their reliance on NO_3^- decreases seasonally as the algae eventually discriminate against this N source and use mostly NH_4^+. The low concentrations of NH_4^+ in the water column could explain the association observed between the SCM and the nitracline, where the phytoplankton can meet their N demand.

The sheer size of the Canadian Arctic combined to the unique and dynamic nature of phytoplankton communities at widespread SCM demonstrate the need to adapt ecosystem models and remote sensing algorithm to the strong temporal and vertical gradients of temperature, irradiance and nutrient concentrations. This is especially relevant in strongly stratified Arctic regions (e.g., Canadian Arctic, Chukchi Sea), which presumably host the most understudied yet strongly perturbed marine ecosystems of the Global Ocean. A more effective parameterization could also consider the vertical and seasonal dynamics of N uptake parameters for different N substrates and the change observed in the ratio of new to total production throughout the growth season.

Tremblay and Gagnon (2009) proposed that the major differences in productivity and trophic status at the pan-Arctic scale are controlled by nutrient supply to the surface, which is typically greater in polynyas or peripheral areas with a short ice-covered season. Within a given region, productivity can increase with the duration of the ice-free season (Pabi et al. 2008; Arrigo et al. 2011) but the relative role of nutrient re-supply versus greater exposure to irradiance on this trend is unknown. Here, we showed how the later may act in synergy with rising temperature and lead to greater productivity by SCM layers, either through more complete NO_3^- usage or by deepening of the nitracline. In this regard, the physical processes that affect the vertical position of the nitracline (e.g., McLaughlin and Carmack 2010) are also expected to influence new production at the SCM.

Chapitre 4 Contribution of subsurface chlorophyll maxima to primary production in the Beaufort Sea (Canadian Arctic): A model assessment

4.1 Résumé

Des études approfondies de l'Arctique canadien ont préalablement révélé l'omniprésence et la persistance de maximums de chlorophylle subsuperficiels (SCM) qui peuvent contribuer largement à la production primaire journalière de la colonne d'eau. Cependant, l'estimation de la contribution annuelle des SCM à la production totale à l'aide de prélèvements *in situ* ou de données satellitaires représente un défi considérable dans l'océan Arctique. Pour cette raison et afin d'estimer l'impact de conditions environnementales fluctuantes ou changeantes, une approche numérique combinant un modèle de turbulence et un modèle d'écosystème a été élaboré pour la mer de Beaufort. L'analyse d'ensembles de simulations indique que les SCM pourraient représenter de 65% à 90% de la production primaire annuelle totale et que cette contribution est peu influencée par le régime de glace, la concentration hivernale d'azote, le paramétrage des processus phytoplanctoniques et les forçages physiques imposés. En conséquence de l'association persistante entre le SCM et la nitracline peu profonde, il appert que l'écosystème de la mer de Beaufort est principalement basé sur la production nouvelle. Ce résultat contraste avec le paradigme voulant que les écosystèmes oligotrophes soient majoritairement supportés par l'azote recyclé et la production régénérée. Par ailleurs, cette étude démontre que l'utilisation d'un modèle simple en combinaison avec l'utilisation des données *in situ* peut apporter un éclairage novateur sur des processus biogéochimiques autrement difficiles à quantifier.

4.2 Abstract

Previous comprehensive investigations of the Canadian Arctic revealed that subsurface chlorophyll maxima (SCM) are widespread and long-lived structures that can contribute significantly to daily primary production in the water column. However, estimating the annual contribution of SCM to production with *in situ* or remote-sensing approaches is challenging in the high Arctic. For this reason and to estimate the impacts of fluctuating or changing environmental conditions on SCM, a numerical approach combining a turbulence model and an ecosystem model was implemented for the coastal Beaufort Sea. An ensemble analysis of simulations suggested that SCM contribute 65 to 90% of total annual primary production and that this proportion is weakly affected by ice regime, winter nitrogen (N) concentration, parameter values determining phytoplankton growth and decay or the physical forcing imposed, all varying within realistic values. Due to the persistent association between the SCM and the shallow nitracline, the pelagic ecosystem of the coastal Beaufort Sea is apparently based on new production, contrasting with the common assumption that oligotrophic systems are predominantly supported by recycled N and

regenerated production. This study demonstrated that the use of a simple model in combination with *in situ* data leads to novel insights into biogeochemical processes that are otherwise very difficult to measure and track.

4.3 Introduction

Recent studies confirmed the importance of subsurface chlorophyll maxima (SCM) in the Canadian Arctic (Martin et al. 2010) and showed that SCM are photosynthetically competent, long-lived and appear at or soon after ice break up (Tremblay et al. 2008; Mundy et al. 2009; Palmer et al. 2011; Martin et al. 2012). While SCM often occur below the depth of maximum phytoplankton biomass and production in oligotrophic tropical waters, due to a photo-acclimatory increase in chlorophyll *a* (chl *a*) per unit carbon (C) with depth (Cullen et al. 1982; Fennel and Boss 2003), the three features closely match in the coastal Canadian Arctic (Martin et al. 2010) due to the relatively shallow and strong haline stratification. This vertical coincidence suggests that phytoplankton at the SCM are a significant source of fresh organic C for the deep ocean and/or the food web, as previously observed in other shallow seas (Scott et al. 2010).

SCM are observed in close association with the nitracline across the Canadian Arctic (Martin et al. 2010). Based on the progressive seasonal deepening of the two features in coastal bays, Tremblay et al. (2008) and Mundy et al. (2009) proposed that SCM communities mediate at least half of the water column nitrate drawdown during summer. In this scenario, the SCM presumably act as a "nutrient trap" (Harrison 1990), limiting the upward diffusion of nitrogen (N) into surface waters and thus reinforcing their own share of water-column productivity. A subsequent, targeted investigation of primary production and nitrogen (N) uptake showed that SCM layers may account for up to 76 and 87% of total and nitrate-based water-column production on a daily basis (Martin et al. 2012). This assessment was made from a few punctual estimates, however, so that the annual contribution of Arctic SCM layers to total, new (i.e. fueled by the input of allochthonous N) and regenerated (i.e. sustained by local N recycling) water column productivity and its response to the changing physical environment remain open questions.

Obtaining concurrent annual estimates of total, new and regenerated SCM productivity is not trivial in highly stratified, oligotrophic sectors of the Arctic Ocean, where modest

nutrient renewal precludes intense vernal blooms at the surface. SCM are often physically isolated from the mixed layer and hardly tractable by orbiting remote sensors that scrutinize the ocean surface (Martin et al. 2010). The acquisition of *in situ* annual time series of vertically-resolved primary production is costly and represents a heavy logistic burden. Even then, classical incubation techniques are unlikely to fully reproduce the rapid and dynamic response of SCM communities to fluctuations in irradiance and nutrient supply (Martin et al. 2012). A complementary modeling approach is thus desirable, insofar as it realistically captures vertical physical processes and satisfactorily parameterizes photosynthetic and nutritive processes in the water column.

In this study we evaluate the contribution of the SCM to water column productivity using a one-dimensional ecosystem model coupled to a turbulence model. This approach is not intended to obtain detailed fluxes across food web compartments, but to provide a model environment where SCM processes can be simulated under different physical forcing scenarios. The model was parameterized using an exhaustive *in situ* biogeochemical dataset assembled from 2002 to 2008 across the Canadian Arctic and complementary information from the literature. A model run was then performed for the year 2008 and compared with field observations that fully resolved the seasonal bloom.

Since phytoplankton cells live in a turbulent environment and have the capacity to acclimate rapidly to varying environmental conditions, parameters used to represent biological processes are potentially subject to significant spatial and temporal variations, as suggested by the large standard deviations associated to field measurements (see section 4.4.3). Physical forcing fields (wind induced turbulence and light, predominantly) are also known within a limited level of certainty so that errors on the model output should not be overlooked. For these reasons we adopted an ensemble-based modeling approach, which consists in performing a large number of simulations (or members) that are slightly perturbed from each other. Once parameter values are changed for one member they were kept constant throughout the simulation. This sensitivity analysis allowed us to characterize model errors arising from sampling uncertainties, forcing scenarios and non-linear terms, thus providing a robust assessment of the SCM contribution to primary production. Two broad categories of ensembles were generated: one where biological parameters were kept

constant and physical environmental conditions varied, and one where the physical forcings were the same among members while biological parameters varied.

4.4 Methods

4.4.1 Model description

The General Ocean Turbulence Model (GOTM; Umlauf and Burchard 2005) was used in association with the nitrogen-based biogeochemical model of Fasham et al. (1990), as adapted by Kuhn and Radach (1997) and described in Burchard et al. (2006). The model has been further modified to accommodate the prescription of initial nutrient profiles specific to a given region. The water column was 200-m deep discretized in 80 vertical levels with exponentially increasing spacing from the surface (1.40 m) to the bottom (3.25 m). Physical and biological equations were iterated with a time step of 300 s. Data were output every 3 hours in order to resolve the diurnal cycle. The background turbulent diffusivity K_z that applies in the absence of any wind or shear-induced mixing was set to 3×10^{-6} m^2 s^{-1} based on *in situ* measurements of turbulence performed in 2008 in the Amundsen Gulf (Bourgault et al. 2011). This one-dimensional configuration was designed to represent average conditions prevailing in the central portion of the Amundsen Gulf, southern Beaufort Sea, where near-shore or shelf-break processes like upwelling, bottom friction, jet currents and riverine freshwater can be neglected. Nutrient profiles and CTD data used to constrain the model and compare with the results were selected accordingly (see section 4.4.2).

Temperature and salinity profiles from the winter station occupied by the *CCGS Amundsen* in Franklin Bay from 10 January to 6 May 2004 were used to weakly constrain the density field with a relaxation time of one week (7 days) and thus initialize the pre-bloom density field. After this pre-bloom period, temperature and salinity were slowly relaxed to the same profile for next January with a relaxation time of 14 days, allowing the wind and buoyancy to affect the stratification on short time scales but preventing temperature and salinity drift on an annual time scale. Ammonium concentrations were also weakly relaxed towards pre-bloom values (0.001 mmol N m^{-3}) in order to avoid unrealistic accumulation in autumn (see Forest et al. 2011). This scheme did not affect estimates of regenerated productivity

(results not shown) but helped the understanding of the dynamic of the SCM during the entire active photosynthetic period. Atmospheric forcing fields (2-m air temperature, relative humidity, 10-m wind velocity, cloud cover and dew point) were taken from the NCEP-NARR Re-analysis, while sea ice concentrations c were obtained from the European Centre for Medium-Range Weather Forecast (ECMWF) ERA-Interim Re-analysis and were used to modulate the ocean surface irradiance as $E_0 = E_+[1-c(1-\tau)]$, where E_+ is the irradiance over the ice and E_0 the irradiance at the water surface, below the ice, and τ is the ice transmissivity. This parameterization is not intended to represent the complex physics of light propagation through ice but rather to study the sensitivity of the model to a phenomenon that can have a large impact on under-ice production (Mundy et al. 2009, Arrigo et al. 2012). PAR transmissivity was estimated at 2% of surface irradiance under bare melting ice, 14% under ponded ice (Perovich et al. 1998) and up to 38–67% directly under melt ponds, which can cover 10–30% of the ice surface during the melt period (Ehn et al. 2011). Based on these estimations, we used three different values of τ (8%, 15% and 30%) to assess the impact of ice transparency on primary production.

After being attenuated by sea ice, light penetrates the ocean and is attenuated following a Jerlov-type exponential decay $E(z)/E_0 = A \exp(-z/\zeta_1) + (1-A) \exp(-z/\zeta_2)$, where the spectral weighing parameter $A = 0.7$, $\zeta_1 = 3.5$ m and $\zeta_2 = 14.0$ m. Generally, waters can be classified as one of the Jerlov (1976) water types. However, light measurements representative of 2004 and 2008 spring seasons could not be represented satisfactorily by either of the standard water types, especially near the surface. The above parameters were thus adjusted to follow the minimum light attenuation level in the water column, which represents the attenuation due only to water without significant amount of phytoplankton (Fig. 4.1). As phytoplankton grows, light is further attenuated by the cells (the bio-shading effect) following the formulation of Kuhn and Radach (1997).

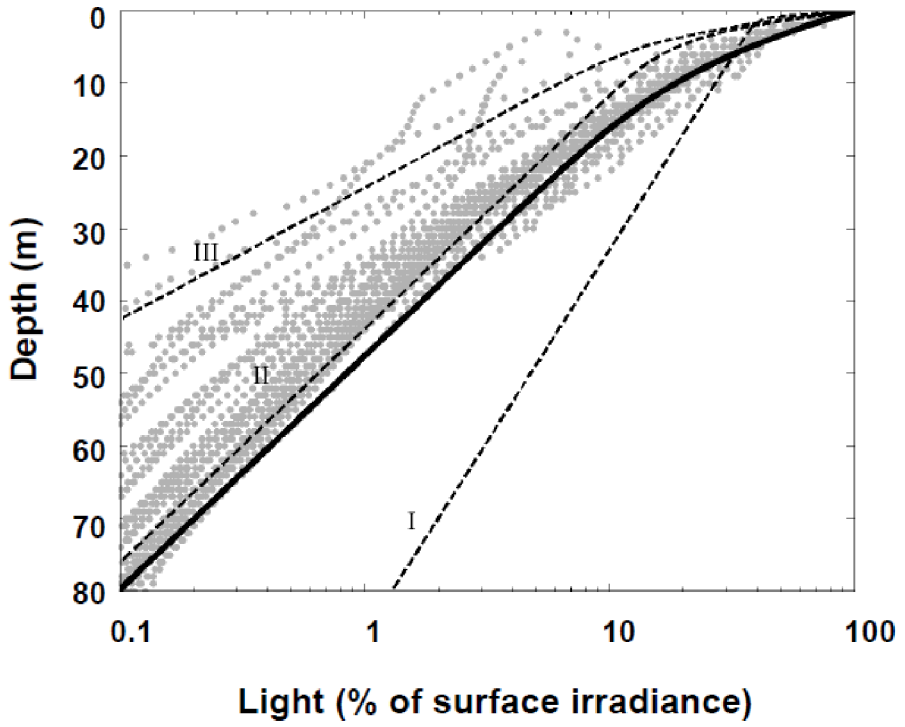

Figure 4.1. Light attenuation profile for the Amundsen Gulf (black line; $A = 0.7$, $\zeta_1 = 3.5$ m and $\zeta_2 = 14.0$ m). This profile was adjusted to measurements made before or during the early stage of phytoplankton blooms in 2004 (4 - 9 June) and 2008 (24 - 29 June), when the shading effect of phytoplankton is minimal (gray circles). The profile is compared to Jerlov water types I, II and III (dashed lines).

The ecosystem model was a typical nitrogen-based NPZD (nutrients (NO_3^- and NH_4^+), phytoplankton, zooplankton and detritus) model supplemented by a microbial loop that mediates N recycling in such a way that new and regenerated production can be distinguished (sensu Dugdale and Goering 1967). The seven model compartments and their interactions are shown in Figure 4.2. This is adequate for stratified offshore Arctic waters, where primary production is primarily limited by the availability of inorganic N (Tremblay and Gagnon 2009). The N and phytoplanktonic components of the model were parameterized and calibrated with our own Arctic data and other compartments (zooplankton, bacteria and detritus) with data from the literature (see section 4.4.3. for details).

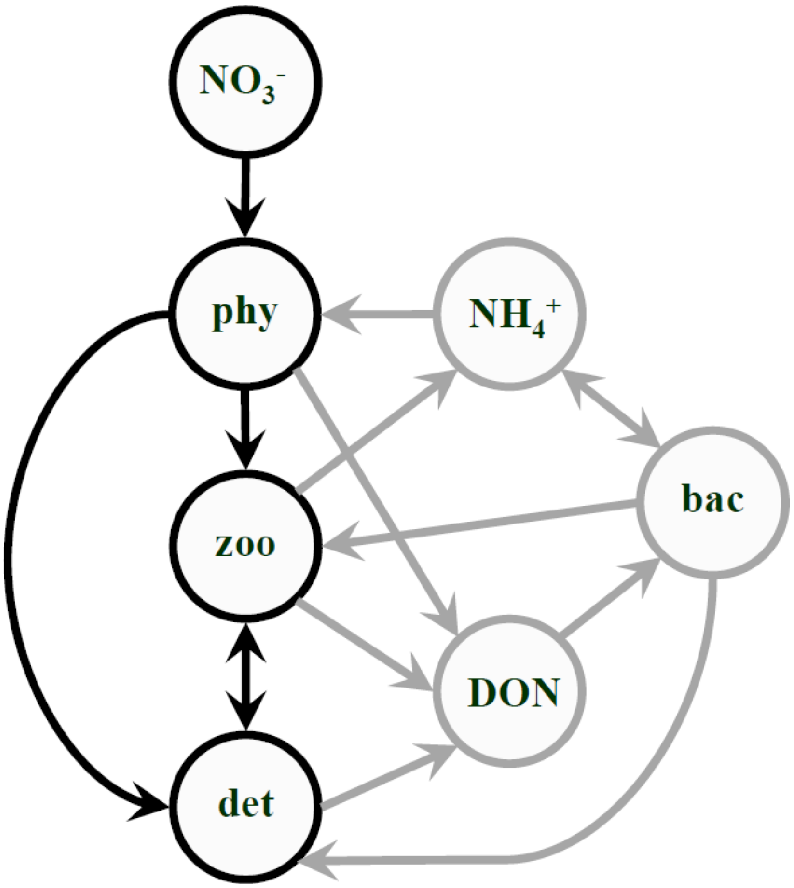

Figure 4.2. The seven-compartments biological model based on Fasham et al. (1990) and modified by Kunh and Radach (1997). The NPZD and the microbial components are represented in black and gray, respectively.

The specific N uptake *versus* irradiance (E) curve for phytoplankton was parameterized by a modified Platt et al. (1980) equation (Smith and Harrison 1991), which includes photoinhibition:

$$V = V_s[1-\exp(-\alpha E/V_s)][\exp(-\beta E/V_s)] \qquad (1)$$

where

$$V_s = V_{max}\{[\alpha/(\alpha+\beta)][\beta/(\alpha+\beta)]^{\beta/\alpha}\}^{-1} \qquad (2)$$

The response of the phytoplankton to nutrients followed a classical Michaelis-Menten equation:

$$Q = Q_1 + Q_2 \qquad (3)$$

with

$$Q_1 = [NO_3^-/K_1][1 + NO_3^-/K_1 + NH_4^+/K_2]^{-1} \qquad (4)$$

and

$$Q_2 = [NH_4^+/K_2][1 + NO_3^-/K_1 + NH_4^+/K_2]^{-1} \qquad (5)$$

where V_{max} is the maximal specific N uptake [d^{-1}], α and β are respectively the photosynthetic efficiency (initial slope of the relationship) and the photoinhibition strength [$m^2\ W^{-1}\ d^{-1}$] and K_1 and K_2 are half-saturation constants for NO_3^- and NH_4^+ [mmol N m^{-3}]. The NO_3^- limitation index and the light limitation index were defined as Q_1 and V/V_{max}, respectively.

Primary production was estimated as:

$$PP = V * Q * [phy] \qquad (6)$$

where [*phy*] is the phytoplankton concentration. Stocks have units of mmol N m^{-3} (or µM) and fluxes have units of mmol N $m^{-3}\ d^{-1}$, and the conversions from N to C and chl *a* were done with ratios obtained from *in situ* data (see below). Values converted to µg chl $a\ l^{-1}$ will be shown hereafter to facilitate comparisons between modeled and observed phytoplankton biomass.

4.4.2 *In situ* data

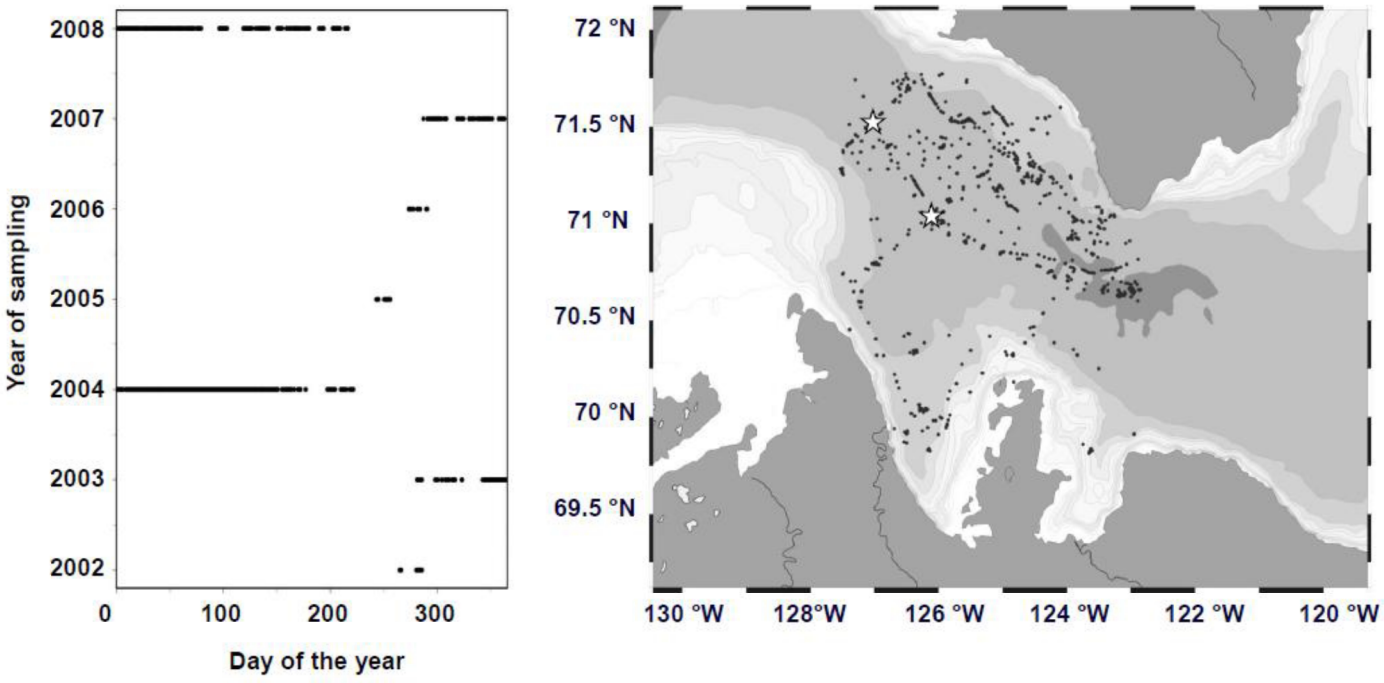

Figure 4.3. Temporal (left) and geographical (right) distributions of the stations sampled in the Amundsen Gulf (2002 to 2008) and used to calibrate the model. Stars indicate the locations of moorings CA05 and CA08.

Data used to calibrate and validate the model were collected from 2002 to 2008 during expeditions of the *CCGS Amundsen* to the Amundsen Gulf (Fig. 4.3). Vertical profiles were obtained at 1322 stations with a CTD-Rosette equipped with sensors to measure *in vivo* fluorescence (SeaPoint Chlorophyll Fluorometer), NO_3^- (SATLANTIC ISUS V1), photosynthetically active radiation (PAR; Biospherical QCP-2300), temperature and salinity (Sea-Bird SBE-911*plus*). All sensors were calibrated at the factory before each expedition. The depth of the nitracline and the depth of the SCM were defined as the depth where the vertical gradient of NO_3^- and the *in vivo* fluorescence had the highest values. A subset of 205 stations was sampled for NO_3^- analysis at standard depths (5, 10, 20, 30, 40, 50, 60, 70, 80, 100, 120, 140, 160, 180, 200, 250, 300 m, then every 100 m and at salinity of 33.1 to capture the nutrient maximum) with 12-l Niskin bottles attached on the

CTD-Rosette. Between 23 October 2007 and 27 July 2008, *in vivo* chlorophyll fluorescence sensors (SeaPoint) were installed on two moorings (at 37 m for CA08 and at 34 and 51 m for CA05).

From 2005 onward, a subset of 58 stations was sampled for NH_4^+ (same depths as NO_3^-) and chl *a* (5 depths: in the upper mixed-layer (5 m), in the upper and the lower tail of the SCM, in the SCM and below the euphotic zone). Measured NO_3^- and chl *a* concentrations were used to post-calibrate NO_3^- and fluorescence sensors, respectively. Out of those stations, 25 were selected to perform light-gradient incubations of water collected at the SCM and 6 to estimate the dependence of N uptake on ambient N concentrations (kinetics) in N-depleted surface waters.

Nitrate was analyzed with a standard colorimetric method adapted for the AutoAnalyzer 3 (Bran + Luebbe) following Grasshoff et al. (1999) and NH_4^+ was determined manually with the sensitive fluorometric method of Holmes et al. (1999) (see Martin et al. 2010 for detection limits and details).

Chl *a* concentrations were determined following the fluorometric method of Parsons et al. (1984) with a Turner Designs AU-10. Settling experiments were conducted with water from the SCM depth (at stations where incubations were performed) to measure the sinking rate of the phytoplankton (w_p) according to the SetCol procedures described in Bienfang (1981). Fractions from the top, middle and bottom parts of the settling column were filtered on GF/F filters and extracted with acetone to determine chlorophyll concentration (see above).

Relationships between irradiance and the uptake of C and N were assessed in lab with two ten-positions light-gradient incubators maintained at *in situ* temperature with a chilling circulator. Optimac metal-halide lamps mimicking solar irradiance were used with blue filter (118 Light Blue Lee Filters Ltd.) and optically neutral filters (Lee Filter Ltd.) in order to simulate the coastal underwater light spectrum and obtain ten different light intensities. Both incubators were spiked with trace amounts of ^{13}C-bicarbonate and ^{15}N (enriched concentrations – minimal effect was observed due to the spike; Martin et al. 2012); one with $^{15}NO_3^-$ and one with $^{15}NH_4^+$ (for detailed method, see Martin et al. 2012). The kinetics

of NO_3^- and NH_4^+ uptake were determined at *in situ* temperature in separate incubators. For each N source, a series of 6 bottles were spiked with a ^{14}N-^{15}N mixture at concentrations ranging from 0 to 6 µM for NO_3^- and 0 to 3 µM for NH_4^+. Incubation times were kept at 4-6 h (to minimize isotopic dilution and avoid nutrient exhaustion) and were terminated by filtration onto 24 mm pre-combusted GF/F filters. The filters were desiccated at 60°C and stored dry for post-cruise, mass-spectrometric analysis as described in Martin et al. (2012).

Uptake-irradiance relationships were parameterized (V_{max}, α, β) by fitting the empirical exponential models of Platt et al. (1980) and the half-saturation constants (K_s) for N uptake were calculated with the Michaelis-Menten equation. The N:chl *a* and C:N ratios were estimated using particulate organic C and N averaged for all light-gradient incubators and the chl *a* concentration measured at SCM depth (C:N = 10.29 and N:chl *a* = 1.11 in mmol C:mmol N and mmol N:µg chl *a* l^{-1}). The uptake-irradiance experiments are discussed in detail by Martin et al. (2012).

4.4.3 Parameterization of biological model

In the ecosystem model, the compartments for N and phytoplankton were almost entirely parameterized with *in situ* data from the Beaufort Sea (see Table 4.1). In order to minimize the impact of stations where photoautotrophs likely made up a small fraction of total nitrogen assimilation or the organic matter pool, photosynthetic parameters were assessed from incubations with particulate C:N $\leq$ 10 (g:g; Martin et al. 2012) and C:chl *a* $\leq$ 200 (Eppley 1968).

The mean V_{max}, α and β were estimated at 0.38 ± 0.34 d^{-1}, 0.11 ± 0.10 m^2 W^{-1} d^{-1} and 0.001 ± 0.001 m^2 W^{-1} d^{-1}, respectively. In the Amundsen Gulf, the half-saturation constant for NO_3^- uptake K_1 followed two patterns: 1) at stations where NO_3^- was low (< 0.20 mmol N m^{-3}), $K_1 = 0.1 \pm 0.05$ mmol N m^{-3} and 2) at stations where NO_3^- was higher (> 0.20 mmol N m^{-3}), $K_1 = 1.0 \pm 0.3$ mmol N m^{-3}. We used the latter since our study focuses on the SCM, which are generally associated with elevated NO_3^- concentrations. For NH_4^+ uptake, the half-saturation constant (K_2) was relatively stable at 0.2 ± 0.05 mmol N m^{-3}. Since phytoplankton maximum mortality rate (μ_1), half-saturation

mortality rate (K_5) and exudation rate (γ) are hardly measurable *in situ*, we used the parameters ($\mu_1 = 0.05$, $K_5 = 0.5$ and $\gamma = 0.05$) initially set by Kuhn and Radach (1997).

The mean phytoplankton settling speed w_p at SCM depth was set to -0.22 ± 0.17 m d^{-1} irrespective of sampling year, season or depth. This value excludes 5 obvious outliers sampled early in the spring, for which $w_p = -1.47 \pm 0.43$ m d^{-1} and likely characterized sinking ice algae.

When possible, other compartments were parameterized with the ecologically nearest estimation found in the literature. Otherwise, parameters from Kuhn and Radach (1997), set for the northern North Sea, were used. For zooplankton, the maximum growth rate ($G_{max} = 0.5$) and assimilation efficiency ($B = 0.7$) were parameterized following Lavoie et al. (2009), whose model included large copepods only. These copepods are known to dominate mesozooplankton in the Beaufort Sea (Lavoie et al. 2009). The bacterial maximum growth rate V_b was set at 0.36 d^{-1}, the mean value observed by Vaqué et al. (2008) in Franklin Bay (Beaufort Sea) between mid-March and May 2004. The bacterial half-saturation uptake constant K_4 was established to 0.05 mmol N m^{-3} according to Furhman et al. (1988), who observed that the affinity of mixed bacteria for NH_4^+ was higher than that of algae. The specific excretion rate μ_3 was adjusted to 0.03 d^{-1} to account for the slower general metabolic rate compared to the North Sea (0.15 d^{-1} as in Kuhn and Radach 1997). The detrital compartment, considered to include fecal pellets, zooplankton carcasses and sedimenting phytoplankton, was attributed a breakdown rate $\mu_4 = 0.33$ d^{-1} as in Lavoie et al. (2009) and a sinking rate $w_d = -10$ m d^{-1} in order to prevent a net loss of bacteria and detritus through sinking (Fasham et al. 1990). Calibrated *in vivo* fluorescence data from two moorings deployed in 2008 were compared with a simulation of the same year using the parameters and forcings mentioned above.

Table 4.1 Parameters used in the biological model.

Variable	Value	Unit	Definition
V_{max}	0.38	d^{-1}	Maximum uptake rate (this study)
α	0.11	$m^2 W^{-1} d^{-1}$	Photosynthetic efficiency (slope of PI curve I→0; this study)
β	0.001	$m^2 W^{-1} d^{-1}$	Photoinhibition (this study)
K_1	1.0	mmol N m^{-3}	Half-saturation constant for NO_3 uptake (this study)
K_2	0.2	mmol N m^{-3}	Half-saturation for NH_4 uptake (this study)
μ_1	0.05	d^{-1}	Phytoplankton mortality rate (Kuhn and Radach; Lavoie et al. 2009)
K_5	0.5	mmol N m^{-3}	Half-saturation constant for phytoplankton mortality (Kuhn and Radach 1997)
γ	0.05	-	Exudation fraction (Kuhn and Radach 1997)
ω_p	-0.22	m d^{-1}	Phytoplankton sinking velocity (this study)
G_{max}	0.5	d^{-1}	Maximum ingestion rate by zooplankton (Lavoie et al. 2009)
K_3	1.0	mmol N m^{-3}	Half-saturation rate constant for ingestion (Kuhn and Radach 1997)
B	0.7	-	Assimilation efficiency of zooplankton (Lavoie et al. 2009)
μ_2	0.3	d^{-1}	Maximum lost rate for zooplankton (Kuhn and Radach 1997)
K_6	0.2	mmol N m^{-3}	Half-saturation constant losses for zooplankton (Kuhn and Radach 1997)
δ	0.1	-	DON fraction of losses by zooplankton (Kuhn and Radach 1997)
ε	0.70	-	NH_4 fraction of losses by zooplankton (Kuhn and Radach 1997)
ρ_1	0.55	-	Grazing preference for phytoplankton (Kuhn and Radach 1997)
ρ_2	0.40	-	Grazing preference for bacteria (Kuhn and Radach 1997)
ρ_3	0.05	-	Grazing preference for detritus (Kuhn and Radach 1997)
V_b	0.36	d^{-1}	Maximum uptake rate by bacteria (Vaqué et al. 2008)
K_4	0.05	mmol N m^{-3}	Half-saturation constant uptake for bacteria (Furhman et al. 1988)
μ_3	0.03	d^{-1}	Excretion rate of bacteria (adjusted from Kuhn and Radach 1997)
μ_4	0.33	d^{-1}	Detritus breakdown rate (Lavoie et al 2009)
ω_d	-10.0	m d^{-1}	Detritus sinking velocity (Fasham et al. 1990)
κ_c	0.03	m^{-1}	Phytoplankton selfshading coefficient (Kuhn and Radach 1997; Lavoie et al. 2009)
A	0.70	-	
ζ_1	3.0	m	Attenuation coefficients (this study; based on Jerlov 1976)
ζ_2	14.0	m	

4.4.4 Defining the SCM

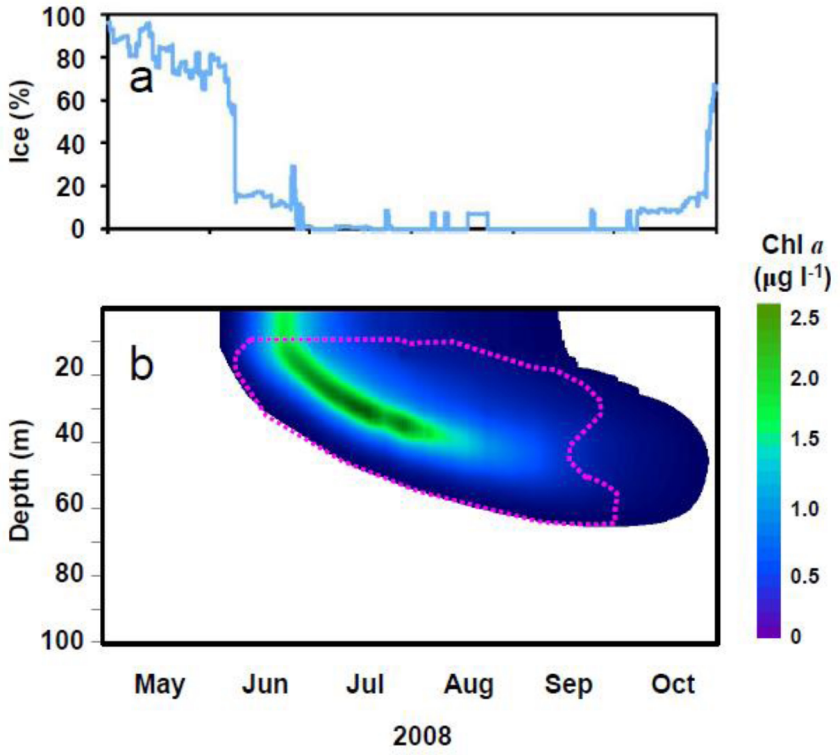

Figure 4.4. Time series of ice concentration data (a; %), modeled chlorophyll biomass in the water column (b; µg chl a l^{-1}). Only concentration above 0.11 µg chl a l^{-1} are shown. The vertical envelope selected for the integration of primary production at the SCM in (b) are given by the dashed line, which represents the zone between the depth where the vertical gradient of phytoplankton concentration reached the threshold of 0.01 µg chl a l^{-1} m^{-1} and where phytoplankton biomasses were ≥ 0.11 µg chl a l^{-1} (pink).

Estimating the contribution of the SCM layer to water-column production required the implementation of a set of criteria (routines) to objectively circumscribe its vertical extent and discriminate it from adjacent layers. The different routines tested (not shown) introduced minute variations in the assessment of production rates in the SCM layer (standard deviation ≤ 3%) so we settled for the one that best defined the layer early in the growing season. Proceeding downward from the surface, the upper limit of the SCM layer was set where (and if) a positive gradient of 0.01 µg chl *a* l^{-1} m^{-1} was attained and chl *a*

equaled or exceeded 0.11 $\mu g\, l^{-1}$, effectively removing profiles where chl *a* was maximum at the surface or vertically homogenous (Fig. 4.4). Then the SCM was identified as the depth where chl *a* was maximum and the base of the SCM layer as the depth where chl *a* reached a negative vertical gradient of 0.01 $\mu g\, l^{-1}\, m^{-1}$ and passed below the 0.11 $\mu g\, l^{-1}$ threshold. Note that this routine is not universal and applies to the range of values simulated here.

The model in its current form only accommodates constant V_{max} and K_1 throughout the water column, which may bias the estimated contribution of SCM layers to water-column production. It is noteworthy, on the one hand, that no significant correlation was observed between experimentally-determined V_{max} values and irradiance at the time of sampling (Martin et al. 2012). In fact, V_{max} was instead correlated significantly to ambient NO_3^- concentration, with slightly lower values at the surface than at SCM depth (Martin et al. 2012). Considering this fact as well as the low ambient N concentrations typical of surface waters, the current lack of depth-dependent parameterization of V_{max} slightly underestimates the relative contribution of SCM. On the other hand, the K_1 values obtained from kinetics experiments varied positively with NO_3^- concentration in this study and others (Kristiansen et al. 1994) so that prescribing the upper estimate in the model elevates the apparent contribution of SCM and counteracts the underestimation caused by a constant V_{max}.

4.4.5 The ensemble approach

Apart from biotic factors, the main determinants of vertical nitrogen fluxes and light availability are turbulence and ice concentration, respectively. Being nonlinear, interactions between the physical environment and the marine ecosystem can turn relatively small variations in the former into large variations in the latter. For example, strong wind events impact primary production and its vertical distribution differently when they occur during a surface bloom or afterward when the SCM is well developed and sheltered by the halocline. In the former case, an earlier and more intense bloom fuelled by additional nutrient entrainment can accelerate zooplankton growth and slow down nitrate uptake by phytoplankton. Over an entire season, even a small change in background diffusivity in the ocean interior can impact total production (e.g. Huisman et al. 2006). To avoid giving too

much weight to any particular forcing time series and to embrace the fundamental uncertainties attached to forcing variables and physical parameters, a few 100-member ensembles of simulations forced by equally realistic but different surface boundary conditions (radiative fluxes, heat and wind) were performed. Each ensemble was constructed by extracting forcing conditions from 20 different geographical locations within the Amundsen Gulf and from 5 different years (2004-2008) of the NCEP-NARR Reanalysis. Two sea ice (called $\mathbf{f}_1$ and $\mathbf{f}_2$) and 3 prior-to-bloom NO_3^- profiles scenarios (called $\mathbf{n}_1$, $\mathbf{n}_2$ and $\mathbf{n}_3$) were constructed based on extremes observed during the period 2004-2008 and observations made in spring 2008, respectively (Fig. 4.5). To each ensemble were associated one sea ice and one prior-to-bloom NO_3^- scenario ($\mathbf{f}_i\mathbf{n}_j$). Sea ice scenarios represented a late and rapid break-up occurring from 10 to 14 May ($\mathbf{f}_1$), and an early slow break-up occurring from 1 April to 25 May ($\mathbf{f}_2$). Finally, pre-bloom NO_3^- profiles scenarios were also tested: $\mathbf{n}_1$ had low NO_3^- in surface waters (1.5 mmol m^{-3}) with a nitracline at 50 m; $\mathbf{n}_2$ had the same surface concentration as $\mathbf{n}_1$ but with a nitracline at 35 m; $\mathbf{n}_3$ had relatively high NO_3^- in surface waters (3.5 mmol m^{-3}) with a nitracline at 35 m. NO_3^- increased linearly to 15 mmol m^{-3} at 80 m ($\mathbf{n}_1$) and 75 m ($\mathbf{n}_2$ and $\mathbf{n}_3$) and remained constant down to the bottom.

It is noteworthy that standard deviations on phytoplanktonic parameters were of the same order of magnitude as the means. In order to characterize the impact of natural variability and parameter error estimation on SCM productivity, we performed a 600-member ensemble of simulations where ice (mean of observations between 2004 and 2008) and NO_3^- ($\mathbf{n}_2$) scenario were kept constant and parameters that have the most significant impact on primary production were varied within the range of observations made over the growth period: V_{max} = 0.02 to 0.72 d^{-1}, α = 0.02 to 0.28 $m^2 W^{-1} d^{-1}$, β = 0.0 to 0.002 $m^2 W^{-1} d^{-1}$ and w_p = –0.05 to –0.45 m d^{-1}. All parameters were kept constant and uniform throughout each simulation, as is done traditionally in classical ecosystem modeling studies. Previous studies showed that photosynthetic parameters are dynamic in the Arctic, changing on the vertical and through time (e.g. Martin et al. 2012; Harrison and Platt 1986) with possible effects on the amplitude and temporal evolution of SCM. However, we argue that the ensemble approach encompasses the uncertainties that would be inherent to a dynamic

parameterization and allows for comparison with other modeling studies. Detailed investigations of more realistic parameterizations will be the subject of future studies. In order to compare model results with *in situ* mooring data, an additional simulation was performed for the year 2008 where forcing conditions were chosen as close as possible to conditions prevailing near the mooring sites. In the next section, this simulation is used for comparison with data, while ensembles are used to characterize model error.

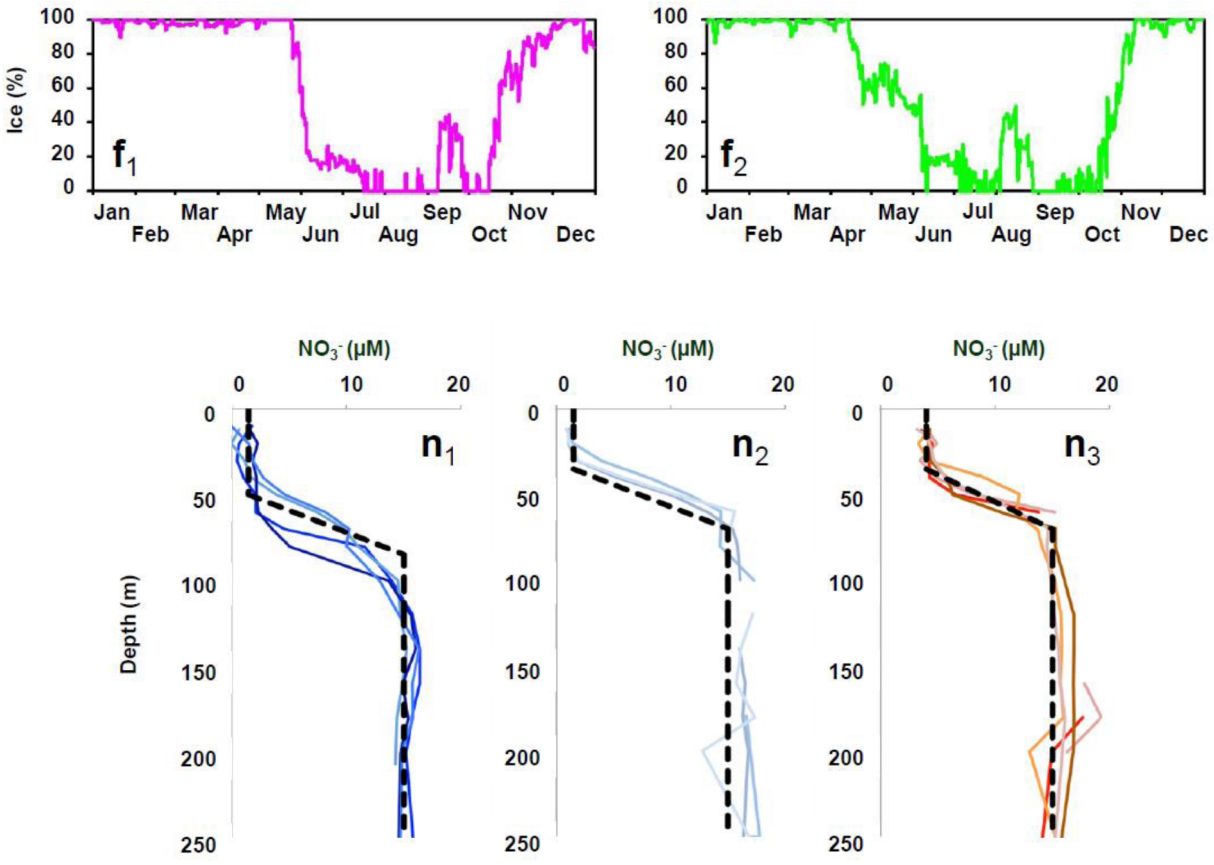

Figure 4.5. The two sea ice ($\mathbf{f}_1$ and $\mathbf{f}_2$) and 3 prior-to-bloom NO_3^- profiles scenarios ($\mathbf{n}_1$, $\mathbf{n}_2$ and $\mathbf{n}_3$) used in the ensemble approach.

4.5 Results

4.5.1 Comparison with 2008 observations

Moored fluorometers at 34 m (CA05) and 37 m (CA08) showed two distinct peaks on 1) 18 (3.22 µg chl *a* l^{-1}) and 10 May (1.09 µg chl *a* l^{-1}) and 2) 21 (3.76 µg chl *a* l^{-1}) and 13 June (2.59 µg chl *a* l^{-1}), respectively (Fig. 4.6). The simulated phytoplankton peak at 35 m reached 2.4 µg chl *a* l^{-1} around 29-30 July (Fig. 4.4). When compared with the second peaks from mooring observations, simulated chl *a* concentrations were within the same range but the peaks were delayed by 38 and 47 days. Prescribing ice transparencies of 8, 15 and 30% advanced the onset of the bloom by 19, 31 and 46 days (Fig. 4.7), respectively, closing the time lag we had in the original simulation with mooring observations. Changing transparency scenarios had a small influence on total annual production, which increased by 7, 11 and 16% for $\tau = 8$, 15 and 30%, and a negligible impact on the relative contribution of the SCM ($\leq$ 1%) and the maximum depth it attained during the year (data not shown).

Peak widths also differed between mooring observations (around 50 days) and model output (around 100 days). However, the growth phase of the bloom (i.e. between the onset and the maximum) lasted approximately the same time (mean of 30 days). The situation was different at ca. 50 m where the chlorophyll concentration estimated by the model never exceeded 0.50 µg chl *a* l^{-1} (maximum on 31 August at 51 m) while mooring data showed two peaks at CA05 (2.36 µg chl *a* l^{-1} on 19 May and 1.81 µg chl *a* l^{-1} on 23 June).

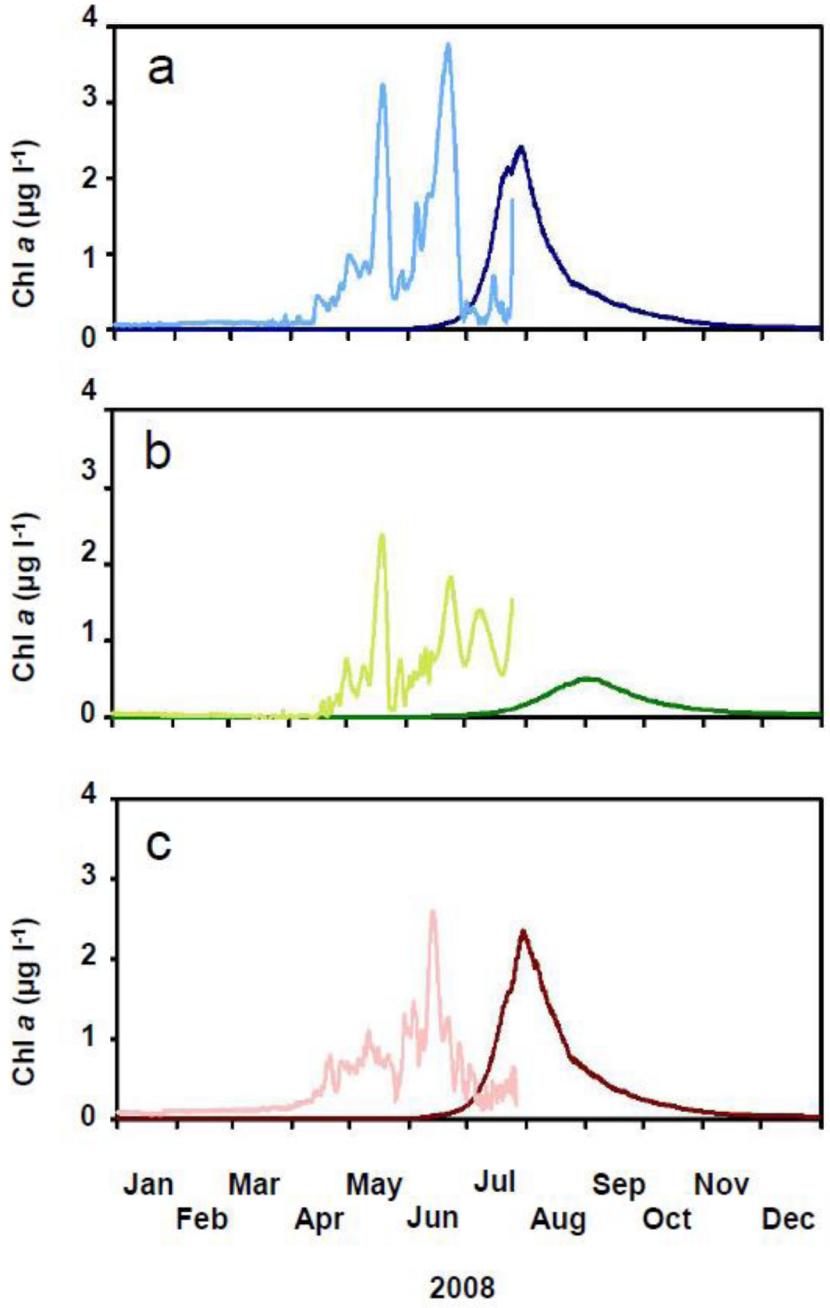

Figure 4.6. Time series of chlorophyll biomass recorded by moored sensors (lightly-coloured solid lines) and produced by the model (darkly-coloured solid lines) for CA05 at 34 m (a; blue) CA05 at 51 m (b; green) and CA08 at 37 m (c; pink) during 2008.

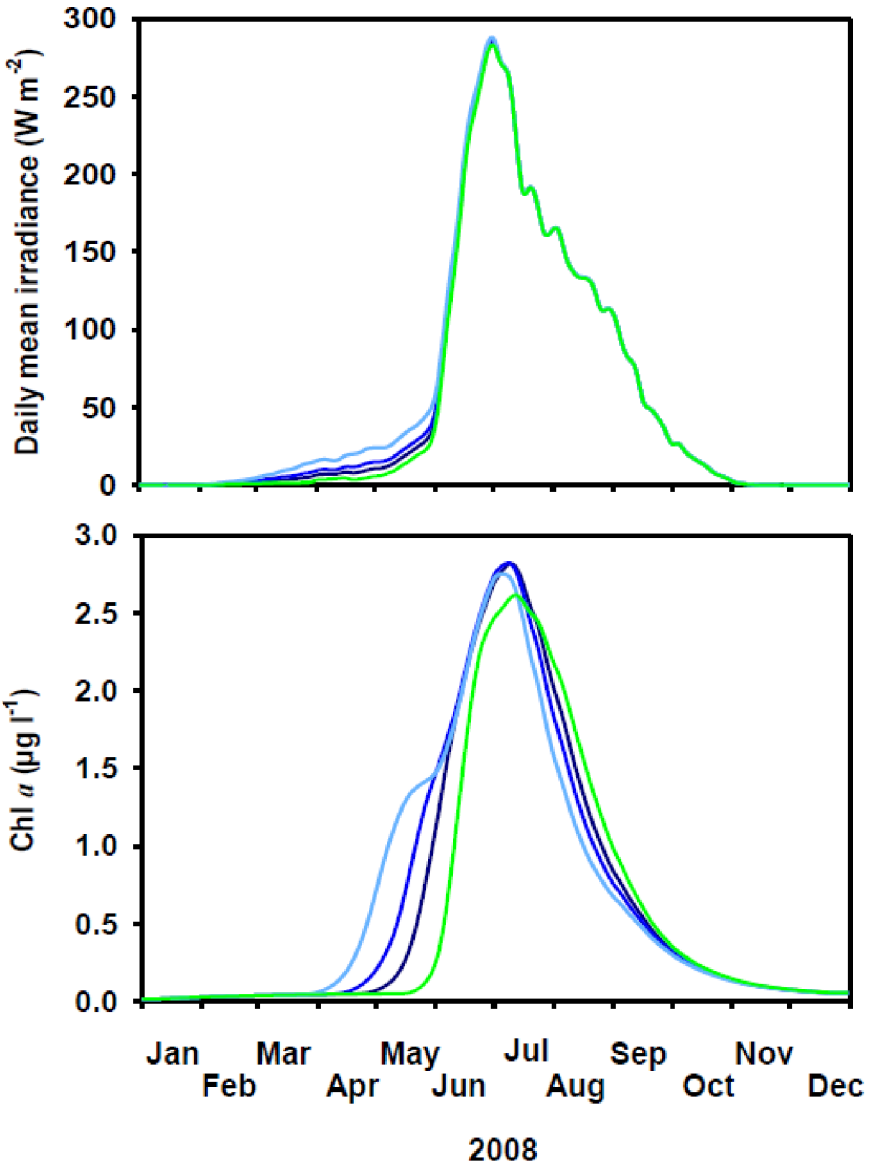

Figure 4.7. Daily mean irradiance available under ice cover (upper panel) and chl *a* concentration at SCM depth (lower panel) for opaque ice (green), 8% (dark blue), 15% (blue) and 30% (light blue) transparency scenarios.

4.5.2 Simulated SCM dynamics

In the 2008 simulation, the SCM (> 0.11 µg chl *a* l^{-1}) formed at ca. 10 m between 5 to 29 June (coinciding with a 65% decline of ice concentrations) and rapidly deepened to 30 m with a maximum of 2.56 µg chl *a* l^{-1} on 18 July (Fig. 4.4). This SCM persisted until

15 October, when maximum biomass was < 0.11 µg chl *a* l^{-1} at 42 m. The NO_3^- limitation index at SCM depth (Q_1) was ≥ 0.8 at the beginning of the season, decreased to 0.3 on 29 June and increased thereafter. The light limitation index at SCM depth (V/V_{max}) reached 0.6 on 5 June, continued to increase until 13 June (0.8) and decreased afterward. The SCM depth was robustly associated to the nitracline depth (Fig. 4.8; $Z_{SCM} = 1.34 \times Z_{nitracline} - 6.07$, $r^2 = 0.98$) until the end of August. After then, the vertical separation between the SCM and the nitracline was ≤ 10 m. Throughout the entire season, a strong relationship was noted between SCM depth and the primary NH_4^+ maximum (PamM; $Z_{PamM} = 0.60 \times Z_{SCM} + 20.73$, $r^2 = 0.70$; Fig. 4.8). Concentrations of NO_3^- were generally moderate (mean = 2.68 ± 1.45 mmol N m^{-3}) but quite variable (range 0.25–4.89 mmol N m^{-3}) at the SCM depth. By contrast, NH_4^+ concentrations were typically very low (mean = 0.25 ± 0.21 mmol N m^{-3}), ranging from 0.001 to 0.58 mmol N m^{-3}.

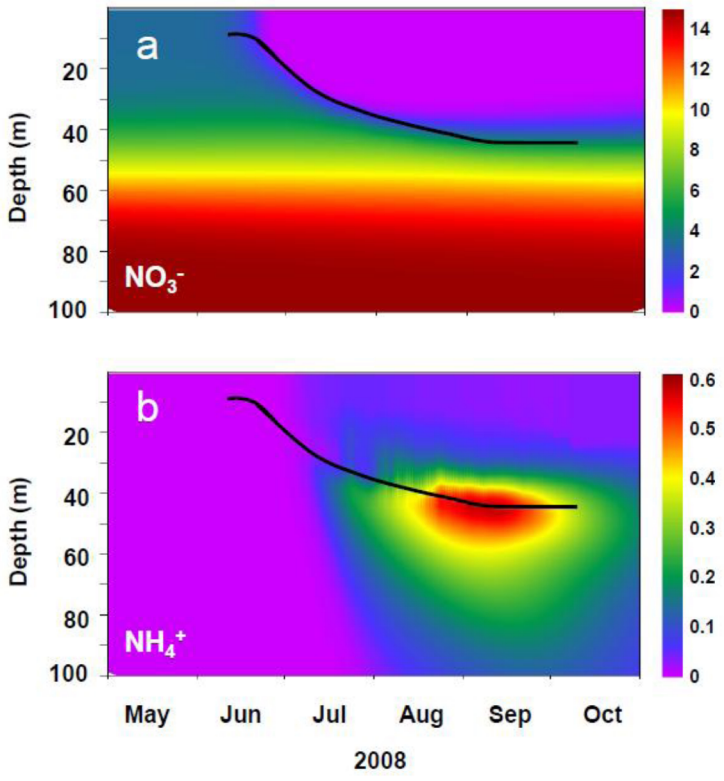

Figure 4.8. Concentrations of NO_3^- (upper panel) and NH_4^+ (lower panel) estimated by the model for 2008. The black line represents the depth of the SCM.

4.5.3 Simulated total, new and regenerated primary production

Total and new water-column production at the onset of SCM formation (5 June) for the 2008 simulation were both 0.03 mmol N m^{-3} d^{-1} (Fig. 4.9) and increased rapidly up to 0.25 mmol N m^{-3} d^{-1} on 18 June. Regenerated production was negligible prior to this date. When the SCM reached a maximum of 2.56 µg chl *a* l^{-1} (18 July), the total, new and regenerated production were 0.26, 0.20 and 0.06 mmol N m^{-3} d^{-1} (*f*-ratio = 0.80; Fig. 4.10) at SCM depth (30 m). During the same period, the maxima of total, new and regenerated production occurred at 32, 32 and 24 m, respectively, with corresponding rates of 0.29, 0.25 and 0.07 mmol N m^{-3} d^{-1}. Production at the SCM was very low after 25 September (0.01 mmol N m^{-3} d^{-1}; *f*-ratio = 0.60).

Slight vertical offsets in the depths of maximum total, new and regenerated production were maintained for an important part of the growth period. From the onset of the bloom to the date of maximum biomass at the SCM on 18 July, maximum total and new production were ca. 2 m below the SCM depth. These three depths coincided between 20 July and 15 August but afterwards the SCM dropped to 4 and 1 m below the maximum of total and new production, respectively. The depth of maximum regenerated production remained at ca. 7 m above the SCM during the entire simulation. Total and new production reached their highest value on 21–22 June (0.32 mmol N m^{-3} d^{-1}) at ca. 10 m, whereas regenerated production peaked on 5 August (0.10 mmol N m^{-3} d^{-1}) at 33 m.

4.5.4 Contribution of the SCM to annual primary production

Total annual primary production for 2008 was 283 mmol N m^{-2} y^{-1} (185 and 98 mmol N m^{-2} y^{-1} for new and regenerated production, respectively) which corresponds to 35, 23 and 12 g C m^{-2} y^{-1} using the C:N ratio specified in section 4.4.2 (Fig. 4.10). Production rates across the SCM layer then represented 231 mmol N m^{-2} y^{-1} (28 g C m^{-2} y^{-1}) for total production, 148 mmol N m^{-2} y^{-1} (18 g C m^{-2} y^{-1}) for new production and 83 mmol N m^{-2} y^{-1} (10 g C m^{-2} y^{-1}) for regenerated production. Overall contributions of the SCM layer to water-column rates spanned 82, 80 and 85% of total, new and regenerated production, respectively.

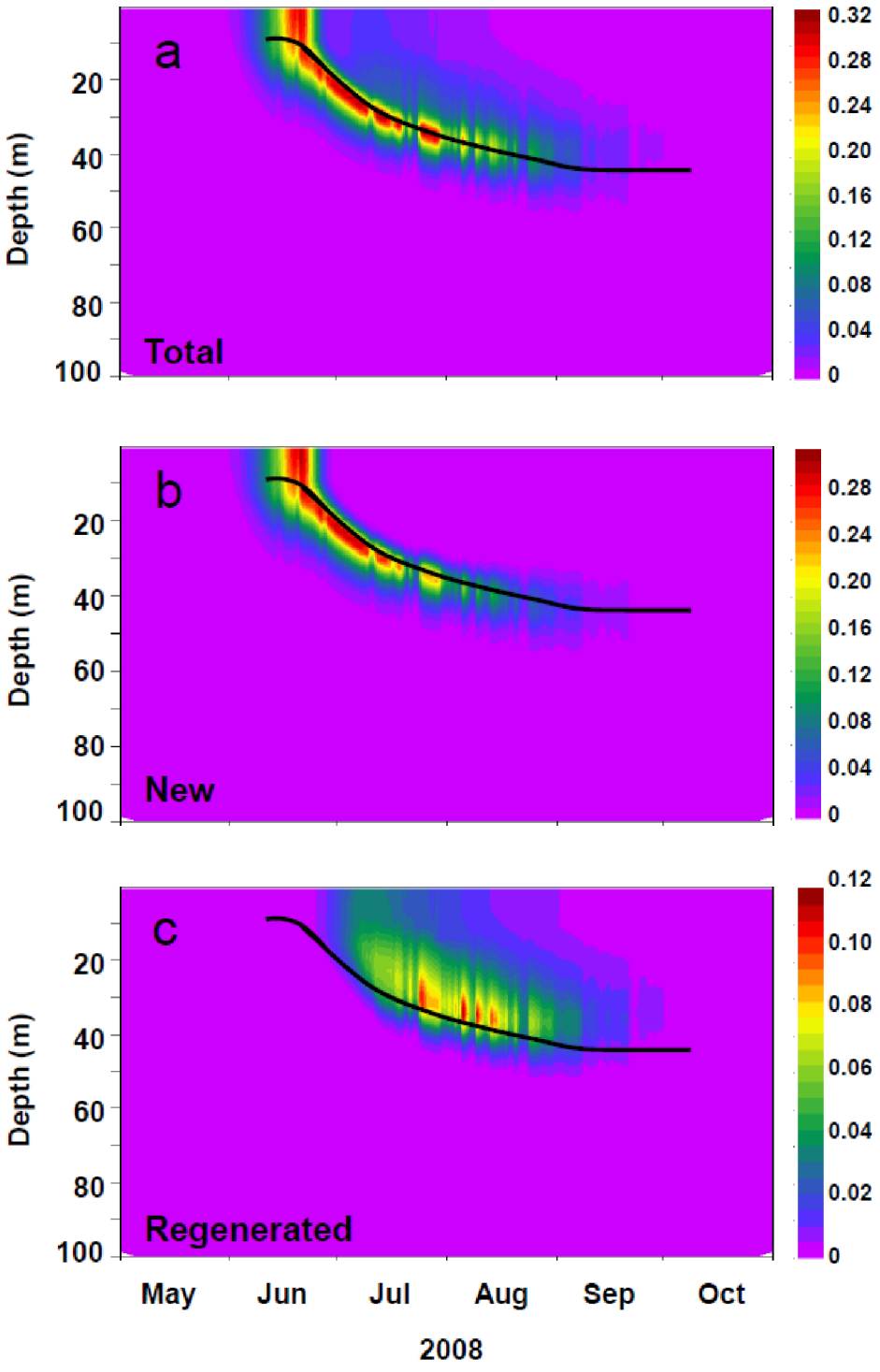

Figure 4.9. Modeled rates (mmol N m^{-3} d^{-1}) of (A) total, (B) new, and (C) regenerated production for 2008. The black line represents the depth of the SCM.

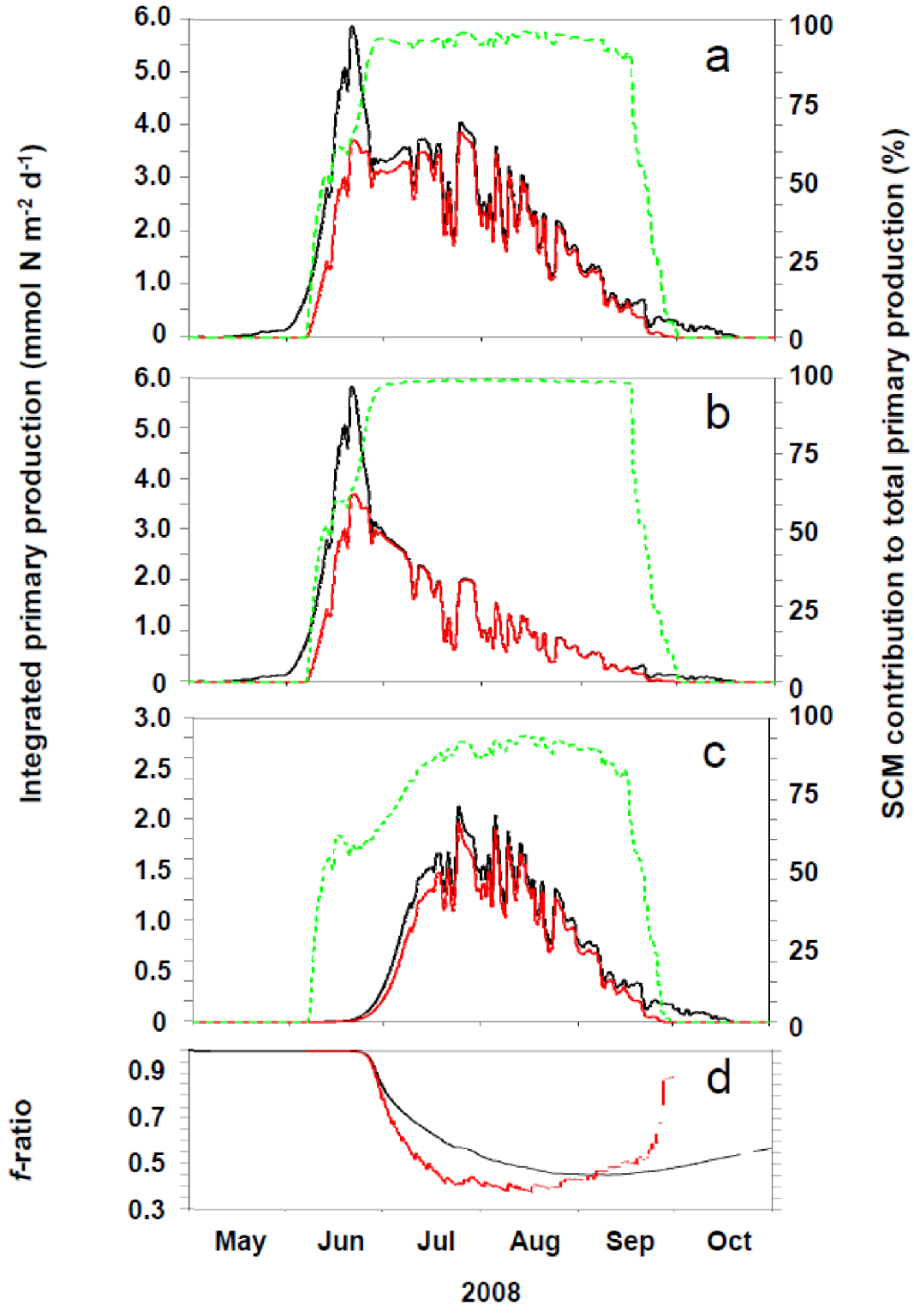

Figure 4.10. Time series of modeled daily rates (mmol N m^{-2} d^{-1}) of (a) total, (b) new, and (c) regenerated production and the *f*-ratio (d) in the water column (black) and in the SCM layer (red; see section 4.4.4 for definition) during 2008. The SCM contribution is given by the dashed green line. Note the different vertical scale in (c).

4.5.5 Inter-annual variability of the model and impact of physical forcing

The overall result of the ensemble analysis is that surface physical forcings during the growing season have a low impact on annual production and the relative contribution of the SCM to this production. The mean ensemble standard deviation represents only $\leq 6\%$ of total, new and regenerated production and $\leq 3\%$ of the contribution of the SCM to total, new and regenerated production (Table 4.2). The response to ice concentration (Table 4.2; tested with a constant NO_3^- scenario $\mathbf{n_3}$) was low but significant, with total, new and regenerated production varying by 28, -28 and 17 mmol N m^{-2} y^{-1} between scenario $\mathbf{f_1}$ and $\mathbf{f_2}$. Corresponding contributions of the SCM were $\leq 77\%$ for $\mathbf{f_1}$ and rose to $\leq 79\%$ for $\mathbf{f_2}$. For the NO_3^- scenarios (Table 4.2; tested with a constant $\mathbf{f_2}$ ice scenario), the total, new and regenerated production varied by 167, 65 and 62 mmol N m^{-2} y^{-1} between $\mathbf{n_1}$ and $\mathbf{n_3}$. For these scenarios, the contribution of the SCM to annual total, new and regenerated production amounted to $\leq 70\%$ for $\mathbf{n_1}$ and $\leq 79\%$ for $\mathbf{n_2}$ and $\mathbf{n_3}$.

Table 4.2 Mean annual production (mmol N m^{-2} y^{-1}) and SCM contribution to this production (%) with their respective relative standard deviation (%) for total, new and regenerated production in the ensemble analysis.

	$\mathbf{f_1n_3}$	$\mathbf{f_2n_1}$	$\mathbf{f_2n_2}$	$\mathbf{f_2n_3}$
Annual total production (mmol N m^{-2} y^{-1} ± %)	258 (4)	119 (5)	168 (6)	286 (4)
Annual new production (mmol N m^{-2} y^{-1} ± %)	180 (4)	87 (4)	127 (6)	152 (4)
Annual regenerated production (mmol N m^{-2} y^{-1} ± %)	77 (5)	32 (6)	35 (8)	94 (5)
SCM contribution to total production (% ± %)	79 (2)	71 (3)	80 (2)	82 (2)
SCM contribution to new production (% ± %)	77 (2)	70 (3)	79 (2)	79 (2)
SCM contribution to regenerated production (% ± %)	83 (4)	75 (4)	84 (3)	87 (2)

The SCM initially formed on 16 June for scenario $\mathbf{f_1n_3}$, 25 May for $\mathbf{f_2n_1}$ and $\mathbf{f_2n_2}$ and 18 May for $\mathbf{f_2n_3}$ but disappeared on 8 November for all ensembles, which results in growth periods of 145, 167 and 174 days, respectively (Fig. 4.11). For $\mathbf{f_1n_3}$, the SCM achieved a maximum concentration of 2.5 µg chl *a* l^{-1} on 30 July. For $\mathbf{f_2}$, the maximum was 1.0 µg chl *a* l^{-1} on 26 July for $\mathbf{n_1}$, 1.8 µg chl *a* l^{-1} on 28 July for $\mathbf{n_2}$ and 2.8 µg chl *a* l^{-1} on 24 July for $\mathbf{n_3}$ (Fig. 4.11). The SCM deepened to a maximum depth of 48, 59, 56 and 51 m for $\mathbf{f_1n_3}$, $\mathbf{f_2n_1}$, $\mathbf{f_2n_2}$ and $\mathbf{f_2n_3}$, respectively (Fig. 4.11).

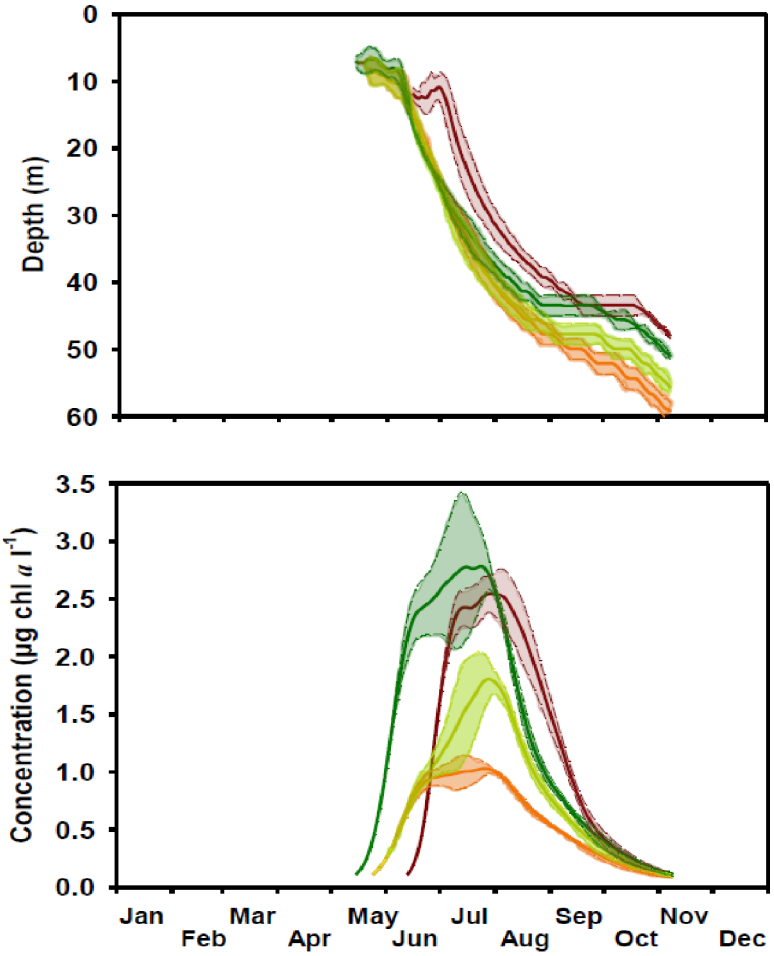

Figure 4.11. Comparison of the temporal evolution of SCM depth (m; upper panel) and the chl *a* concentration at this depth (µg chl *a* l^{-1}; lower panel) between scenarios $\mathbf{f_1n_3}$ (purple), $\mathbf{f_2n_1}$ (orange), $\mathbf{f_2n_2}$ (light green) and $\mathbf{f_2n_3}$ (dark green). Shaded areas represent the standard deviation on mean SCM depths and chl *a* concentrations, respectively.

4.5.6 Biological variability of the model

The response of total production and the relative SCM contribution to changes in w_p and β was small in the biological ensemble. For this reason, only the two extreme scenarios are shown in Fig. 4.12. Unlike w_p and β, changes in $V_{\max}$ and α had a greater impact on overall rates. With $V_{\max} \geq 0.22$ and $\alpha \geq 0.08$, the annual total production varied from 94 to 311 mmol N $m^{-2}y^{-1}$ and SCM contribution was $\geq 65\%$ over the ranged of parameters (Fig. 4.12). An increase in this contribution also occurred with rising total annual production in the water column (Fig. 4.12).

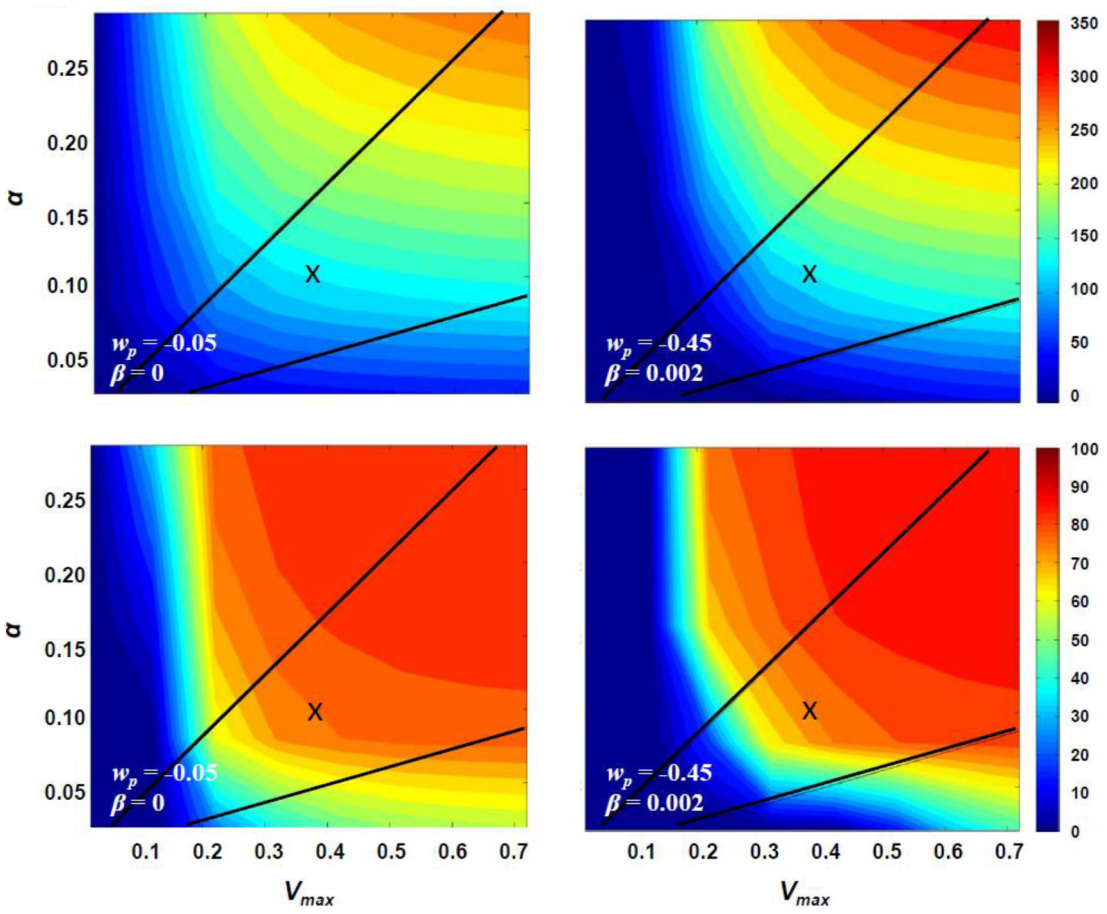

Figure 4.12. Impact of changes in the parameters V_{max} and α under two w_p and β scenarios (w_p = -0.05 and β = 0 on the left side and w_p = -0.45 and β = 0.002 on the right side) on estimates of annual production (mmol N m^{-2} y^{-1}; upper panels) and the relative contribution of the SCM layer (%; lower panels). The "x" stands for the mean condition used in the 2008 simulation (see section 4.4.3) and the solid lines give the range of photo-acclimation indices ($E_k = V_{max} / \alpha$) observed at the surface and at the SCM depth by Martin et al. (2012).

4.6 Discussion

Model results clearly support the fact that SCM can mediate a large fraction of water-column primary production on a daily basis, which is consistent with field observations made by Martin et al. (2012) for the Canadian Beaufort Sea, as well as on an annual basis. This is largely due to the typically low concentration of nitrogen available in the upper euphotic zone. With the exception of a brief period at the onset of the spring bloom, SCM are present during the entire growth period and, with the adjoining layer of elevated chl *a*, account for 65 to 90% of the total annual primary production under the whole range of observed phytoplankton parameters.

Notable differences in the timing and vertical distribution of primary production were observed when comparing simulations and mooring data. The absence of the first peak, observed around mid-May in mooring data, most probably resulted from the absence of ice algae in the model. The concordance of near-synchronous chlorophyll peaks at 35 and 50 m with rapid ice break-up (ice concentration dropped from ~90% to ~35% in the first half of May) and a temporary spike in sedimentation rates in the region is consistent with the export of newly released ice algae (Forest et al. 2011). The omission of ice algae from the model should nevertheless have a minor impact on primary production estimates since bottom-ice communities contribute to less than 5% of total annual production in Arctic coastal waters (Gosselin et al. 1997; Lavoie et al. 2009).

The single chlorophyll peaks produced by the model at ca. 35 m were delayed by 38 and 47 days when compared to the second peak observed at CA05 and CA08, respectively. This situation is neither surprising nor invalidating considering that we used regionally-averaged ice concentrations and opaque ice conditions as a baseline. Prescription of an opaque ice cover can forestall the beginning of the season by up to 46 days (Fig. 4.7). Moreover, ice retreat (concentration $\leq$ 5%) occurred on 5 June above the moorings (Forest et al. 2011) but on 29 June in the model. The resulting delay in chlorophyll peaks is consistent with the correlation observed between ice retreat and the initiation of the bloom in the ensemble analysis (Fig. 4.11). The key point, however, is that timing is inconsequential in the present exercise because sensitivity tests showed that different transparency scenarios have a small

effect on total annual production (≤ 16%) and the contribution of the SCM (≤ 1%) to this production.

The absence of ice algae and under-ice bloom in the model also delays the consumption of NO_3^- in the upper few meters of the water column so that the simulated SCM initially develops in open water very close to the surface (ca. 10 m). Nevertheless, ice transparency tests produced only slight differences in the depth where the SCM attains the highest chl *a* concentration during the growth period (32, 34, 36 and 38 m for $\tau = 0$, 8, 15 and 30%, respectively). For the 2008 simulation, the nitracline reached a maximum depth of 34 m during the growth period (Fig. 4.8). The ensemble analysis showed similar maximum depth for the nitracline (the effect of initial nutrient availability on primary production is discussed later), which could explain why chlorophyll persisted longer at 30 m (ca. 50 days longer than at the mooring locations) and never showed conspicuous increases at 50 m. Nevertheless, the SCM depths obtained with the 2008 simulation (Fig. 4.4) was within the range of observations made in the Beaufort Sea and Amundsen Gulf in late summer and fall 2005 and 2006, when SCM occurred between 20 and 35 m (except off the shelf break where SCM were between 40 and 62 m; Martin et al. 2010), and throughout the entire growth period across the whole Canadian Arctic from 2005 to 2008, where the mean SCM depth was 35±16 m (Martin et al. 2012).

Integrated over a year, modeled water column primary production (35 g C m^{-2} y^{-1}) was tightly bracketed by different field-based estimates for the same area and year (49 g C m^{-2} y^{-1} by Forest et al. 2011; 25 g C m^{-2} y^{-1} by Shadwick et al. 2011), but slightly higher or within range of estimates for other years and sectors (e.g., 15–40 g C m^{-2} y^{-1} by Subba Rao and Platt 1984; 12–28 g C m^{-2} y^{-1} based on Carmack et al. 2004 and Lavoie et al. 2009; 20 – 70 g C m^{-2} y^{-1} by Hill and Cota 2005 for the Chukchi Sea). Overall, these values are characteristic of oligotrophic waters and much lower than those attained (>150 g C m^{-2} y^{-1}) in productive sectors of the Arctic.

In agreement with the field data analyzed by Martin et al. 2012 (*f*-ratio of 0.74 ± 0.26 for spring and early-summer and 0.37 ± 0.20 for late-summer and fall) and by Simpson et al. 2013 (*f*-ratio between 0.6 and 0.9 during the peak of production and between 0.1 and 0.2

and 0.4 and 0.6 for the pre-bloom and autumn period), we noted a decrease of the *f*-ratio at the depth of the SCM throughout the growth season. This phenomenon can be explained by the combined effect of the decrease in NO_3^-, the buildup of the NH_4^+ pool and the higher affinity of the phytoplankton for NH_4^+ than NO_3^- in the range of concentrations observed at the SCM. Nevertheless, the integrated *f*-ratio for the entire period (annual new production / annual total production) was 0.66 for the whole euphotic zone and 0.64 for the SCM (Fig. 4.10). These values fall in the middle of the range (0.48-0.95) estimated by Forest et al. 2011 using field data from the central Beaufort Sea for spring-summer 2008. This can be explained by the fact that a large share of the SCM production takes place during spring, when NO_3^- concentrations are favorable in the upper part of the water column. We thus conclude that new production supports a large portion of total annual production in the Beaufort Sea. The system appears to be N-limited since we noted an important increase in productivity with rising NO_3^- concentrations in the ensemble analysis (increase of 170 mmol N m^{-2} y^{-1} between $\mathbf{n}_1$ and $\mathbf{n}_3$), while the change in the length of the growth period ($\mathbf{f}_1$ and $\mathbf{f}_2$) had a minor effect on overall productivity (difference of 28 mmol N m^{-2} y^{-1} between the two ice scenarios; Table 4.2).

4.6.1 Dynamics of SCM development

Estimates of annual primary production and of the SCM contribution showed a low sensitivity to surface boundary conditions (radiative fluxes, heat and wind) in the ensemble analysis, implying a relative independence of SCM dynamics to varying surface conditions. In the Canadian Arctic, snow thickness, ice melting and underwater irradiance are known to control the timing of blooms (Fortier et al. 2002). Under-ice phytoplankton blooms have also been recognized as a potentially widespread, under-documented and increasingly frequent phenomenon (Fortier et al. 2002; Mundy et al. 2009; Arrigo et al. 2012). In the 2008 simulation, we noted a synchrony between the initiation of the bloom and a threshold ice concentration of 65%. The SCM then hovered near 10 m until the ice concentration dropped below 5%. Ice transparency scenarios point in the same direction (Fig. 4.7). On 29 June, the NO_3^- limitation index reached its minimum value and the SCM started to rapidly deepen with the nitracline in response to the rapid development of N shortage in surface waters. Rapid deepening of the SCM was also noted by Palmer et al. (2011) during spring 2008 in Darnley Bay (Beaufort Sea), where it passed from 10 to 34 m within 6 days.

Subsequent to the onset of nutrient limitation at the surface, a close association develops between the SCM and the nitracline, which approximates the relationship previously observed in the Canadian Arctic ($Z_{SCM} = 1.00 \times Z_{nitracline} - 2.57$; Martin et al. 2012). Proximity with the nitracline allows the phytoplankton to avoid prolonged conditions of N limitation (i.e. the increase in the NO_3^- limitation index) but induces light limitation of short-term production rates (see also Martin et al. 2012). This is reflected in the depth of maximum total and new production, which goes from below the SCM depth at the beginning of the open-water period (to avoid N limitation under favorable light condition) to above the SCM depth later on (to counteract light limitation; Fig. 4.9), the decline of chl *a* concentrations at the SCM after 18 July (Fig. 4.4) and the appearance of maximum regenerated production 7 m above the SCM. The latter results from the greater availability of light and NH_4^+ above the nitracline as well as the prescribed higher affinity of phytoplankton for NH_4^+ in the model ($K_2 = 0.2$). The SCM presumably deepens the nitracline until irradiance become insufficient to support net growth (i.e. the compensation irradiance; Klausmeier and Litchman 2001). In the model this threshold was attained on 15 October (SCM at 42 m), when the daily mean irradiance dropped below 0.1 W m^{-2} (similar to the value estimated by Holm-Hansen et al. (1977) in Antarctica).

4.6.2 Contribution of the SCM layer to water-column productivity

Model results indicate that SCM layers mediate a very large share of total, new and regenerated primary production under the strongly stratified and oligotrophic conditions that prevail in the Canada Basin and the Amundsen Gulf. Throughout the range of significant photosynthetic parameters, the SCM contribution always represented more than half of total, water column production (contribution $\geq$ 65%; Fig. 4.12). Whether this result extends to other less stratified sectors of the Arctic is unclear at present. The modeling study of Popova et al. (2010) obtained SCM contributions ranging from 10 to 90% depending on sectors (pan-Arctic average of 46%). Based on remote sensing approaches and historical field data (ARCSS-PP database), Hill et al. (2013) proposed that SCM account for 50% of pan-Arctic primary production on average, whereas Arrigo et al. (2011) found a much lower average of 8% (see also Ardyna et al. 2013). We refer the reader to Martin et al. (2012) for a discussion of possible causes behind these contrasted results; those include limitations inherent to the ARCSS-PP database as well as differences in the

algorithms used to infer water-column productivity from surface properties and in the procedures used for temporal and spatial averaging.

4.6.3 Impact of environmental change on the fate of SCM productivity

A marked decrease in the duration of the ice-covered period was observed in the Arctic in recent decades (Serreze et al. 2007; Markus et al. 2009). The apparent response of primary production, estimated by remote-sensing techniques, is generally modest but variable in sign, ranging from negative in some areas to null or positive in others (Arrigo et al. 2008; Bélanger et al. 2012). For the Canada Basin, a study of the partial pressure of CO_2 indicated a lack of increase in carbon drawdown by primary producers (Cai et al. 2010). This observation was recently extended to the southeast Beaufort Sea (Else et al. 2013) and is consistent with the results of the present simulation, in which an increase of nearly one month in the ice-free period translated into a production increment of only ca. 10% (28 mmol N m^{-1} y^{-1}; Table 4.2) and a 3% rise in the contribution of the SCM in Amundsen Gulf. This can probably be attributed to more favorable light conditions in surface waters when the ice breaks up late (the midnight sun prevails in June and July), which presumably allows higher production rates at the SCM (Fig. 4.11). In this case, the maintenance of relatively high subsurface production rates after the end of the surface bloom likely counteracts the effect of a shorter growth period.

A prior review of published time courses of primary production showed that environmental forcing of N supply exerts a major influence on annual primary production in seasonally ice-free waters (Tremblay and Gagnon 2009). This pattern is consistent with the leading role of pre-bloom NO_3^- concentrations in setting the concentrations of chl *a* at SCM depth (Fig. 4.11) and total water-column primary production (e.g., annual production in scenario $\mathbf{n}_1$ represents only 42% of the production in scenario $\mathbf{n}_3$) in our simulations. The weak response ($\leq$ 8%; Table 4.2) of annual primary production to changes in external physical forcings in the ensemble analysis suggests that it will stay low as long as the Beaufort Sea remains strongly stratified by low-salinity water from the Pacific Ocean and freshwater input from rivers and melting ice (see also Tremblay et al. 2008). Note that the 1-D approach used here tackles the overall impact of vertical mixing but does not resolve

episodic nutrient supply by internal waves, convection, eddies or upwelling, which can drive substantial increases in productivity on shelves (Tremblay et al. 2011).

4.7 Conclusion

Results obtained from the ensemble analysis of numerical simulations indicate that the SCM contributes 65 to 90% of total annual primary production in the stratified oceanic waters of the Beaufort Sea (Canadian Arctic), based on realistic prescriptions of photosynthetic parameters for the area. The persistent association of the SCM with the nitracline throughout the growth period supports a system based primarily on NO_3^-, challenging the classical view that stratified oligotrophic waters rely primarily on N recycling and regenerated production.

In contrast to other studies advocating a rise in annual primary production in different sectors of the Arctic Ocean, a one month extension of the ice-free period in Amundsen Gulf induced a small 10% increase in annual primary production. This result is explained by the strong vertical stratification, which opposes mixing processes and dampens the fluctuations and changes in N replenishment that would otherwise ensue from a greater exposure of the surface ocean to direct atmospheric forcing (see also Tremblay et al. 2008 and Codispoti et al. 2013). We therefore hypothesize that, in the long run, changes in productivity resulting directly from convection or wind-driven mixing in the Canada Basin will be minor unless the upper halocline weakens over time.

Overall, this study underscores how simple models can lead to a better grasp of phenomena that are difficult or even impossible to fully quantify in the field. The inclusion of a dynamic parameterization, where photosynthetic parameters are allowed to respond to recent light history and improved upper ocean physics, would be the next logical step. There is little doubt that a judicious combination of field sampling and modeling can lead to novel insights into the changing Arctic ecosystem, allow to formulate new hypotheses and generate plausible scenarios for the future.

Chapitre 5 Conclusion

5.1 Conclusion générale

La production primaire océanique joue un rôle primordial au sein de l'écosystème Arctique. Cependant, les producteurs se retrouvant à la base du réseau alimentaire marin rencontrent des conditions de croissance particulièrement variables et contraignantes à ces latitudes (Smith et Harrison 1991; Sakshaug 2004; Tremblay et Gagnon 2009). La compréhension des différents phénomènes et mécanismes entourant ces communautés clés est donc d'une importance fondamentale pour la compréhension globale de la dynamique écosystémique. L'échantillonnage effectué lors de la présente étude a mené à l'obtention d'une couverture spatiale et temporelle étendue de l'environnement biophysicochimique et des processus phytoplanctoniques associés. Motivée par l'observation préalable que les maximums de chlorophylle subsuperficiels (SCM) sont des structures majeures se formant tôt en saison, persistantes durant l'été et possiblement responsables d'une grande part de l'utilisation du nitrate dans la colonne d'eau, cette première thèse consacrée à la structure verticale de la production primaire arctique avait pour but d'étudier les propriétés, la phénologie et l'écophysiologie des SCM dans les eaux canadiennes.

Dans un premier temps, l'objectif était d'établir la quantité et la répartition verticale de la chlorophylle en fonction des conditions océanographiques de l'Arctique canadien (chapitre 2) et, parallèlement, de vérifier si la chlorophylle de surface pouvait permettre de prédire la chlorophylle totale dans la colonne d'eau (par exemple, dans le but de faire des estimations de biomasse ou de production primaire à l'aide de la télédétection). Ce chapitre nous a permis d'observer que les SCM sont des structures extrêmement répandues et responsables d'une part non-négligeable de la biomasse phytoplanctonique en Arctique canadien. L'utilisation rapide du nitrate dans les eaux de surface (Tremblay et al. 2008; Mundy et al 2009) cause l'apparition hâtive des SCM qui se retrouveront par la suite associés à la nitracline. Ces SCM étant en lien avec les maximums de biomasse (et non la conséquence d'une augmentation du ratio de chlorophylle : carbone), ils contiennent une partie

importante et difficilement prévisible du carbone disponible dans la colonne d'eau. Ces conditions font en sorte que l'estimation de la chlorophylle et de la production primaire à partir des observations satellitaires représente un défi considérable en Arctique canadien, puisqu'une portion importante de la chlorophylle totale y est difficilement estimable à partir de la chlorophylle de surface.

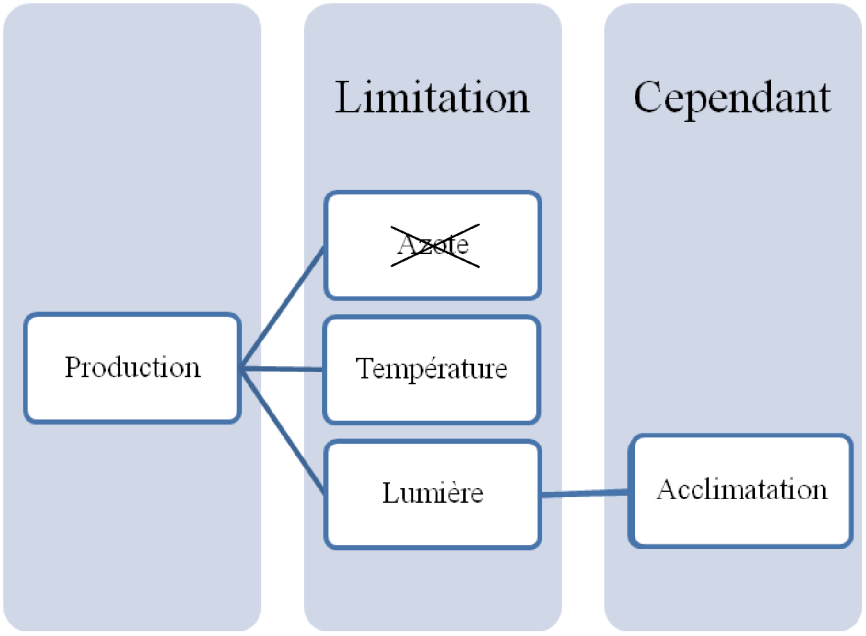

Figure 5.1. Schématisation des principaux résultats de la thèse en ce qui concerne les facteurs pouvant freiner ou aider la production primaire du SCM.

Puisque les SCM sont localisés en profondeur, en association avec la nitracline, il a été supposé que leurs taux photosynthétiques seraient limités en lumière, par opposition aux communautés de surface, et qu'elles consommeraient principalement de l'azote nouveau (nitrate) provenant des eaux profondes plutôt que l'azote recyclé localement (ammonium, urée). Afin de vérifier cette hypothèse, les relations entre la lumière, les nutriments et la prise de carbone et d'azote en surface et au SCM ont été évaluées de manière expérimentale au chapitre 3. Conjointement, l'étude avait pour objectif d'évaluer la contribution des SCM à la production totale de la colonne d'eau ainsi que de réviser les paramètres

photosynthétiques utilisés par plusieurs modèles et algorithmes de télédétection. Les résultats ont permis de démontrer que la production primaire du phytoplancton des SCM est généralement limitée en lumière et/ou en température durant l'été et l'automne, bien que les algues soient photosynthétiquement compétentes, apparemment bien acclimatées à leurs conditions de croissance et qu'elles montrent une forte photoinhibition aux intensités lumineuses se rapprochant de celles observées en surface (étude des F_v/F_m). Un calcul ponctuel basé sur les différences de paramètres photosynthétiques observées entre la surface et le SCM a montré que la strate verticale composant le SCM pouvait supporter jusqu'à 76% de la production de carbone (et jusqu'à 98% de la prise de nitrate) dans la colonne d'eau. Les algues du SCM consommaient majoritairement le nitrate au printemps, mais leur dépendance à cette forme d'azote diminuait avec l'avancement de la période de croissance (Fig. 5.2). Cette transition est probablement due au déclin saisonnier de l'énergie lumineuse disponible, ce qui favoriserait la prise d'ammonium dont le coût énergétique d'assimilation est moindre que celui du nitrate (Behrenfeld et al. 2008). Bien qu'à tout moment de l'année les algues du SCM semblent préférer l'ammonium lorsque l'éclairement est faible, la faible disponibilité de ce nutriment contraint le phytoplancton à utiliser du nitrate pour combler ses besoins en azote, d'où l'association entre la profondeur du SCM et celle de la nitracline.

Afin de vérifier l'hypothèse selon laquelle les SCM contribuent de façon significative à la production annuelle totale, nouvelle et régénérée, l'estimation de la production primaire ainsi que l'évolution temporelle et la contribution des SCM ont été effectuées à l'aide d'une approche numérique (chapitre 4). Cette approche a permis d'évaluer que la couche d'algues englobant le SCM en mer de Beaufort contribuait à plus de 65% de la production totale de la colonne d'eau, indépendamment des conditions initiales imposées. Les résultats obtenus à l'aide du modèle permettent aussi de conclure que la persistance des SCM fait en sorte que la production nouvelle contribue fortement à la production totale au cours d'une année de production en mer de Beaufort, en accord avec leur association avec la nitracline. Somme toute, les valeurs de production primaire annuelle estimées à l'aide de l'approche numérique démontrent bien le caractère oligotrophe de la mer de Beaufort, un système limité en azote où les concentrations de nitrate disponibles en surface déterminent le niveau de productivité.

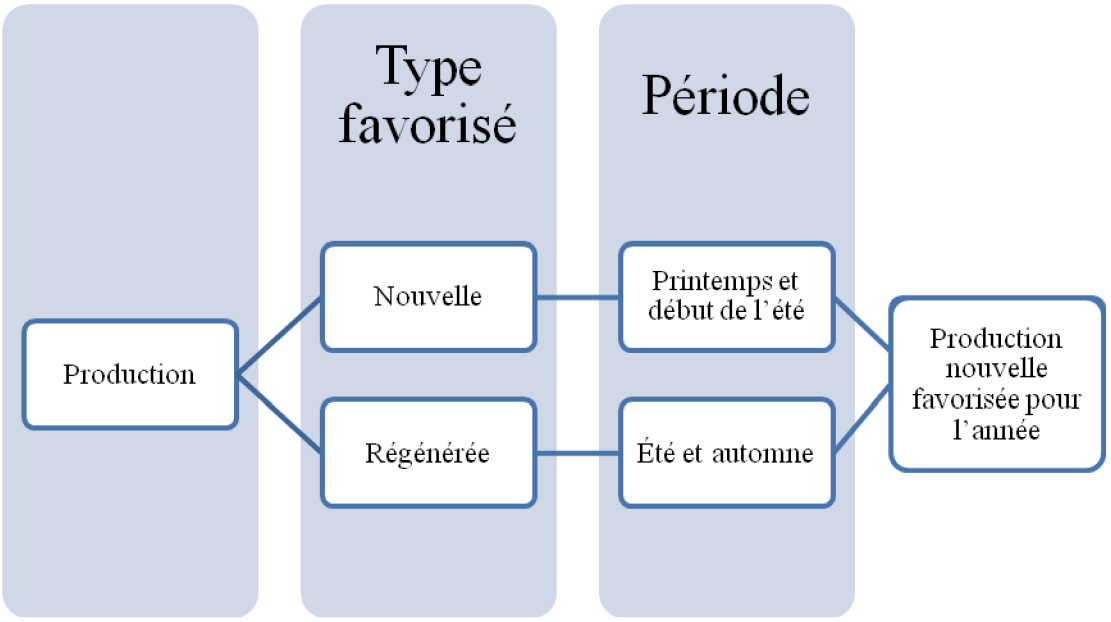

Figure 5.2. Résumé des types de production primaire qui dominent sur une base saisonnière et annuelle en Arctique canadien.

Le modèle élaboré dans le cadre des travaux de la présente thèse a aussi permis de révéler la dynamique du SCM à travers une saison de production et de compléter la vision découlant des observations effectuées sur le terrain. Cette dynamique est d'ailleurs schématisée à la Figure 5.3. Tout d'abord, on note une apparition rapide de la chlorophylle et du SCM lors du retrait de la glace. On observe par la suite un approfondissement du SCM, qui suivra la nitracline jusqu'à l'atteinte de la profondeur seuil où les algues passent d'une limitation en nitrate à une limitation en lumière. C'est la quantité de nitrate disponible au dessus de ce seuil en début de saison qui détermine l'intensité du SCM. L'approfondissement du SCM se poursuit ensuite alors que les algues poussent la nitracline encore plus bas pour se procurer de l'azote. La limitation en lumière devient éventuellement suffisamment sévère pour conduire au déclin du SCM et sa disparition, lorsque la production nette, n'est plus possible en fin de saison.

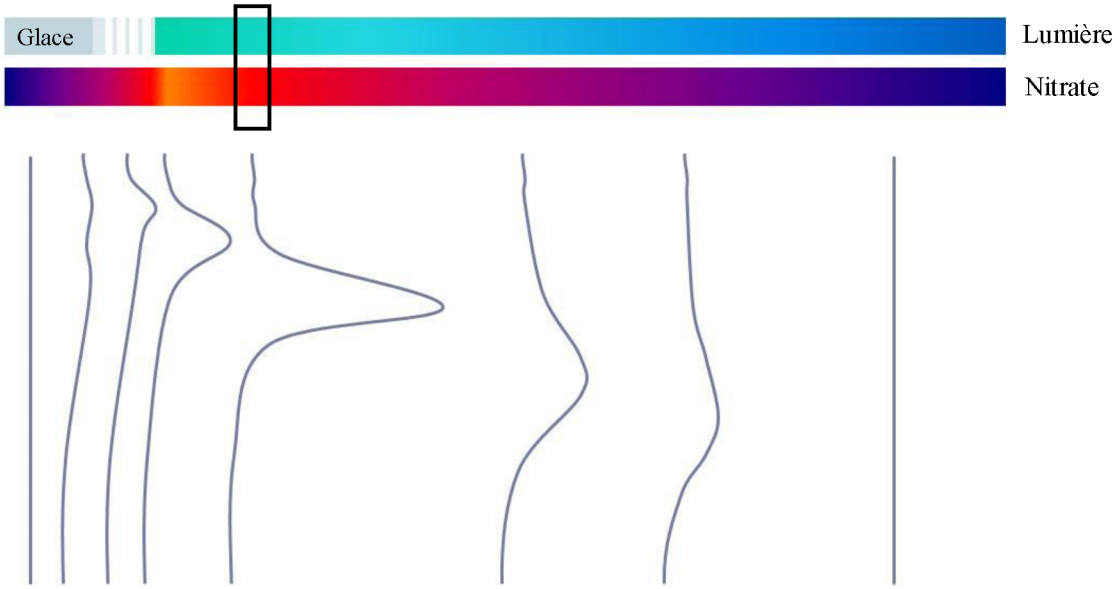

Figure 5.3. Évolution schématisée du profil vertical de chlorophylle (traits bleus) ainsi que de l'intensité lumineuse (du vert au bleu) et de la concentration en nitrate (du orange au violet) au SCM pendant la saison de croissance. Le période optimale pour la productivité du SCM est représentée par le rectangle noir.

Dans une perspective élargie, la zone d'étude couverte par cette thèse représente environ 27% de la superficie de l'Arctique, ce qui est considérable. Deux études récentes indiquent que les SCM représenteraient environ la moitié de la production annuelle totale à l'échelle de l'Arctique (Popova et al. 2010; Hill et al. 2013). Il semble donc que les SCM soient des structures répandues et importantes dans cet océan et qu'omettre de les considérer peut potentiellement mener à une sous-estimation substantielle de la production primaire. Quoique seul un échantillonnage intensif des SCM pour l'ensemble de l'Arctique puisse apporter des certitudes en la matière, il est permis de penser que des résultats similaires à ceux observés en Arctique canadien seront aussi retrouvés dans les autres régions. À titre d'exemple, McLaughlin et Carmack (2010) ont observé la présence de SCM en association avec la nitracline dans le basin du Canada. Ces SCM ont par ailleurs été observés plus profondément qu'en Arctique canadien, soit entre 50 (entre 2003 et 2005) et 65 m (entre 2008 et 2009). Dans les basins de Marakov et de Nansen, les SCM peuvent être retrouvés

jusqu'à 85 m sous la surface (Gosselin et al. 1997). Cette situation contraste avec les environnements côtiers, où ils sont le plus souvent observés à des profondeurs moindres, soit entre 20 et 45 m (dans la baie d'Hudson par Martini 1986; dans le détroit de Fram par Hirche et al. 1991; en mer de Laptev par Heiskanen et Keck 1996; en mer de Chukchi central par Cota et al. 1996 et Gosselin et al. 1997; en mer de Beaufort par Carmack et al. 2004; en mer de Kara par Romankevich et Vetrov 2004; en mer de Beaufort et de Chukchi par Hill et Cota 2005). Malgré les différences physiques entre les régions arctiques, Popova et al. (2010) ont conclu que même dans les zones influencées par les apports d'eau Pacifique et Atlantique (par exemple le sud de la mer de Chukchi), où les nutriments sont retrouvés en concentrations relativement élevés, les SCM représenteraient de 30 à 40% de la quantité totale de chlorophylle dans la colonne d'eau. La contribution du SCM à la production totale augmente de 46%, pour l'ensemble de l'Arctique, à 68% lorsque ces zones sont exclues du calcul (Popova et al. 2010).

Un objectif concomitant de cette thèse était de fournir des pistes de réponses quant à l'implication des modifications de l'écosystème Arctique sur la productivité biologique marine dans un contexte de changements climatiques. Dans cette optique, l'influence positive de l'adoucissement des eaux de surface par les apports fluviaux, l'augmentation des précipitations et la fonte des glaces sur la stratification verticale (Peterson et al. 2002) feront en sorte que les algues dépendront davantage des apports en nutriment à la base de la zone euphotique (McLaughlin et Carmack 2010). De plus, les simulations effectuées en mer de Beaufort suggèrent que l'augmentation de la saison libre de glace n'a qu'un impact modeste sur l'augmentation de la productivité (environ 10%). Toutefois, l'augmentation de la lumière disponible en synergie avec une augmentation de la température pourrait causer une augmentation de la productivité de la zone du SCM, soit par l'utilisation plus complète du nitrate ou par l'approfondissement de la nitracline. Tel que suggéré par les différents scénarios de disponibilité de nitrate (« prior-to-bloom ») simulés au chapitre 4, l'upwelling en fin de saison de production peut aussi renouveler les nutriments en surface, produisant des conditions initiales de nitrate favorisant la production primaire de surface au printemps subséquent (voir aussi Tremblay et al. 2011).

Finalement, la présente thèse a permis d'observer que les SCM de l'Arctique canadien présentent des caractéristiques distinctes lorsque comparés à ceux des autres régions océaniques. Par contraste avec les eaux tempérées (Mann et Lazier 2006; Pommier et al. 2009), par exemple, on note que les SCM arctiques sont persistants tout au long de la saison de production, sont relativement « isolés » de la zone de mélange de surface et contiennent une portion importante et difficilement prévisible de la biomasse totale disponible dans la zone euphotique. Néanmoins, et dans un contexte de changements climatiques rapides, l'augmentation globale des températures de surface et de la stratification tend à amincir la couche de mélange et à limiter l'apport en nutriments à la surface (Peterson et al. 2002; Boyce et al. 2010). Cette situation, en plus de mener à une diminution de la biomasse totale (Boyce et al. 2010), s'apparente fortement aux conditions qui prévalent déjà en Arctique et pourrait donc affecter la distribution verticale du phytoplancton en favorisant la présence de SCM dans d'autres régions du monde. De part leur longévité et leur présence généralisée, les SCM arctiques partagent des points communs avec ceux retrouvés dans les gyres subtropicales où la quasi-absence d'azote dans les eaux de surfaces mène à la formation de SCM (Huisman et al. 2006; Mann et Lazier 2006). Cependant, les SCM des zones subtropicales se distinguent par leur positionnement profond, parfois sous la zone euphotique mais au dessus de la nitracline. Ils ne correspondent ni au maximum de biomasse carbonée ni au maximum de productivité primaire (Steele 1964; Kiefer et al. 1976; Cullen 1982; Falkowski et Kiefer 1985; Fennel et Boss 2003). Somme toute, les SCM de l'Arctique canadien sont situés peu profondément dans la zone euphotique et démontrent un couplage unique à la nitracline, ce qui leur permet vraisemblablement de contrecarrer les effets négatifs de la faible température et de présenter des taux de production primaire substantiels.

5.2 Perspective d'avenir

Les travaux réalisés au cours de cette thèse doctorale ont permis d'affirmer que les SCM sont des structures largement répandues dans les différentes régions de l'Arctique canadien et que ces derniers y jouent un rôle majeur pour la production primaire de la colonne d'eau. De part leur importance et leur dynamisme, il apparait primordial d'inclure les communautés composant les SCM aux algorithmes d'estimation de la chlorophylle et de la

production primaire par la télédétection (ainsi que de quantifier la répercussion des SCM s'ils sont ignorés). L'optimisation des modèles, pour sa part, devra passer par la considération de la limitation en température et les variations verticales de la réponse photosynthétique, l'inclusion des changements de dynamique de la production nouvelle et régénérée observés durant la saison de production et, dans le cas de la prise d'azote, l'introduction d'une paramétrisation dynamique pour tenir compte des variations liées à la profondeur et au moment de l'année. De plus, il est à noter que la présente étude se limite à l'estimation de la réponse photosynthétique à deux profondeurs seulement (à la surface et au SCM) et pour une unique saison (l'automne 2006). Un échantillonnage intensif, effectué à plusieurs profondeurs dans la zone euphotique et s'étendant sur l'ensemble de la période de croissance phytoplanctonique, apporterait un éclairage essentiel à la compréhension de la dynamique de l'écosystème. L'insertion de différentes formes d'azotes (comme l'urée et les acides aminés), tant dans les modèles que pour la compréhension de l'écologie nutritive du phytoplancton pourrait s'avérer judicieuse.

Certains processus du cycle de l'azote, n'ont pas été abordés dans le cadre de cette thèse, malgré qu'ils aient un impact probable, mais à ce jour peu documenté, sur la production nouvelle et régénérée en Arctique. Par exemple, il a été observé que la fixation de l'azote en mer de Beaufort, quoique présentant des taux relativement bas (0.14 nmol N l^{-1} j^{-1}) en comparaison avec d'autres océans, pourrait soutenir environ 4% de la production nouvelle (représentant 0.6 mg C m^{-2} j^{-1}; Blais et al. 2012). De plus, ce processus est susceptible d'être d'une plus grande importance à proximité des grands fleuves Arctique (par exemple, la fixation de l'azote atteint 4.45 nmol N l^{-1} j^{-1} à l'embouchure du fleuve Mackenzie; Blais et al. 2012). Par ailleurs, la nitrification peut être responsable d'une portion substantielle des apports en nitrate dans les eaux stratifiés des autres océans (entre 20% et 100% du nitrate y serait, en fait, de l'azote recyclé; Raimbault et al. 1999, Yool et al. 2007). Même s'il est permis de supposer que les conditions lumineuses feront en sorte que la nitrification bactérienne sera inhibée pendant l'été en Arctique (Horrigan et al. 1981), près d'un tiers du nitrate qui s'accumule dans la couche de mélange pendant l'hiver provient possiblement de la nitrification en zone côtière de la mer de Beaufort (Tremblay et al. 2008). De plus, il a été récemment observé que les archaea, tel *Thaumarchaeota*, serait abondant et participerait à la nitrification de l'ammonium, mais aussi de l'urée dans l'océan Arctique (Alonso-Saez

et al. 2012). En ce sens, il serait intéressant de se pencher sur le rôle de la fixation de l'azote gazeux, de la nitrification ainsi que de l'assimilation de l'azote organique par le phytoplancton (à la suite de la minéralisation photochimique ou bactérienne) lors de l'estimation de la production phytoplanctonique en Arctique canadien. De plus, la dilution isotopique n'a pas été considérée lors de nos incubations bien qu'elle pourrait mener à une surestimation du *f*-ratio qui pourrait s'additionner à celle possiblement causée par la nitrification ou encore compenser la sous-estimation du *f*-ratio attribuable à la fixation de l'azote gazeux. Toutefois la courte durée des incubations diminue l'impact de ces processus à l'intérieur des bouteilles (Dugdale et Goering 1967) et la dilution isotopique semble avoir un impact moindre en régions arctiques et subarctiques (Kanda et al. 1987). Bien que certains des paramètres clés (E_k et contribution relative de la prise au noir à la prise totale) discutés dans la thèse ne soient pas touchés par ces considérations, il serait utile de quantifier un plus grand nombre de processus azotés dans les études futures.

L'utilisation des nouveaux outils maintenant disponibles pour les études écosystémiques, telle la modélisation, permettra de mieux comprendre la dynamique de la colonne d'eau (entre autres d'estimer la contribution des SCM à la production primaire) ainsi que de caractériser la réponse biologique des échelons primaires ainsi que suivants des réseaux alimentaires aux changements climatiques. En effet, quoique non discuté dans le cadre de cette thèse, des modèles simples, tel que celui présenté au chapitre 4, pourraient être utilisés pour étudier la réponse des communautés bactériennes et zooplanctoniques aux changements physicochimique de la colonne d'eau ainsi que pour estimer l'exportation du matériel organique vers les communautés benthiques. Dans ce cas, une paramétrisation complète des différents compartiments du modèle deviendrait possible suivant un échantillonnage intensif et complet des différentes zones de l'Arctique canadien, et ce, à différents moments de l'année. De plus, l'utilisation d'une approche 3D couplant un modèle d'écosystème à un modèle de circulation océanique permettrait de tenir compte de l'influence des apports horizontaux et verticaux (par exemple les upwellings) de nutriments sur la productivité relative des SCM.

Finalement, un programme de déploiement de lignes de mouillages enregistrant des données en continu de chacune des régions mentionnées ainsi que l'échantillonnage à haute résolution verticale de la colonne d'eau permettraient aussi d'obtenir de précieuses données nécessaires à la calibration des modèles et des algorithmes de calcul de la production primaire annuelle ainsi qu'à une meilleure compréhension de la dynamique de la colonne d'eau en Arctique canadien. . En définitive, une combinaison judicieuse d'observations *in situ*, de modélisation et de télédétection s'impose comme une voie d'avenir menant à une meilleure compréhension de l'écosystème marin arctique.

Bibliographie

ACIA (2005) Scientific report: Arctic Climate Impact Assessment. Cambridge, Cambridge University Press.

Allen, A. E., Howart-Jones, M. H., Booth, M. G., Frisher, M. E., Verity, P. G., Bronk, D. A. and Sanderson, M. P. (2002) Importance of heterotrophic bacterial assimilation of ammonium and nitrate in the Barents Sea during summer. *Journal of Marine Systems,* 38**,** 93-108.

Alonso-Saez, L., Waller, A. S., Mende, D. R., Bakker, K., Farnelid, H., Yager, P. L., Lovejoy, C., Tremblay, J.-E., Potvin, M., Heinrich, F., Estrada, M., Riemann, L., Bork, P., Pedros-Alio, C. & Bertilsson, S. (2012) Role for urea in nitrification by polar marine Archaea. *Proceedings of the National Academy of Sciences,* 109**,** 17989-17994.

Anderson, G. C. (1969) Subsurface chlorophyll maximum in the Northeast Pacific Ocean. *Limnology and Oceanography,* 14**,** 386-391.

Ardyna, M., Babin, M., Gosselin, M., Devred, E., Bélanger, S., Martsuoka, A. & Tremblay, J. E. (2013) Parameterization of vertical chlorophyll a in the Arctic Ocean: impact of the subsurface chlorophyll maximum on regional, seasonal and annual primary production estimates. *Biogeosciences Discuss,* 10**,** 1345-1399.

Ardyna, M., Gosselin, M., Michel, C., Poulin, M. and Tremblay, J. E. (2011) Environmental forcing of phytoplankton community structure and function in the Canadian High Arctic: contrasting oligotrophic and eutrophic regions. *Marine Ecology Progress Series,* 442**,** 37-53.

Arrigo, K. R., Dijken, G. and Pabi, S. (2008) Impact of a shrinking Arctic ice cover on marine primary production. *Geophysical Research Letters,* 35**,** doi:10.1029/2008GL035028.

Arrigo, K. R., Matrai, P. A. and Dijken, G. (2011) Primary productivity in the Arctic Ocean: Impacts of complex optical properties and subsurface chlorophyll maxima on large-scale estimates. *Journal of Geophysical Research,* 116**,** doi:10.1029/2011JC007273.

Arrigo, K. R., Perovich, D. K., Pickart, R. S., Brown, Z. W., van Dijken, G. L., Lowry, K. E., Mills, M. M., Palmer, M. A., Balch, W. M., Bahr, F., Bates, N. R., Benitez-Nelson, C., Bowler, B., Brownlee, E., Ehn, J. K., Frey, K. E., Garley, R., Laney, S. R., Lubelczyk, L., Mathis, J., Matsuoka, A., Mitchell, B. G., Moore, G. W. K., Ortega-Retuerta, E., Pal, S., Polashenski, C. M., Reynolds, R. A., Schieber, B., Sosik, H. M., Stephens, M. and Swift, J. H. (2012) Massive Phytoplankton Blooms Under Arctic Sea Ice. *Science,* 336**,** 1408.

Babin, M., Morel, A. and Gagnon, R. (1994) An incubator designed for extensive and sensitive measurements of phytoplankton photosynthetic parameters. *Limnology and Oceanography,* 39, 694-702.

Ban, A., Aikawa, S., Hattori, H., Sasaki, H., Sampei, M., Kudoh, S., Fukuchi, M., Satoh, K. and Kashino, Y. (2006) Comparative analysis of photosynthetic properties in ice algae and phytoplankton inhabiting Franklin Bay, the Canadian Arctic, with those in mesophilic diatoms during CASES 03-04. *Polar Biosciences,* 19, 11-28.

Beckmann, A. and Hense, I. (2007) Beneath the surface: Characteristics of oceanic ecosystems under weak mixing conditions - A theoretical investigation. *Process in Oceanography,* 75, 771-796.

Bédard-Therriault, L., Poulin, M. and Bossé, L. (1999) Guide d'identification du phytoplancton marin de l'estuaire et du golfe du Saint-Laurent incluant également certains protozoaires. *Publication Spéciale Canadienne des Sciences Halieutiques et Aquatiques,* 128, 1-387.

Behrenfeld, M. J., Halsey, K. H. and Milligan, A. J. (2008) Evolved physiological responses of phytoplankton to their integrated growth environment. *Philosophical Transactions of the Royal Society B,* 363, 2687-2703.

Bélanger, S., Babin, M. and Tremblay, J.-E. (2012) Increasing cloudiness in Arctic damps the increase in phytoplankton due to sea ice receding. *Biogeosciences Discuss,* 9, 13987-14012.

Berrouard, M. (2011) Contribution des bactéries hétérotrophes au cycle marin de l'azote dans l'océan Arctique canadien. *Biology.* Quebec City, Laval University.

Bienfang, P. K. (1981) SETCOL - A Technologically Simple and Reliable Method for Measuring Phytoplankton Sinking Rates. *Canadian Journal of Fisheries and Aquatic Sciences,* 38, 1289-1294.

Blais, M., Tremblay, J. E., Lovejoy, C., Jungblunt, A. D., Gagnon, J., Martin, J. and Thaler, M. (2012) Nitrogen fixation and identification of potential diazotrophs in the Canadian Arctic. *Global Biogeochemical Cycles,* 26, doi:10.1029/2011GB004096.

Booth, B. C., Larouche, P., Belanger, S., Klein, B., Amiel, D. and Mei, Z.-P. (2002) Dynamics of *Chaetoceros socialis* blooms in the North Water. *Deep-Sea Research II,* 49, 5003-5025.

Bourgault, D., C. Hamel, F. Cyr, J.-E. Tremblay, P. S. Galbraith, D. Dumont, and Y. Gratton (2011), Turbulent nitrate fluxes in the Amundsen Gulf during ice-covered conditions, *Geophysical Research Letter,* 38, L15602,doi:10.1029/2011GL047936

Boyce, D. G., Lewis, M. R. and Worm, B. (2010) Global phytoplankton decline over the past century. *Nature,* 466, 591-596.

Brugel, S., Nozais, C., Poulin, M., Tremblay, J. E., Miller, L. A., Simpson, K. G., Gratton, Y. and Demers, S. (2009) Phytoplankton biomass and production in the southeastern Beaufort Sea in autumn 2002 and 2003. *Marine Ecology Progress Series,* 377, 63-77.

Brunelle, C. B., Larouche, P. and Gosselin, M. (2012) Variability of phytoplankton light absorption in Canadian Arctic seas. *Journal of Geophysical Research,* 117, doi:10.1029/2011JC007345.

Burchard, H., Bolding, K., Kuhn, W., Meister, A., Neumann, T. and Umlauf, L. (2006) Description of a flexible and extendable physical–biogeochemical model system for the water column. *Journal of Marine Systems,* 61, 180-211.

Cai, W.-J., Chen, L., Chen, B., Gao, Z., Lee, S. H., Chen, J., Pierrot, D., Sullivan, K., Wang, Y., Hu, X., Huang, W.-J., Zhang, Y., Xu, S., Murata, A., Grebmeier, J. M., Jones, E. P. and Zhang, H. (2010) Decrease in the CO2 Uptake Capacity in an Ice-Free Arctic Ocean Basin. *Science,* 329, 556-559.

Calbet, A. and Prairie, Y. T. (2003) Mesozooplankton Grazing and Primary Production: Reply to the Comment by Laws. *Limnology and Oceanography,* 48, 1359-1362.

Carmack, E. C. and Chapman, D. C. (2003) Wind-driven shelf/basin exchange on an Arctic shelf: The joint roles of ice cover extent and shelf-break bathymetry. *Geophysical Research Letters,* 30, 1778, doi:10.1029/2003GL017526,2003.

Carmack, E. C., Macdonald, R. W. and Jasper, S. (2004) Phytoplankton productivity on the Canadian Shelf of the Beaufort Sea. *Marine Ecology Progress Series,* 277, 37-50.

Carpenter, J. H. (1965) The accuracy of the Winkler method for dissolved oxygen analysis. *Limnology and Oceanography,* 10, 135-140.

Chung, P. C., Gardner, W. D., Landry, M. R., Richardson, M. J. and Walsh, I. D. (1998) Beam attenuation by microorganisms and detrital particles in the equatorial Pacific. *Journal of Geophysical Research,* 103, 12669-12281.

Cochlan, W. P. (1986) Seasonal study of uptake and regeneration on nitrogen on the Scotian Shelf. *Continental Shelf Research,* 5, 555-577.

Cochlan, W. P., Harrison, P. J. and Denman, K. L. (1991) Diel Periodicity of Nitrogen Uptake by Marine Phytoplankton in Nitrate-Rich Environments. *Limnology and Oceanography,* 36, 1689-1700.

Codispoti, L. A., V. Kelly, A. Thessen, P. Matrai, S. Suttles, V. Hill, M. Steele, and B. Light (2013), Synthesis of primary production in the Arctic Ocean. III : Nitrate and phosphate based estimated of net community production, *Progress in Oceanography*, 110, 126–150.

Collos, Y. (1987) Calculations of ^{15}N Uptake Rates by Phytoplankton Assimilating One or Several Nitrogen-Sources. *Applied Radiation and Isotopes,* 38, 275-282.

Coon, T. G., Lopez, M., Richerson, J., Powell, T. M. and Goldman, C. R. (1987) Summer dynamics of the deep chlorophyll maximum in Lake Tahoe. *Journal of Plankton Research,* 9, 327-344.

Cota, G. F., Pomeroy, L. R., Harrison, W. G., Jones, E. P., Peters, F., Sheldon, W. M. and Weingartner, T. R. (1996) Nutrients, primary production and microbial heterotrophy in the southeastern Chukchi Sea: Arctic summer nutrient depletion and heterotrophy. *Marine Ecology Progress Series,* 135, 274-258.

Cullen, J. J. (1982) The deep chlorophyll maximum: comparing vertical profiles of chlorophyll *a*. *Canadian Journal of Fisheries and Aquatic Sciences,* 39, 791-803.

DeVries, T., Deutsch, C., Primeau, F., Chang, B. and Devol, A. (2012) Global rates of waters-column denitrification derived from nitrogen gas measurements. *Nature Geoscience,* 5, 547-550.

Dolan, J. R. and Marrasé, C. (1995) Planktonic ciliate distribution relative to a deep chlorophyll maximum: Catalan Sea, N.W Mediterranean, June 1993. *Deep-Sea Research I,* 42, 1965-1987.

Dortch, Q. (1982) Effect of growth conditions on accumulation of internal nitrate, ammonium, amino acids, and protein in three marine diatoms. *Journal of Experimental Marine Biology and Ecology,* 61, 243-264.

Dugdale, R. C. and Goering, J. J. (1967) Uptake of new and regenerated forms of nitrogen in primary productiviy. *Limnology and Oceanography,* 12, 196-206.

Ehn, J., Mundy, C. J., Barber, D. G., Hop, H., Rossnagel, A. and Stewart, J. (2011) Impact of horizontal spreading on light propagation in melt pond covered seasonal sea ice in the Canadian Arctic. *Journal of Geophysical Research,* 116, doi:10.1029/2010JC006908.

Else, B. G. T., R. J. Galley, B. Lansard, D. G. Barber, K. Brown, L. A. Miller, A. Mucci, T. N. Papakyriakou, J.-E. Tremblay, and S. Rysgaard (2013), Further observations of a decreasing atmospheric CO2 uptake capacity in the Canada Basin (Arctic Ocean) due to sea ice loss, *Geophysical Research Letter*, 40, 1132–1137, doi:10.1002/grl.50268.

Eppley, R. W. (1968) An incubation method for estimating the carbon content of phytoplankton in natural samples. *Limnology and Oceanography,* 13, 574-582.

Eppley, R. W. and Peterson, B. J. (1979) Particulate organic matter flux and phytoplanktonic new production in the deep ocean. *Nature,* 282, 677-680.

Estrada, M., Marrasé, C., Latasa, M., Berdalet, Delgado, M. and Riera, T. (1993) Variability of deep chlorophyll maximum characteristic in the Northwestern Mediterranean. *Marine Ecology Progress Series,* 92, 289-300.

Falkowski, P. G., Barber, R. T. and Smetacek, V. (1998) Biogeochemical Controls and Feedback on Ocean Primary Production. *Science,* 281.

Falkowski, P. G. and Kiefer, D. A. (1985) Chlorophyll a fluorescence in phytoplankton: relationship to photosynthesis and biomass. *Journal of Plankton Research,* 7, 715-731.

Fasham, M. J. R., Ducklow, H. W. and McKelvie, S. M. (1990) A nitrogen-based model of plankton dynamics in the oceanic mixed layer. *Journal of Marine Research,* 48, 591-639.

Fennel, K. and Boss, E. (2003) Subsurface maxima of phytoplankton and chlorophyll: steady-state solutions from a simple model. *Limnology and Oceanography,* 48, 1521-1534.

Field, C. B., Behrenfeld, M. J., Randerson, J. T. and Falkowski, P. (1998) Primary Production of the Biosphere: Integrating Terrestrial and Oceanic Components. *Science,* 281, 237-240.

Forest, A., Tremblay, J.-É., Gratton, Y., Martin, J., Gagnon, J., Darnis, G., Sampei, M., Fortier, L., Ardyna, M., Gosselin, M., Hattori, H., Nguyen, D., Maranger, R., Vaqué, D., Marrasé, C., Pedros-Alio, C., Sallon, A., Michel, C., Kellogg, C., Deming, J., Shadwick, E., Thomas, H., Link, H., Archambault, P. and Piepenburg, D. (2011) Biogenic carbon flows through the planktonic food web on the Amundsen Gulf (Arctic Ocean): A synthesis of field measurments and inverse modeling analyses. *Progress in Oceanography,* 91, 410-436.

Fortier, M., Fortier, L., Michel, C. and Legendre, L. (2002) Climatic and biological forcing of vertical flux and biogenic particles under seasonal Arctic sea ice. *Marine Ecology Progress Series,* 225, 1-16.

Fouilland, E., Gosselin, M., Rivkin, R. B., Vasseur, C. and Mostajir, B. (2007) Nitrogen uptake by heterotrophic bacteria and phytoplankton in Arctic surface waters. *Journal of Plankton Research,* 29, 369-379.

Frenette, J.-J., Demers, S., Legendre, L. and Dodson, J. (1993) Lack of Agreement Among Models for Estimating the Photosynthetic Parameters. *Limnology and Oceanography,* 38, 679-687.

Fuhrman, J. A., Horrigan, S. G. and Capone, D. G. (1998) Use of ^{13}N as tracer for bacterial and algal uptake of ammonium from seawater. *Marine Ecology Progress Series,* 45, 271-278.

Gallegos, C. L., Platt, T., Harrison, W. G. and Irving, B. (1983) Photosynthetic Parameters of Arctic Marine Phytoplankton: Vertical Variations and Time Scales of Adaptation. *Limnology and Oceanography,* 28, 698-708.

Glibert, P. M., Biggs, D. C. and McCarthy, J. J. (1982) Utilization of ammonium and nitrate during austral summer in the Scotia Sea. *Deep Sea Research,* 29, 837-350.

Goeyens, L., Kindermans, N., Abu Yusulf, M. and Elskens, M. (1998) A Room Temperature Procedure for the Manual Determination of Urea in Seawater. *Estuarine, Coastal and Shelf Science,* 47, 415-418.

Gosselin, M., Legendre, L., Therriault, J. C., Demers, S. and Rochet, M. (1986) Physical control of the horizontal patchiness of sea-ice microalgae. *Marine Ecology Progress Series,* 29, 289-298.

Gosselin, M., Levasseur, M., Wheeler, P. A., Horner, R. A. and Booth, B. C. (1997) New measurement of phytoplankton and ice algal production in the Arctic Ocean. *Deep-Sea Research II,* 44, 1623-1644.

Grasshoff, K., Kremling, K. and Ehrhardt, M. (Eds.) (1999) *Methods of seawater analysis,* New York, Wiley-VCH.

Gruber, N. and Sarmiento, J. (1997) Global patterns of marine nitrogen fixation and denitrification. *Global Biogeochemical Cycles,* 11, 235-266.

Harrison, P. J., Conway, H. L., Holmes, R. W. and Davis, C. O. (1977) Marine Diatoms Grown in Chemostats under Silicate and Ammonium Limitation, III. Cellular Chemical Composition and Morphology of Chaetoceros debilis, Skeletonema costatum, and Thalassiosira gravida. *Marine Biology,* 43, 19-31.

Harrison, W. G. (1986) Photosynthesis-Irradiance Relationships in Polar and Temperate Phytoplakton Populations. *Polar Biology,* 5, 153-164.

Harrison, W. G. (1990) Nitrogen utilisation in chlorophyll and primary productivity maximum layers: an analysis based on the f-ratio. *Marine Ecology Progress Series,* 60, 85-90.

Harrison, W. G. and Cota, G. F. (1991) Primary production in polar waters: relation to nutrient availability. IN Sakshaug, E. and Hopkins, C. C. E. (Eds.) *Pro Mare Symposium on Polar Marine Ecology.* Trondheim, Polar Research.

Harrison, W. G. and Platt, T. (1980) Variations in assimilation number of coastal marine phytoplankton: Effects of environment co-variates. *Journal of Plankton Research,* 2, 249-260.

Harrison, W. G. and Platt, T. (1986) Photosynthesis-Irradiance Relationships in Polar and Temperate Phytoplakton Populations. *Polar Biology,* 5, 153-164.

Harrison, W. G., Platt, T. and Irwin, B. (1982) Primary Production and Nutrient Assimilation by Natural Phytoplankton Populations of the Eastern Canadian Arctic. *Canadian Journal of Fisheries and Aquatic Sciences,* 39, 335-345.

Heinkanen, A. S. and Keck, A. (1996) Distribution and sinking rates of phytoplankton, detritus, and particulate biogenic silica in the Laptev Sea and Lena River (Arctic Siberia). *Marine Chemistry,* 53, 229-245.

Herbland, A. and Voituriez, B. (1979) Hydrological structure analysis for estimating the primary production in the tropical Atlantic Ocean. *Journal of Marine Research,* 37, 87-101.

Hill, V. and Cota, G. F. (2005) Spatial patterns of primary production on the shelf, slope and basin of the Western Arctic in 2002. *Deep Sea Research II,* 52, 3344-3354.

Hill, V., Matrai, P. A., Olson, E., Suttles, S., Steele, M., Codispoti, L. A. and Zimmerman, R. C. (2013) Synthesis of integrated primary production in the Arctic Ocean: II. In situ and remotely sensed estimated. *Progress in Oceanography,* 110, 107-125.

Hirche, H.-J., Baumann, M. E. M., Kattner, G. and Gradinger, R. (1991) Plankton distribution and the impact of copepod grazing on primary production in Fram Strait, Greenland Sea. *Journal of Marine Systems,* 2, 477-494.

Hodges, B. A. and Rudnick, D. L. (2004) Simple models of steady deep maxima in chlorophyll and biomass. *Deep-Sea Research I,* 51, 999-1015.

Holmes, R. M., Aminot, A., Kerouel, R., Hooker, B. A. and Peterson, J. B. (1999) A simple and precise method for measuring ammonium in marine and freshwater ecosystems. *Canadian Journal of Fisheries and Aquatic Sciences,* 56, 1801-1808.

Holm-Hansen, O., El-Sayed, S. Z., Franceschini, G. A. and Cuhel, R. L. (1977) Primary production and the factors controlling phytoplankton growth in the Southern Ocean. IN Llano, G. A. (Ed.) *Adaptations within antarctic ecosystems: proceedings of the Third SCAR Symposium on Antarctic Biology.* Washington DC, Smithsonian Institution.

Holm-Hansen, O. and Hewes, C. D. (2004) Deep chlorophyll-a maxima (DCMs) in Antarctic waters: I-Relationships between DCMs and the physical, chemical, and optical conditions in the upper water column. *Polar Biology,* 27, 699-710.

Horrigan, S. G., Carlucci, A. F. and Williams, R. G. (1981) Light inhibition of nitrification in sea-surface films. *Journal of Marine Research,* 39, 557-565.

Huisman, J., Pham Thi, N. N., Karl, D. M. and Sommeijer, B. (2006) Reduced mixing generates oscillations and chaos in the oceanic deep chlorophyll maximum. *Nature,* 439, 322-325.

Huszar, V., Kruk, C. and Nina, C. (2003) Steady-state assemblages of phytoplankton in four temperate lakes (NE U.S.A.). *Hydrobiologia,* 502, 97-109.

IPCC (2001) *Climate Change 2001: Impacts, Adaptation, and Vulnerability,* Cambridge, Cambridge University Press.

Jerlov, N. G. (1976) *Marine Optics,* Amsterdam, Elsevier.

Jones, E. P., Swift, J. H., Anderson, L. G., Lipizer, M., Civitarese, G., Falkner, K. K., Kattner, G. and McLaughlin, F. A. (2003) Tracking Pacific water in the North Atlantic Ocean. *Journal of Geophysical Research,* 108, 1-10.

Kanda, J., Laws, E. A., Saino, T. and Hattori, A. (1987) An evaluation of isotope dilution effect from conventional data sets of ^{15}N uptake experiments. *Journal of Plankton Research,* 9, 79-90.

Kiefer, D. A., Olson, R. J. and Holm-Hansen, O. (1976) Another look at the nitrite and chlorophyll maxima in the central North Pacific. *Deep-Sea Research,* 23, 1199-1208.

Kirchman, D. L. and Wheeler, P. A. (1998) Uptake of ammonium and nitrate by heterotrophic bacteria and phytoplankton in the sub-Arctic Pacific. *Deep-Sea Research I,* 45, 347-365.

Klausmeier, C. A. and Litchman, E. (2001) Algal games: The vertical distribution of phytoplankton in poorly mixed water columns. *Limnology and Oceanography,* 46, 1998-2007.

Klein, B., LeBlanc, B., Mei, Z.-P., Beret, R., Michaud, J., Mundy, C.-J., von Quillfeldt, C. H., Garneau, M.-E., Roy, S., Gratton, Y., Cochran, J. K., Belanger, S., Larouche, P., Pakulski, J. D., Rivkin, R. B. and Legendre, L. (2002) Phytoplankton biomass, production and potential export in the North Water. *Deep Sea Research Part II: Topical Studies in Oceanography (The International North Water Polynya Study),* 49, 4983-5002.

Knapp, G. P., Stalcup, M. C. and Stanley, R. J. (1990) Automated oxygen titration and salinity determination. Woods Hole, Woods Hole Oceanographic Institution.

Konneke, M., Bernhard, A. E., de la Torre, J. R., Walker, C. B., Waterbury, J. B. and Stahl, D. A. (2005) Isolation of an autotrophic ammonia-oxidizing marine archaeon. *Nature,* 437, 543-546.

Kristiansen, S. and Farbrot, T. (1991) Nitrogen uptake rates in phytoplankton and ice algae in the Barents Sea. IN Sakshaug, E., Hopkins, C. C. E. and Britsland, N. A. (Eds.) *Proceedings of the Pro Mare Symposium on Polar Marine Ecology. Trondheim. 12-16 May 1990.* Polar Research.

Kristiansen, S., Farbrot, T. and Wheeler, P. A. (1994) Nitrogen cycling in the Barents Sea - Seasonal dynamics of new and regenerated production in the marginal ice zone. *Limnology and Oceanography,* 39**,** 1630-1642.

Kristiansen, S. and Lund, B. A. (1989) Nitrogen cycling in the Barent Sea - I. Uptake of nitrogen in the water column *Deep Sea Research,* 36**,** 255-268.

Kuhn, W. and Radach, G. (1997) A one-dimensional physical-biological model study of the pelagic nitrogen cycling during the spring bloom in the northern North Sea (FLEX '76). *Journal of Marine Research,* 55**,** 687-734.

Lalli, C. M. and Parsons, T. R. (1997) *Biological oceanography: an introduction.,* Oxford, Butterworth-Heinemann.

Lavoie, D., Macdonald, R. W. and Denman, K. L. (2009) Primary productivity and export fluxes on the Canadian shelf of the Beaufort Sea: A modelling study. *Journal of Marine Systems,* 75**,** 17-32.

Laws, E. A. and Archie, J. W. (1981) Appropriate Use of Regression Analysis in Marine Biology. *Marine Biology,* 65**,** 13-16.

Lee, S. H. and Whitledge, T. E. (2005) Primary and new production in the deep Canada Basin during summer 2002. *Polar Biology,* 28**,** 190-197.

Lewis, M. R. and Smith, J. C. (1983) A small volume, short-incubation-time method for measurement of photosynthesis aas a function of incident irradiance. *Marine Ecology Progress Series,* 13**,** 99-102.

Li, W. (1985) Photosynthetic response to temperature on marine phytoplankton along a latitudinal gradient (16°N to 74°N). *Deep Sea Research,* 32**,** 1381-1391.

Li, W., McLaughlin, F. A., Lovejoy, C. and Carmack, E. C. (2009) Smallest Algae Thrive As the Arctic Ocean Freshens. *Science,* 326**,** 539.

Lomas, M. W. and Lipschultz, F. (2006) Forming the primary nitrite maximum: nitrifiers or phytoplankton? *Limnology and Oceanography,* 51**,** 2453-2467.

Lovejoy, C., Vincent, W. F., Bonilla, S., Roy, S., Martineau, M.-J., Terrado, R., Potvin, M., Massana, R. & Pedros-Alio, C. (2007) Distribution, phylogeny, and growth of cold-adapted picoprasinophytes in Arctic Seas. *Journal of Phycology,* 43**,** 78-89.

Lung, J. W. G., Kipling, C. and Le Cren, E. D. (1958) The inverted microscope method of estimating algal numbers and the statistical basis of estimations by counting. *Hydrobiologia,* 11, 143-170.

Mann, K. H. and Lazier, J. R. N. (2006) *Dynamics of marine ecosystems: biological-physical interactions in the oceans,* Malden, Blackwell Publishing.

Markus, T., Stroeve, J. C. and Miller, J. (2009) Recent changes in Arctic sea ice melt onset, freezeup, and melt season length. *Journal of Geophysical Research,* 114, doi:10.1029/2009JC005436.

Martin, J., Tremblay, J. E., Gagnon, J., Tremblay, G., Lapoussiere, A., Jose, C., Poulin, M., Gosselin, M., Gratton, Y. and Michel, C. (2010) Prevalence, structure and properties of subsurface chlorophyll maxima in Canadian Arctic waters. *Marine Ecology Progress Series,* 412, 69-84.

Martin, J., Tremblay, J. E. and Price, N. M. (2012) Nutritive and photosynthetic ecology of subsurface chlorophyll maxima in Canadian Arctic waters. *Biogeosciences,* 9, 6445-6488.

Martini, I. P. (1986) *Canadian inland seas,* New York, Elsevier.

McCarthy, J. J., Taylor, W. R. and Taft, J. L. (1977) Nitrogenous Nutrition of the Plankton in the Chesapeake Bay. 1. Nutrient Availability and Phytoplankton Preferences. *Limnology and Oceanography,* 22, 996-1011.

McLaughlin, F. A. and Carmack, E. C. (2010) Deepening of the nutricline and chlorophyll maximum in the Canada Basin interior, 2003-2009. *Geophysical Reasearch Letters,* 37, doi:10.1029/2010GL045459.

Mei, Z.-P., Legendre, L., Gratton, Y., Tremblay, J. E., LeBlanc, B., Mundy, C., Klein, B., Gosselin, M., Larouche, P., Papakyriakou, T. N., Lovejoy, C. and von Quillfeldt, C. G. (2002) Physical control of spring-summer phytoplankton dynamics in the North Water, April-July 1998. *Deep Sea Research II,* 49, 4959-4982.

Miller, C. B. (2004) *Biological Oceanography,* United Kingdom, Blackwell Publishing.

Morel, A. and Berthon, J.-F. (1989) Surface pigments, algal biomass profiles, and potential production of the euphotic layer: Relationships reinvestigated in view of remote-sensing applications. *Limnology and Oceanography,* 34, 1545-1562.

Mulvenna, P. F. and Savidge, G. (1992) A Modified Manual Method for the Determination of Urea in Seawater using Diacetylmonoxime Reagent. *Estuarine, Coastal and Shelf Science,* 34, 429-438.

Mundy, C.-J., Gosselin, M., Ehn, J., Gratton, Y., Rossnagel, A., Barber, D., Martin, J., Tremblay, J.-É., Palmer, M. R., Arrigo, K. R., Darnis, G., Fortier, L., Else, B. and Papakyriakou, T. (2009) Contribution of under-ice primary production to an ice-edge upwelling phytoplankton bloom in the Canadian Beaufort Sea. *Geophysical Research Letters,* 36, L17601, doi:10.1029/2009GL038837.

Neori, A. and Holm-Hansen, O. (1982) Effect of temperature on rate of photosynthesis in Antarctic phytoplankton. *Polar Biology,* 1, 33-38.

NSIDC (2009) State of the cryosphere: sea ice. www-nsidc.colorado.edu/sotc/sea_ice.html.

NSIDC (2011) State of the cryosphere: sea ice. www.nsidc.org.

Pabi, S., Dijken, G. and Arrigo, K. R. (2008) Primary production in the Arctic Ocean, 1998-2006. *Journal of Geophysical Research,* 113, doi:10.1029/2007JC004578.

Palmer, M., Arrigo, K., Mundy, C., Ehn, J., Gosselin, M., Barber, D., Martin, J., Alou, E., Roy, S. and Tremblay, J.-É. (2011) Spatial and temporal variation of photosynthetic parameters in natural phytoplankton assemblages in the Beaufort Sea, Canadian Arctic. *Polar Biology,* 34, 1915-1928.

Parsons, T. R., Maita, Y. and Lalli, C. M. (1984) *A manual of chemical and biological methods for seawater analysis,* Toronto, Pergamon Press.

Perovich, D. K., Roesler, C. S. and Pegau, W. S. (1998) Variability in Arctic sea ice optical properties. *Journal of Geophysical Research,* 103, 1193-1208.

Peterson, J. B., Holmes, R. M., McClelland, J. W., Vörösmarty, C. J., Lammers, R. B., Shiklomanov, A. I., Shiklomanov, I. A. and Rahmstorf, S. (2002) Increasing River Discharge to the Arctic Ocean. *Science,* 298, 2171-2173.

Platt, T., Gallegos, C. L. and Harrison, W. G. (1980) Photoinhibition of photosynthesis in natural assemblages of marine phytoplankton. *Journal of Marine Research,* 38, 687-701.

Platt, T., Harrison, W. G., Irwin, B., Horne, E. P. and Gallegos, C. L. (1980) Photosynthesis and photoadaptation of marine phytoplankton in the Arctic. *Deep Sea Research,* 29, 1159-1170.

Pommier, J., Gosselin, M. and Michel, C. (2009) Size-fractionated phytoplankton production and biomass during the decline of the northwest Atlantic spring bloom. *Journal of Plankton Research,* 31, 429-446.

Popova, E. E., Yool, A., Coward, A. C., Aksenov, Y. K., Alderson, B. A., de Cuevas, B. A. and Anderson, T. R. (2010) Control of primary production in the Arctic by nutrients and light: insights from a high resolution ocean general circulation model. *Biogeosciences,* 7, 3569-3591.

Price, N. M., Cochlan, W. P. and Harrison, P. J. (1985) Time course of uptake of inorganic and organic nitrogen by phytoplankton in the Strait of Georgia: comparison of frontal and stratified communities. *Marine Ecology Progress Series,* 27**,** 39-53.

Prinsenberg, S. J. (1986) On the physical oceanography of Foxe Basin. IN Martini, I. P. (Ed.) *Canadian inland seas.* New York, Elsevier Oceanography Series.

Priscu, J. C. (1989) Photon dependence of inorganic nitrogen transport by phytoplankton in perennially ice-covered antarctic lakes. *Hydrobiologia,* 172**,** 173-182.

Probyn, T. A., Waldron, H. N., Searson, S. and Owens, N. J. P. (1996) Diel vaiability in nitrogenous nutrient uptake at photic and sub-photic depths. *Journal of Plankton Research,* 118**,** 2063-2079.

Raimbault, P., Slawyk, G., Boudjellal, B., Coatanoan, C., Conan, P., Coste, B., Garcia, N., Moutin, T. and Pujo-Pay, M. (1999) Carbon and nitrogen uptake and export in the equatorial Pacific at 150°W: evidence of an efficient regenerated production cycle. *Journal of Geophysical Research,* 104**,** 3341-3356.

Redfield, A. C., Ketchum, B. H. and Richards, F. A. (1963) The influence of organisms on the composition of sea-water, IN Holl, M. N. (Eds) *The Sea,* vol. 2 New York, Interscience.

Rysgaard, S., Nielsen, T. G. and Hansen, B. W. (1999) Seasonal variation in nutrients, pelagic primary production and grazing in a high-Arctic coastal marine ecosystem, Young Sound, Northeast Greenland. *Marine Ecology Progress Series,* 179**,** 13-25.

Sakshaug, E. (2004) Primary and secondary production in the Arctic seas. IN Stein, R. and Macdonald, R. W. (Eds.) *The organic carbon cycle in the Arctic Ocean.* Berlin, Springer-Verlag.

Sakshaug, E. and Slagstad, D. (1991) Light and productivity of phytoplankton in polar marine ecosystems: a physiological view. IN Sakshaug, E., Hopkins, C. C. E. and Britsland, N. A. (Eds.) *Proceedings of the Pro Mare Symposium on Polar Marine Ecology. Trondheim. 12-16 May 1990.* Polar Research.

Sambrotto, R. N. and Mace, B. J. (2000) Coupling of biological and physical regimes across the Antarctic Polar Front as reflected by nitrogen production and recycling. *Deep-Sea Research II,* 47**,** 3339-3367.

Scott, B. E., Sharples, J., Ross, O. N., Wang, J., Pierce, G. J. and Camphuysen, C. J. (2010) Sub-surface hotspots in shallow seas: fine-scale limited locations of top predator foraging habitat indicated by tidal mixing and sub-surface chlorophyll. *Marine Ecology Progress Series,* 408**,** 207-226.

Serreze, M. C., Holland, M. M. and Stroeve, J. (2007) Perspectives on the Arctic's Shrinking Sea-Ice Cover. *Science,* 315**,** 1533-1536.

Shadwick, E., Thomas, H., Chierici, M., Else, B., Fransson, A., Michel, C., Miller, L. A., Mucci, A., Niemi, A., Papakyriakou, T. and Tremblay, J.-É. (2011) Seasonal variability of inorganic carbon system in the Amundsen Gulf region of the southeastern Beaufort Sea. *Limnology and Oceanography,* 56**,** 303-322.

Sharples, J., Moore, C. M., Rippeth, T. P., Holligan, P. M., Hydes, D. J., Fisher, N. R. and Simpson, J. H. (2001) Phytoplankton distribution and survival in the thermocline. *Limnology and Oceanography,* 46**,** 486-496.

Sharples, J., Tweddle, J. F., Green, J. A. M., Palmer, M. R., Kim, Y.-N., Hickman, A. E., Holligan, P. M., Moore, C. M., Rippeth, T. P., Simpson, J. H. and Krivtsov, V. (2007) Spring-neap modulation on internal tide mixing and vertical nitrate fluxes at a shelf edge in summer. *Limnology and Oceanography,* 52**,** 1735-1747.

Simpson, K. G., J. E. Tremblay, S. Brugel, and N. M. Price (2013), Nutrient dynamics in the western Canadian Arctic, II. Estimates of new and regenerated production over the Mackenzie Shelf and Cape Bathurst Polynya, *Marine Ecology Progress Series*, 484**,** 47–62.

Smith, W. O. and Harrison, W. G. (1991) New production in polar regions: the role of environmental controls. *Deep Sea Research,* 38**,** 1463-1479.

Steele, J. H. (1964) A study of production in the Gulf of Mexico. *Journal of Marine Research,* 22**,** 211-222.

Steele, J. H. and Yentsch, C. S. (1960) The vertical distribution of chlorophyll. *Journal of Marine Biology Association,* 39**,** 217-226.

Stein, R. and Macdonald, R. W. (2004) *The Organic Carbon Cycle in the Arctic Ocean,* Berlin, Springer-Verlag.

Subba Rao, D. V. and Platt, T. (1984) Primary Production of Arctic Waters. *Polar Biology,* 3**,** 191-201.

Taylor, A. H., Harris, J. R. W. and Aiken, J. (1986) The interaction of physical and biological processes in a model of the vertical distribution of phytoplankton under stratification. *Elsevier Oceanograghy Serie* 42**,** 313-330.

Tomas, C. R. (1997) *Identifying marine phytoplankton,* San Diego, CA, Academic Press.

Tremblay, G., Belzile, C., Gosselin, M., Poulin, M., Roy, S. and Tremblay, J. É. (2009) Late summer phytoplankton distribution along a 3500 km transect in Canadian Arctic waters: strong numerical dominance by picoeukaryotes. *Aquatic Microbial Ecology,* 54**,** 55-70.

Tremblay, J. E., Bélanger, S., Barber, D. G., Asplin, M. G., Martin, J., Darnis, G., Fortier, L., Gratton, Y., Link, H., Archambault, P., Sallon, A., Michel, C., Williams, W. J., Phillippe, B. and Gosselin, M. (2011) Climate forcing multiplies biological productivity in the coastal Arctic Ocean. *Geophysical Reasearch Letters,* 38, doi:10.1029/2011GL048825.

Tremblay, J. E. and Gagnon, J. (2009) The effect of irradiance and nutrient supply on the productivity of Arctic waters: a perspective on climate change. IN Nihoul, J. C. J. and Kostianoy, A. G. (Eds.) *Influence of Climate Change on the Changing Arctic and Sub-Arctic Conditions.* Dordrecht, The Netherlands, Springer Verlag.

Tremblay, J. É., Gratton, Y., Carmack, E. C., Payne, C. D. and Price, N. M. (2002) Impact of the large-scale Arctic circulation and the North Water Polynya on nutrient inventories in Baffin Bay. *Journal of Geophysical Research,* 107, 3112, doi:10.1029/2000JC000595.

Tremblay, J. É., Michel, C., Hobson, K. A., Gosselin, M. and Price, N. M. (2006) Bloom dynamics in early opening waters of the Arctic Ocean. *Limnology and Oceanography,* 51, 900-912.

Tremblay, J. É., Simpson, K., Martin, J., Miller, L., Gratton, Y., Barber, D. and Price, N. M. (2008) Vertical stability and the annual dynamics of nutrients and chlorophyll fluorescence in the coastal, southeast Beaufort Sea. *Journal of Geophysical Research,* 113, C07S09, doi:10.1029/2007JC004547.

Uitz, J., Claustre, H., Morel, A. and Hooker, S. B. (2006) Vertical distribution of phytoplankton communities in open ocean: an assessment based on surface chlorophyll. *Journal of Geophysical Research,* 111, C08005, doi:10.1029/2005JC003207.

Umlauf, L. and Burchard, H. (2005) Second-order turbulence closure models for geophysical boundary layers. A review of recent work. *Continental Shelf Research,* 25, 795-827.

Vaqué, D., Guadayol, O., Peters, F., Felipe, J., Angel-Ripoll, L., Terrado, R., Lovejoy, C. and Pedros-Alio, C. (2008) Seasonal changes in planktonic bacterivory rates under the ice-covered coastal Arctic Ocean. *Limnology and Oceanography,* 53, 2427-2438.

Vetrov, A. A. and Romankevich, E. A. (2004) *Carbon Cycle in the Russian Arctic Seas,* Moscow, Ed.: Berlin, New-York: Springer.

Vidussi, F., Roy, S., Lovejoy, C., Gammelgaard, M., Thomsen, H. A., Booth, B. C., Tremblay, J. É. and Mostajir, B. (2004) Spatial and temporal variability of the phytoplankton community structure in the North Water Polynya, investigated using

pigment biomarkers. *Canadian Journal of Fisheries and Aquatic Sciences,* 61, 2038-2052.

Wallace, D. W. R., Minnett, P. J. and Hopkins, T. S. (1995) Nutrients, oxygen, and inferred new production in the Northeast Water Polynya, 1992. *Journal of Geophysical Research,* 100, 4323-4340.

Ward, B. B. (2002) Nitrification in aquatic in aquatic system. IN Capone, D. G. (Ed.) *Encyclopedia of environmental microbiology.* Wiley.

Webb, W. L., Newton, M. and Starr, D. (1974) Carbon dioxide exchange of Alnus rubra: A mathematical model. *Oecologia,* 17, 281-291.

Weiss, R. F. (1970) The solubility of nitrogen, oxygen and argon in water and seawater. *Deep Sea Research,* 17, 721-735.

Weston, K., Fernand, L., Mills, D. K., Delahunty, R. and Brown, J. (2005) Primary production in the deep chlorophyll maximum of the central North Sea. *Journal of Plankton Research,* 27, 909-922.

Williams, R. G. and Follows, M. J. (2003) Physical transport of nutrients and the maintenance of biological production. IN Fasham, M. (Ed.) *Ocean Biogeochemistry: The Role of the Ocean Carbon Cycle in Global Change,*. New-York, Springer.

Williams, W. J. and Carmack, E. C. (2008) Combined effect of wind-forcing and isobath divergence on upwelling at Cape Bathurst, Beaufort Sea. *Journal of Marine Research,* 66, 645-663.

Wu, P., Wood, R. and Stott, P. (2005) Human influence on increasing Arctic river discharges. *Geophysical Research Letters,* 32, L02703, doi:10.1029/2004GL021570.

Yang, J., Comiso, J., Walsh, I. D., Krishfield, R. and Honjo, S. (2004) Storm-driven mixing and potential impact on the Arctic Ocean. *Journal of Geophysical Research*, doi: 10.1029/2001JC001248.

Yool, A., Martin, A. P., Fernández, C. and Clark, D. R. (2007) The significance of nitrification for oceanic new production. *Nature,* 447, doi:10.1038/nature05885.

Zakardjian, B. A., Gratton, Y. and Vézina, A. F. (2000) Late spring phytoplankton bloom in the Lower St. Lawrence Estuary: the flushing hypothesis revisited. *Marine Ecology Progress Series,* 192, 31-48.

Zehr, J. P. and Ward, B. B. (2002) Nitrogen Cycling in the Ocean: New Perspectives on Processes and Paradigms. *Applied and Environmental Microbiology,* 68, 1015-1024.

Annexe A

Table A1 Significant correlations between water-column variables and uptake-irradiance parameters for the data set where SCM communities were incubated with trace (T) or enriched (E) N additions.

	Carbon											
	P_m^B				E_k				α			
	NH_4^+ T	NO_3^- T	NH_4^+ E	NO_3^- E	NH_4^+ T	NO_3^- T	NH_4^+ E	NO_3^- E	NH_4^+ T	NO_3^- T	NH_4^+ E	NO_3^- E
Temperature (°C)	0.85***	0.73***	-	0.86***	0.88***	0.79***	-	0.88***	-	-	-	-
Day of the year	-	-	-0.53**	-	-	-	-	-	-	-	-	-
[chl *a*] (µg l^{-1})	-	-	0.51**	-	-	-	0.43*	-	-	-	-	-
[NO_3^-] (µM)	-	-	-	-	-	-	-	-	-	-	-	-
[NO_2^-] (µM)	-	-	-	-	-	-	-	-	-0.39*	-	-	-
[NH_4^+] (µM)	-	-	-	-	-	-	-	-	0.46*	-	-	-
Total [N] (µM)	-	-	-	-	-	-	-	-	-	-	-	-
E_{SCM}	-	-	0.49*	-	-	-	0.48*	-	-	-	-	-

	Nitrogen											
	N_m^B				E_k				α			
	NH_4^+ T	NO_3^- T	NH_4^+ E	NO_3^- E	NH_4^+ T	NO_3^- T	NH_4^+ E	NO_3^- E	NH_4^+ T	NO_3^- T	NH_4^+ E	NO_3^- E
Temperature (°C)	-	-	-	-	-	-	-	-	-	-	-	-
Day of the year	-	-0.36*	-0.50**	-0.60***	-	-	-	-	-	-	-0.44*	-0.61***
[chl *a*] (µg l^{-1})	-	-	0.53**	0.58***	-	-	-	-	-	0.36*	0.37*	0.54**
[NO_3^-] (µM)	-	0.52**	-	-	-	-	-	-	-	0.35*	-	0.35*
[NO_2^-] (µM)	-	0.53**	-	-	-	-	-	-	-	-	-	-
[NH_4^+] (µM)	-	-	-	-	-	-	-	-	-	-	-	-
Total [N] (µM)	-	0.52**	-	-	-	-	-	-	-	0.36*	-	-
E_{SCM}	-	-	0.67***	0.62***	-	-	0.44*	-	-	-	-	-

* : $p < 0.05$; ** : $p < 0.01$; *** : $p < 0.001$

Table A2 Significant correlations between water-column variables and uptake-irradiance parameters for the data set where surface and SCM communities were incubated with trace (T) or enriched (E) NO_3^- additions.

Carbon

	P_m^B				E_k				α			
	NO_3^- T Surface	NO_3^- T SCM	NO_3^- E Surface	NO_3^- E SCM	NO_3^- T Surface	NO_3^- T SCM	NO_3^- E Surface	NO_3^- E SCM	NO_3^- T Surface	NO_3^- T SCM	NO_3^- E Surface	NO_3^- E SCM
Temperature (°C)	0.93***	-	0.97***	-	-	0.72*	0.74*	-	0.76*	-	0.81*	-
Day of the year	-	-	-	-	-	-	-	-	-	0.68*	-	0.78*
[chl *a*] (µg l^{-1})	-	-	-	-	-	0.68*	-	-	-	-	-	-
[NO_3^-] (µM)	-	-	-	-	-	-	-	-	-	-	-	-
[NO_2^-] (µM)	-	-	-	-	-	-0.69*	-	-	-	-	-	-
[NH_4^+] (µM)	-	-	-	0.72*	-	0.74*	-	0.82*	-	-	-	-
Total [N] (µM)	-	-	-	-	-	-	-	-	-	-	-	-
E_{SCM}	-	-	-	0.90**	-	-	-	0.95***	-	-	-	-

Nitrogen

	N_m^B				E_k				α			
	NO_3^- T Surface	NO_3^- T SCM	NO_3^- E Surface	NO_3^- E SCM	NO_3^- T Surface	NO_3^- T SCM	NO_3^- E Surface	NO_3^- E SCM	NO_3^- T Surface	NO_3^- T SCM	NO_3^- E Surface	NO_3^- E SCM
Temperature (°C)	-	-	-	-	0.71*	0.82**	-	0.94***	-	-	-	-
Day of the year	-	-	-0.84**	-	-	-	-	-	-	0.70*	-	-
[chl *a*] (µg l^{-1})	-	-	-	-	-	0.87**	0.86**	0.82*	-	-	-	-
[NO_3^-] (µM)	-	-	-	-	-	-	0.81*	-	-	-	-	-
[NO_2^-] (µM)	-	-	-	-	-	-	-	-	-	-	-	-
[NH_4^+] (µM)	-	-	-	0.85**	0.93***	-	-	-	0.95**	0.72*	-	-
Total [N] (µM)	-	-	-	-	0.94***	-	-	-	0.90**	-	-	-
E_{SCM}	-	-	-	0.86**	-	-	0.77*	-	-	-	-	0.73*

* : $p < 0.05$; ** : $p < 0.01$; *** : $p < 0.001$

Annexe B

Table B1 Summary of uptake-irradiance parameters for N uptake (trace ^{15}N additions) at the SCM.

	NO_3^-				
	N_m^B µg N (µg chl *a*)$^{-1}$ h^{-1}	α µg N (µg chl *a*)$^{-1}$ h^{-1} (µmol quanta m^{-2} s^{-1})$^{-1}$	E_k µmol quanta m^{-2} s^{-1}	D^B µg N (µg chl *a*)$^{-1}$ h^{-1}	Relative D^B %
Mean (±SD)	0.042 ± 0.043	0.004 ± 0.003	18 ± 12	0.010 ± 0.030	14 ± 17
Minimum	0.001	0	1	0	0
Maximum	0.210	0.040	57	0.210	64

	NH_4^+				
	N_m^B µg N (µg chl *a*)$^{-1}$ h^{-1}	α µg N (µg chl *a*)$^{-1}$ h^{-1} (µmol quanta m^{-2} s^{-1})$^{-1}$	E_k µmol quanta m^{-2} s^{-1}	D^B µg N (µg chl *a*)$^{-1}$ h^{-1}	Relative D^B %
Mean (±SD)	0.016 ± 0.017	0.005 ± 0.008	7 ± 8	0.008 ± 0.009	26 ± 24
Minimum	0	0	1	0	0
Maximum	0.070	0.039	43	0.030	80

Annexe C

Table C1 Uptake-irradiance parameters for the data set where SCM and surface communities were incubated with trace (T) or enriched (E) NO_3^- additions. N_m^B is presented without dark uptake. Experimental stations located in the coastal Beaufort Sea (CBS), North-West Passage (NWP), central and eastern Baffin Bay (CBB and EBB, respectively) for late summer-fall 2006.

					Carbon											
					P_m^B µg C (µg chl *a*)$^{-1}$ h^{-1}				E_k µmol quanta m^{-2} s^{-1}				α µg C (µg chl *a*)$^{-1}$ h^{-1} (µmol quanta m^{-2} s^{-1})$^{-1}$			
Region	Station	Depth (m)	Date	Day of the year	NO_3^- T SCM	NO_3^- T Surface	NO_3^- E SCM	NO_3^- E Surface	NO_3^- T SCM	NO_3^- T Surface	NO_3^- E SCM	NO_3^- E Surface	NO_3^- T SCM	NO_3^- T Surface	NO_3^- E SCM	NO_3^- E Surface
CBB	132	5	09-09-2006	252		0.397		0.512		31		41		0.013		0.013
CBB	132	34	09-09-2006	252	0.227		0.229		17		13		0.014		0.018	
EBB	131	5	11-09-2006	254		0.819		0.664		32		32		0.026		0.021
EBB	131	35	11-09-2006	254	0.602		0.684		22		32		0.028		0.021	
CBB	108	5	17-09-2006	260		0.651		0.807		30		43		0.022		0.019
CBB	108	40	17-09-2006	260	0.737		0.743		32		32		0.023		0.023	
NWP	303	5	21-09-2006	264		0.547				42				0.013		
NWP	303	22	21-09-2006	264	0.691				30				0.023			
NWP	307	5	23-09-2006	266		1.377		2.067		31		22		0.054		0.093
NWP	307	31	23-09-2006	266	1.714		1.647		26		90		0.056		0.018	
CBS	405	5	01-10-2006	274		1.106		1.292		41		50		0.027		0.026
CBS	405	48	01-10-2006	274	0.228		0.227		8		11		0.027		0.020	
CBS	408	5	03-10-2006	276		0.971		0.788		42		39		0.023		0.020
CBS	408	67	03-10-2006	276	0.322		0.297		10		11		0.031		0.028	
CBS	SH (409)	5	04-10-2006	277		1.113		1.066		31		34		0.036		0.031
CBS	SH (409)	35	04-10-2006	277	0.856		0.809		20		21		0.042		0.038	
CBS	435	5	12-10-2006	285		0.390		0.349		22		25		0.018		0.014
CBS	435	55	12-10-2006	285	0.400		0.387		7		9		0.055		0.044	

					Nitrogen (without dark uptake)															
					N_m^B µg N (µg chl *a*)$^{-1}$ h^{-1}				E_k µmol quanta m^{-2} s^{-1}				α µg N (µg chl *a*)$^{-1}$ h^{-1}) (µmol quanta m^{-2} s^{-1})$^{-1}$				D^B µg N (µg chl *a*)$^{-1}$ h^{-1})			
Region	Station	Depth (m)	Date	Day of the year	NO_3^- T SCM	NO_3^- T Surface	NO_3^- E SCM	NO_3^- E Surface	NO_3^- T SCM	NO_3^- T Surface	NO_3^- E SCM	NO_3^- E Surface	NO_3^- T SCM	NO_3^- T Surface	NO_3^- E SCM	NO_3^- E Surface	NO_3^- T SCM	NO_3^- T Surface	NO_3^- E SCM	NO_3^- E Surface
CBB	132	5	09-09-2006	252		0.009		0.051		5		4		0.002		0.013				0.064
CBB	132	34	09-09-2006	252	0.016		0.015		14		5		0.001		0.003		0.002		0.002	
EBB	131	5	11-09-2006	254		0.023		0.032		23		35		0.001		0.001		0.000		0.002
EBB	131	35	11-09-2006	254	0.028		0.025		17		25		0.002		0.001		0.003		0.005	
CBB	108	5	17-09-2006	260		0.011		0.032		19		36		0.001		0.001		0.002		0.001
CBB	108	40	17-09-2006	260	0.014		0.030		28		34		0.001		0.001		0.000		0.000	
NWP	303	5	21-09-2006	264		0.018				13				0.001				0.007		
NWP	303	22	21-09-2006	264	0.042				23				0.002				0.011			
NWP	307	5	23-09-2006	266		0.070		0.044		12		15		0.006		0.003		0.020		0.022
NWP	307	31	23-09-2006	266	0.077		0.060		26		15		0.003		0.004		0.000		0.000	
CBS	405	5	01-10-2006	274		0.002		0.018		46		6		0.000		0.003		0.003		0.007
CBS	405	48	01-10-2006	274	0.027		0.013		6		11		0.005		0.001		0.036		0.011	
CBS	408	5	03-10-2006	276				0.018				11				0.002				0.006
CBS	408	67	03-10-2006	276	0.040		0.014		9		8		0.005		0.002		0.000		0.008	
CBS	SH (409)	5	04-10-2006	277		0.005		0.014		11		20		0.001		0.001		0.003		0.010
CBS	SH (409)	35	04-10-2006	277	0.006		0.006		13		21		0.001		0.000		0.000		0.007	
CBS	435	5	12-10-2006	285		0.001		0.010		14		3		0.000		0.003		0.001		0.001
CBS	435	55	12-10-2006	285	0.031		0.003		3		10		0.010		0.000		0.032			

Table C2 Uptake-irradiance parameters for the data set where SCM communities were incubated with trace (T) or enriched (E) NO_3^- and NH_4^+ additions. N_m^B is presented without dark uptake. Experimental stations located in the coastal Beaufort Sea (CBS), offshore Beaufort Sea (OBS), North-West Passage (NWP), western, central and eastern Baffin Bay (WBB, CBB and EBB, respectively) and Hudson Bay (HB) for spring-early summer and late summer-fall. "N/d" indicates that no data were available.

					Carbon											
					P_m^B µg C (µg chl *a*)$^{-1}$ h^{-1}				E_k µmol quanta m^{-2} s^{-1}				α µg C (µg chl *a*)$^{-1}$ h^{-1}) (µmol quanta m^{-2} s^{-1})$^{-1}$			
Region	Station	Depth (m)	Date	Day of the year	$NH_4^+{}_T$	$NO_3^-{}_T$	$NH_4^+{}_E$	$NO_3^-{}_E$	$NH_4^+{}_T$	$NO_3^-{}_T$	$NH_4^+{}_E$	$NO_3^-{}_E$	$NH_4^+{}_T$	$NO_3^-{}_T$	$NH_4^+{}_E$	$NO_3^-{}_E$
EBB	BA01-05	24	16-08-2005	228	n/d	n/d	n/d	n/d	n/d	n/d	n/d	n/d	n/d	n/d	n/d	n/d
WBB	BA03-05	42	18-08-2005	230	n/d	n/d	n/d	n/d	n/d	n/d	n/d	n/d	n/d	n/d	n/d	n/d
CBB	BA04-05	25	22-08-2005	234	0.558	0.465	0.570	0.490	28	23	24	22	0.020	0.021	0.024	0.022
NWP	S3	33	23-08-2005	235	0.256	0.287	n/d	0.228	16	20	n/d	15	0.016	0.015	n/d	0.015
CBS	S201	19	02-09-2005	245	0.153	0.159	0.143	0.157	26	28	48	42	0.006	0.006	0.003	0.004
OBS	S10	52	05-09-2005	248	0.168	0.131	0.172	0.141	19	18	23	25	0.009	0.007	0.007	0.006
CBS	CA08-05	43	09-09-2005	252	0.343	0.263	0.195	0.307	30	36	35	37	0.011	0.007	0.006	0.008
CBS	CA18-05	30	12-09-2005	255	0.492	0.462	0.509	0.521	20	24	21	25	0.025	0.020	0.024	0.021
HB	S22	35	06-10-2005	279	0.387	0.345	0.309	0.442	25	22	24	29	0.015	0.015	0.013	0.015
HB	NR24	17	10-10-2005	283	7.751	5.323	n/d	11.131	451	207	n/d	546	0.017	0.026	n/d	0.020
WBB	118	50	14-09-2006	257	0.510	0.535	0.486	0.516	21	34	22	34	0.025	0.016	0.022	0.015
CBS	436	18	09-10-2006	282	0.688	0.714	0.689	0.716	24	16	15	17	0.029	0.045	0.046	0.043
WBS	101	41	20-09-2007	272	0.427	0.466	0.523	0.530	8	14	22	14	0.053	0.034	0.024	0.037
EBB	115	80	01-10-2007	274	0.195	0.188	0.215	0.149	17	15	20	12	0.011	0.012	0.011	0.013
NWP	302	37	07-10-2007	280	0.885	0.791	0.777	0.794	17	16	19	13	0.053	0.051	0.042	0.062
CBS	435	16	17-10-2007	290	0.233	0.241	0.248	0.247	13	17	15	11	0.018	0.014	0.017	0.022
CBS	1806	22	19-10-2007	292	0.509	0.484	0.428	0.484	13	20	13	20	0.039	0.025	0.034	0.025
CBS	408	12	22-10-2007	295	0.845	0.858	0.660	0.901	32	34	23	31	0.027	0.025	0.029	0.029
CBS	405	31	25-10-2007	298	0.479	0.501	0.518	0.500	11	18	9	14	0.043	0.028	0.056	0.037
CBS	D43	30	28-04-2008	119	0.863	1.029	1.259	1.144	27	34	29	34	0.032	0.030	0.043	0.034
CBS	1020A	44	06-05-2008	127	0.528	0.513	0.504	0.501	25	29	18	19	0.022	0.018	0.029	0.026
CBS	1806	50	23-05-2008	144	0.698	1.080	0.820	0.703	18	20	23	13	0.040	0.055	0.036	0.053
CBS	405b	16	10-06-2008	140	1.919	2.770	2.086	2.202	59	97	70	73	0.033	0.029	0.030	0.030
CBS	405	37	01-06-2008	153	0.303	0.503	0.568	0.438	20	18	19	17	0.016	0.029	0.030	0.027
CBS	405b	37	10-06-2008	162	0.829	1.225	0.969	0.549	35	43	32	29	0.024	0.029	0.031	0.019
CBS	FB07	37	21-06-2008	173	0.711	0.685	0.746	0.615	19	21	20	18	0.038	0.032	0.037	0.034
CBS	1216	33	23-06-2008	175	0.520	0.677	0.567	0.725	13	11	12	21	0.039	0.061	0.048	0.035
CBS	F7	33	24-06-2008	176	1.099	1.467	1.170	1.156	21	28	23	20	0.052	0.053	0.050	0.057
CBS	1208	35	28-06-2008	180	0.495	0.707	0.626	0.603	22	25	26	26	0.023	0.029	0.024	0.023
CBS	6006	54	04-07-2008	186	0.152	0.133	0.156	0.126	16	12	16	11	0.010	0.012	0.010	0.011
CBS	2010	29	06-07-2008	188	0.471	0.326	0.533	0.324	39	19	26	21	0.012	0.017	0.021	0.015
CBS	416	73	10-07-2008	192	0.571	0.627	0.859	0.439	27	31	33	22	0.021	0.020	0.026	0.020

					Nitrogen (without dark uptake)															
					N_m^B µg N (µg chl *a*)$^{-1}$ h^{-1}				E_k µmol quanta m^{-2} s^{-1}				α µg N (µg chl *a*)$^{-1}$ h^{-1}) (µmol quanta m^{-2} s^{-1})$^{-1}$				D^B µg N (µg chl *a*)$^{-1}$ h^{-1}			
Region	**Station**	**Depth (m)**	**Date**	**Day of the year**	$NH_4^+{}_T$	$NO_3^-{}_T$	$NH_4^+{}_E$	$NO_3^-{}_E$	$NH_4^+{}_T$	$NO_3^-{}_T$	$NH_4^+{}_E$	$NO_3^-{}_E$	$NH_4^+{}_T$	$NO_3^-{}_T$	$NH_4^+{}_E$	$NO_3^-{}_E$	$NH_4^+{}_T$	$NO_3^-{}_T$	$NH_4^+{}_E$	$NO_3^-{}_E$
EBB	BA01-05	24	16-08-2005	228	0.037	0.014	0.062	0.038	15	17	6	35	0.003	0.001	0.010	0.001	0.017	0.001	0.011	0.001
WBB	BA03-05	42	18-08-2005	230	0.008	0.009	0.020	0.028	3	22	12	26	0.003	0.0004	0.002	0.001	0.007	0.002	0.039	0.005
CBB	BA04-05	25	22-08-2005	234	0.037	0.059	0.098	0.038	7	33	10	13	0.005	0.002	0.010	0.003	0.016	0.005	0.069	0.000
NWP	S3	33	23-08-2005	235	0.024	0.029	0.039	0.032	5	26	5	11	0.004	0.001	0.008	0.003	0.003	0.004	0.010	0.004
CBS	S201	19	02-09-2005	245	0.028	0.041	0.032	0.030	8	41	11	43	0.004	0.001	0.003	0.001	0.021	0.002	0.044	0.004
OBS	S10	52	05-09-2005	248	0.025	0.110	0.039	0.025	4	19	12	22	0.006	0.006	0.003	0.001	0.019	0.011	0.041	0.005
CBS	CA08-05	43	09-09-2005	252	0.024	0.024	0.088	0.023	6	34	6	25	0.004	0.001	0.014	0.001	0.006	0.000	0.037	0.005
CBS	CA18-05	30	12-09-2005	255	0.009	0.097	0.036	0.061	2	12	4	31	0.004	0.008	0.009	0.002	0.015	0.017	0.040	0.007
HB	S22	35	06-10-2005	279	0.014	0.016	0.017	0.012	12	12	9	23	0.001	0.001	0.002	0.001	0.012	0.010	0.030	0.002
HB	NR24	17	10-10-2005	283	0.051	0.054	0.092	0.051	12	27	25	47	0.004	0.002	0.004	0.001	0.029	0.002	0.056	0.000
WBB	118	50	14-09-2006	257	0.014	0.029	0.022	0.051	9	22	10	30	0.002	0.001	0.002	0.002	0.006	0.001	0.012	0.000
CBS	436	18	09-10-2006	282	0.012	0.004	0.031	0.015	6	10	5	9	0.002	0.0004	0.006	0.002	0.002	0.001	0.013	0.003
WBS	101	41	20-09-2007	272	0.004	0.001	0.012	0.006	3	23	9	9	0.002	0.00003	0.001	0.001	0.000	n/d	0.010	0.006
EBB	115	80	01-10-2007	274	0.000	0.003	0.005	0.007	8	17	24	13	0.00004	0.0002	0.0002	0.001	0.000	n/d	n/d	0.010
NWP	302	37	07-10-2007	280	0.004	0.003	0.011	0.009	10	13	10	18	0.0004	0.0002	0.001	0.001	0.002	0.000	0.014	0.002
CBS	435	16	17-10-2007	290	0.001	0.004	0.008	0.006	2	21	8	63	0.001	0.0002	0.001	0.0001	0.005	0.002	0.008	0.008
CBS	1806	22	19-10-2007	292	0.002	0.003	0.009	0.006	0	26	7	10	0.005	0.0001	0.001	0.001	0.003	0.000	0.009	0.002
CBS	408	12	22-10-2007	295	0.005	0.002	0.014	0.005	4	16	6	76	0.001	0.0001	0.002	0.0001	0.001	0.001	0.004	0.000
CBS	405	31	25-10-2007	298	0.002	0.006	0.007	0.001	1	9	5	5	0.002	0.001	0.001	0.0003	0.004	0.000	0.005	0.006
CBS	D43	30	28-04-2008	119	0.006	0.042	0.040	0.069	7	14	10	25	0.001	0.003	0.004	0.003	0.004	0.011	0.009	0.009
CBS	1020A	44	06-05-2008	127	0.005	0.114	0.031	0.093	7	29	10	20	0.001	0.004	0.003	0.005	0.000	0.000	0.000	0.000
CBS	1806	50	23-05-2008	144	0.013	0.061	0.124	0.200	43	7	5	11	0.000	0.009	0.023	0.018	0.003	0.008	0.000	0.033
CBS	405b	16	10-06-2008	140	0.005	0.008	0.243	0.355	8	17	24	37	0.001	0.001	0.010	0.010	0.014	0.016	0.047	0.191
CBS	405	37	01-06-2008	153	0.005	0.049	0.061	0.024	27	30	41	20	0.000	0.002	0.002	0.001	0.022	0.032	0.049	0.008
CBS	405b	37	10-06-2008	162	0.043	0.062	0.122	0.091	13	21	17	12	0.003	0.003	0.007	0.008	0.030	0.003	0.033	0.000
CBS	FB07	37	21-06-2008	173	0.026	0.029	0.049	0.041	7	4	7	11	0.004	0.007	0.007	0.004	0.006	0.000	0.000	0.000
CBS	1216	33	23-06-2008	175	0.007	0.062	0.048	0.087	5	17	5	14	0.001	0.004	0.010	0.006	0.000	0.000	0.001	0.000
CBS	F7	33	24-06-2008	176	0.070	0.013	0.107	0.056	2	26	8	22	0.039	0.001	0.013	0.003	0.000	0.000	0.000	0.000
CBS	1208	35	28-06-2008	180	0.009	0.012	0.040	0.052	1	7	7	9	0.018	0.002	0.006	0.006	0.000	0.000	0.019	0.000
CBS	6006	54	04-07-2008	186	0.000	0.037	0.004	0.021	0	17	6	13	0.000	0.002	0.001	0.002	0.000	0.007	n/d	0.004
CBS	2010	29	06-07-2008	188	0.004	0.027	0.021	0.023	0	6	2	4	0.024	0.005	0.009	0.005	0.000	0.003	0.018	0.013
CBS	416	73	10-07-2008	192	0.000	0.210	0.000	0.129	0	5	0	11	0.000	0.040	0.000	0.012	0.000	0.000	0.000	0.000

Table C3 Uptake-irradiance parameters for the data set where SCM communities were incubated with trace (T) or enriched (E) NO_3^- and urea additions. N_m^B is presented without dark uptake. Experimental stations located in the coastal Beaufort Sea (CBS) for spring-early summer and late summer-fall.

					Carbon											
					P_m^B µg C (µg chl *a*)$^{-1}$ h^{-1}				E_k µmol quanta m^{-2} s^{-1}				α µg C (µg chl *a*)$^{-1}$ h^{-1} (µmol quanta m^{-2} s^{-1})$^{-1}$			
Region	Station	Depth (m)	Date	Day of the year	Urea $_T$	$NO_3^-{}_T$	Urea $_E$	$NO_3^-{}_E$	Urea $_T$	$NO_3^-{}_T$	Urea $_E$	$NO_3^-{}_E$	Urea $_T$	$NO_3^-{}_T$	Urea $_E$	$NO_3^-{}_E$
CBB	108	30	03-10-2007	276	0.326	0.221	0.375	0.739	22	13	8	26	0.015	0.017	0.048	0.028
CBS	9008	37	27-05-2008	148	0.707	0.540	0.860	0.545	28	22	40	19	0.025	0.025	0.022	0.029
CBS	F7	12	08-06-2008	160	1.306	1.390	1.895	1.807	32	40	57	72	0.041	0.035	0.033	0.025
CBS	F7	33	19-06-2008	171	0.692	0.921	0.951	0.670	20	25	26	19	0.034	0.036	0.037	0.036
CBS	1200	36	27-06-2008	179	1.031	0.936	0.931	1.029	46	37	42	43	0.022	0.025	0.022	0.024
CBS	421	62	01-07-2008	183	0.353	0.434	0.421	0.469	10	13	12	8	0.037	0.033	0.035	0.058
CBS	410	54	08-07-2008	190	0.279	0.305	0.376	0.352	17	18	20	14	0.016	0.017	0.019	0.024

					Nitrogen (without dark uptake)															
					N_m^B µg N (µg chl *a*)$^{-1}$ h^{-1}				E_k µmol quanta m^{-2} s^{-1}				α µg N (µg chl *a*)$^{-1}$ h^{-1} (µmol quanta m^{-2} s^{-1})$^{-1}$				D^B µg N (µg chl *a*)$^{-1}$ h^{-1}			
Region	Station	Depth (m)	Date	Day of the year	Urea $_T$	$NO_3^-{}_T$	Urea $_E$	$NO_3^-{}_E$	Urea $_T$	$NO_3^-{}_T$	Urea $_E$	$NO_3^-{}_E$	Urea $_T$	$NO_3^-{}_T$	Urea $_E$	$NO_3^-{}_E$	Urea $_T$	$NO_3^-{}_T$	Urea $_E$	$NO_3^-{}_E$
CBB	108	30	03-10-2007	276	0.002	0.024	0.003	0.011	2	40	2	22	0.001	0.001	0.002	0.001	0.000	0.001	0.000	0.000
CBS	9008	37	27-05-2008	148	0.000	0.027	0.000	0.057	0	6	0	7	0.000	0.004	n/d	0.008	0.000	0.014	0.000	0.053
CBS	F7	12	08-06-2008	160	0.040	0.152	0.032	0.364	28	18	36	47	0.001	0.009	0.001	0.008	0.013	0.000	0.000	0.000
CBS	F7	33	19-06-2008	171	0.000	0.100	0.002	0.083	0	10	8	7	0.000	0.010	0.000	0.012	0.000	0.211	0.000	0.049
CBS	1200	36	27-06-2008	179	0.054	0.087	0.034	0.075	7	14	7	21	0.008	0.006	0.005	0.004	0.027	0.006	0.000	0.006
CBS	421	62	01-07-2008	183	0.000	0.030	0.000	0.097	0	1	0	3	0.000	0.021	n/d	0.030	0.000	0.000	0.000	0.000
CBS	410	54	08-07-2008	190	0.003	0.085	0.003	0.110	2	10	9	31	0.002	0.009	0.000	0.004	0.004	0.000	0.000	0.000

Table C4 Uptake-irradiance parameters for the data set where SCM communities were incubated with trace (T) or enriched (E) NO_3^- and NO_2^- additions. N_m^B is presented without dark uptake. Experimental stations located in the coastal Beaufort Sea (CBS) for spring-early summer and late summer-fall.

					Carbon											
					P_m^B µg C (µg chl *a*)$^{-1}$ h^{-1}				E_k µmol quanta m^{-2} s^{-1}				α µg C (µg chl *a*)$^{-1}$ h^{-1}) (µmol quanta m^{-2} s^{-1})$^{-1}$			
Region	Station	Depth (m)	Date	Day of the year	NO_2^- T	NO_3^- T	NO_2^- E	NO_3^- E	NO_2^- T	NO_3^- T	NO_2^- E	NO_3^- E	NO_2^- T	NO_3^- T	NO_2^- E	NO_3^- E
CBS	407	30	18-10-2006	291	1.280	1.530	1.335	1.325	22	20	24	21	0.057	0.078	0.057	0.064
CBS	407	34	23-10-2007	296	0.861	1.184	1.066	1.383	24	31	29	37	0.036	0.038	0.036	0.037
CBS	1011	63	21-05-2008	142	0.919	1.457	1.010	0.861	42	40	44	42	0.022	0.037	0.023	0.020

					Nitrogen (without dark uptake)															
					N_m^B µg N (µg chl *a*)$^{-1}$ h^{-1}				E_k µmol quanta m^{-2} s^{-1}				α µg N (µg chl *a*)$^{-1}$ h^{-1}) (µmol quanta m^{-2} s^{-1})$^{-1}$				D^B µg N (µg chl *a*)$^{-1}$ h^{-1})			
Region	Station	Depth (m)	Date	Day of the year	NO_2^- T	NO_3^- T	NO_2^- E	NO_3^- E	NO_2^- T	NO_3^- T	NO_2^- E	NO_3^- E	NO_2^- T	NO_3^- T	NO_2^- E	NO_3^- E	NO_2^- T	NO_3^- T	NO_2^- E	NO_3^- E
CBS	407	30	18-10-2006	291	0.007	0.023	0.018	0.017	6	13	16	12	0.001	0.002	0.001	0.001	0.003	0.006	0.003	0.005
CBS	407	34	23-10-2007	296	0.001	0.036	0.004	0.046	1	24	37	28	0.001	0.002	0.000	0.002	0.001	0.009	0.003	0.004
CBS	1011	63	21-05-2008	142	0.008	0.151	0.007	0.102	27	58	23	68	0.000	0.003	0.000	0.002	0.000	0.000	0.001	0.000